STRUCTURAL AND FUNCTIONAL IMPACTS OF CHEMICAL MODIFICATIONS IN PEPTIDES AND SMALL PROTEINS

by

Halina Marie Werner

B.Sc. Biochemistry, Seattle University, 2012

Submitted to the Graduate Faculty of

The Dietrich School of Arts & Sciences in partial fulfillment

of the requirements for the degree of

Doctor of Philosophy

University of Pittsburgh

2018

UNIVERSITY OF PITTSBURGH

DIETRICH SCHOOL OF ARTS & SCIENCES

This dissertation was presented

by

Halina Marie Werner

It was defended on

July 18th, 2018

and approved by

W. Seth Childers, Assistant Professor, Department of Chemistry

Stephen G. Weber, Professor, Department of Chemistry

Jeffrey L. Brodsky, Professor, Avinoff Chair of Biological Sciences

Dissertation Advisor: W. Seth Horne, Associate Professor, Department of Chemistry

STRUCTURAL AND FUNCTIONAL IMPACTS OF CHEMICAL MODIFICATIONS IN PEPTIDES AND SMALL PROTEINS

Halina M. Werner, PhD

University of Pittsburgh, 2018

Due to their presence in all forms of life, proteins have remained at the forefront of research in myriad disciplines. Chemists employ covalent modifications to probe protein structure and function. At the simplest level of structure, a naturally occurring protein comprises a linear sequence of L-α-amino acids, each of which displays one of twenty sidechains. Simple primary sequence modifications can impact the complex structure and function of proteins in interesting ways. In this dissertation, we document our efforts to understand this relationship through chemical modification of peptides and small proteins.

The sequences of natural proteins can be partially substituted with unnatural amino acids, generating heterogeneous-backbone foldamers. The structures and functions of bioactive proteins have been recreated by heterogeneous-backbone foldamers. These protein mimics show increased resistance to proteolytic digestion; however, no effort has yet determined the relative protection efficiencies of unnatural residues. Thus, we ranked the proteolytic protection imparted by four commonly utilized unnatural residues substituted into a host peptide. These rankings have since been employed in the design of bioactive protein mimics.

Covalent cross-linking of protein sidechains is one type of modification employed to stabilize protein structures. Cross-links made across α-helices are thought to impart structural stability by preorganizing the backbone into an α-helical conformation; however, there is limited

evidence bearing directly on this hypothesis. Thus, we compared the thermodynamic impacts of three cross-link types on folding in a small α-helix rich protein. Our results support the preorganization hypothesis, showing a decreased entropic penalty of folding for all three cross-linked proteins. This finding should help inform the endeavors of the peptide and protein cross-linking community.

The ability of heterogeneous-backbone foldamers to mimic bioactive proteins highlights their potential use as therapeutics. While our group has been developing design principles, we have not yet achieved structural and functional mimicry of a protein larger than 56 residues. Thus, we use native chemical ligation to generate a library of heterogeneous-backbone ubiquitin foldamers, some of which fold and function comparably to native ubiquitin. In addition to refining our design principles, this is the first example of a heterogeneous-backbone foldamer of this size and functional ability.

TABLE OF CONTENTS

LIST OF TABLES

LIST OF FIGURES

LIST OF EQUATIONS

1.0 INTRODUCTION

Note: Parts of this chapter were published as Werner, H. M.; Horne, W. S. "Folding and function in α/β-peptides: Targets and therapeutic applications." *Curr. Opin. Chem. Biol.* **2015,** *28,* 75-82. It is reproduced from reference [1] with permission from Elsevier Publishing Company.

Proteins have received considerable attention among countless disciplines because they are essential for life. Their many functions are possible because proteins are arranged into a variety of organized structures. Accordingly, a significant branch of chemical biology research is devoted to elucidating the relationship between protein structure and function.

1.1 PROTEIN STRUCTURE

One approach toward investigating the protein structure-function relationship is to study protein folding, the process that transforms an expansive, linear chain of atoms into a compact, three-dimensional protein conformation. Remarkably, the complex transformations involved in protein folding are dictated solely by the primary level of protein structure, a simple linear sequence of amino acids.[2] In nature, amino acids have a consistent chemical connectivity comprising an L-α-backbone that bears one of twenty canonical side chains (**Figure 1**).

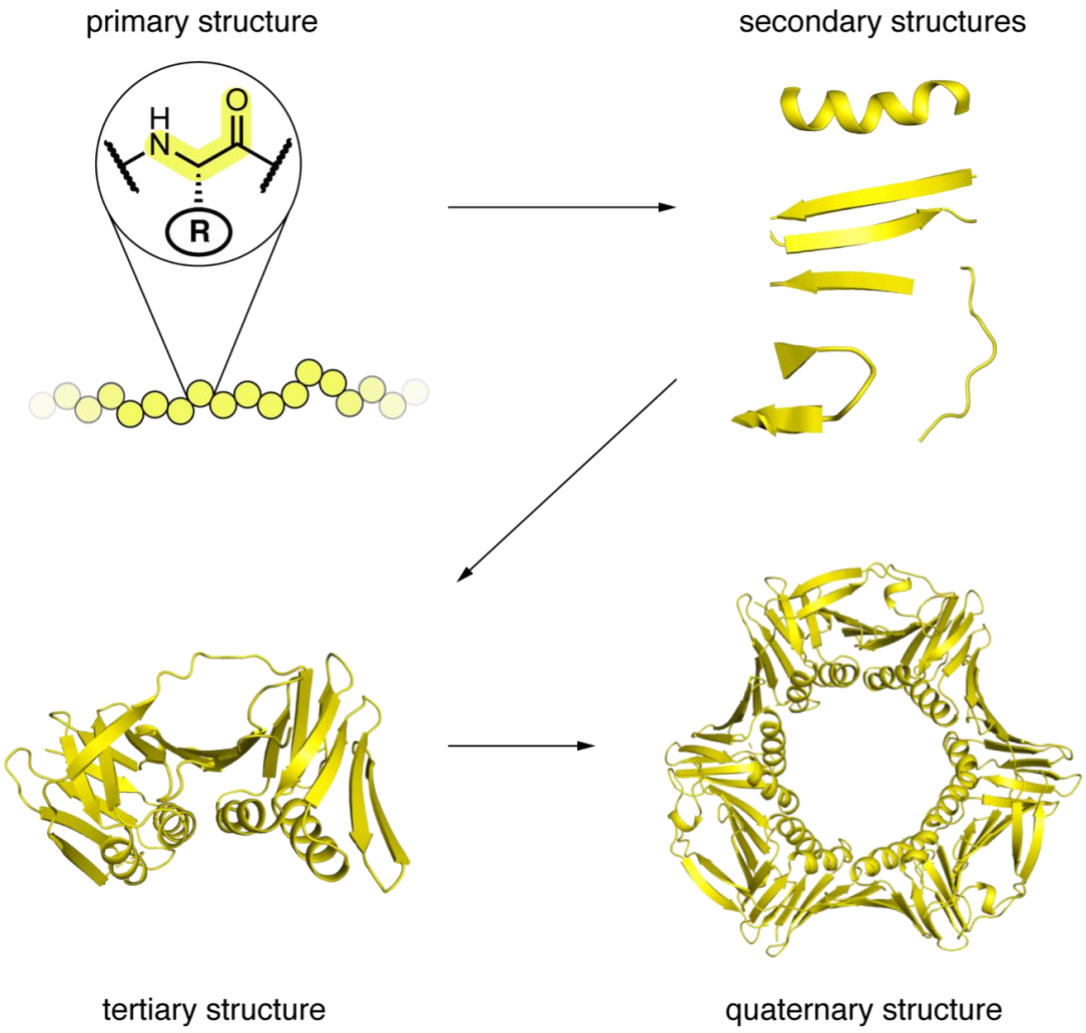

Figure 1. Structural hierarchy of the PCNA protein (yellow highlight=backbone, R=sidechain). PDB: 1AXC

Local effects and interactions within amino acids of the primary structure, such as their conformational preferences and hydrogen bonding interactions, dictate folding into discrete secondary structures—helices, β-sheets, tight turns, and flexible loops.[3] Hydrophobic and polar interactions between secondary structures form the tertiary structure of a protein, at the center of which the hydrophobic core is found.[4] Tertiary structure represents the most complex conformation achieved by a single chain of amino acids; at the height of protein structural and functional complexity are quaternary structures, which are formed by the assembly of several tertiary structure subunits.[5] The organized intricacy of protein structure and function provides an excellent setting in which to study the effects of chemical modifications.

While the diversity of protein building blocks is limited in terms of covalent connectivity, nature commonly expands this diversity through post-translational modifications.[6] Such chemical modifications, which include phosphorylation and acetylation, regulate countless cellular and metabolic processes.[7-8] Taking inspiration from nature, scientists have made modifications to protein side chains and backbones to introduce artificial covalent connectivities. Modifying proteins at this molecular level is a sophisticated way to probe the relationships between protein primary sequence, higher-order structures, and functions.

1.2 PEPTIDE MACROCYCLIZATION THROUGH SIDE CHAIN CROSS-LINKING

Protein stability often arises from the generation of covalent macrocycles. For instance, nature does this in the form of localized cyclizations such as disulfide bonds[9] and N-terminal pyroglutamate formation, [10] or global "head-to-tail" macrocyclizations—i.e. N- to C-terminus—exemplified by proteins such as Cyclosporin A.[11] From this, chemists have been inspired to

leverage natural and unnatural protein side chains to form peptide macrocycles.[12] Through this approach, naturally occurring side chains or installed unnatural moieties can be chemoselectively tethered together to form a cross-link, typically across a helical face (residues $i \rightarrow i+4$, $i \rightarrow i+7$, or $i \rightarrow i+11$) (**Figure 2**).

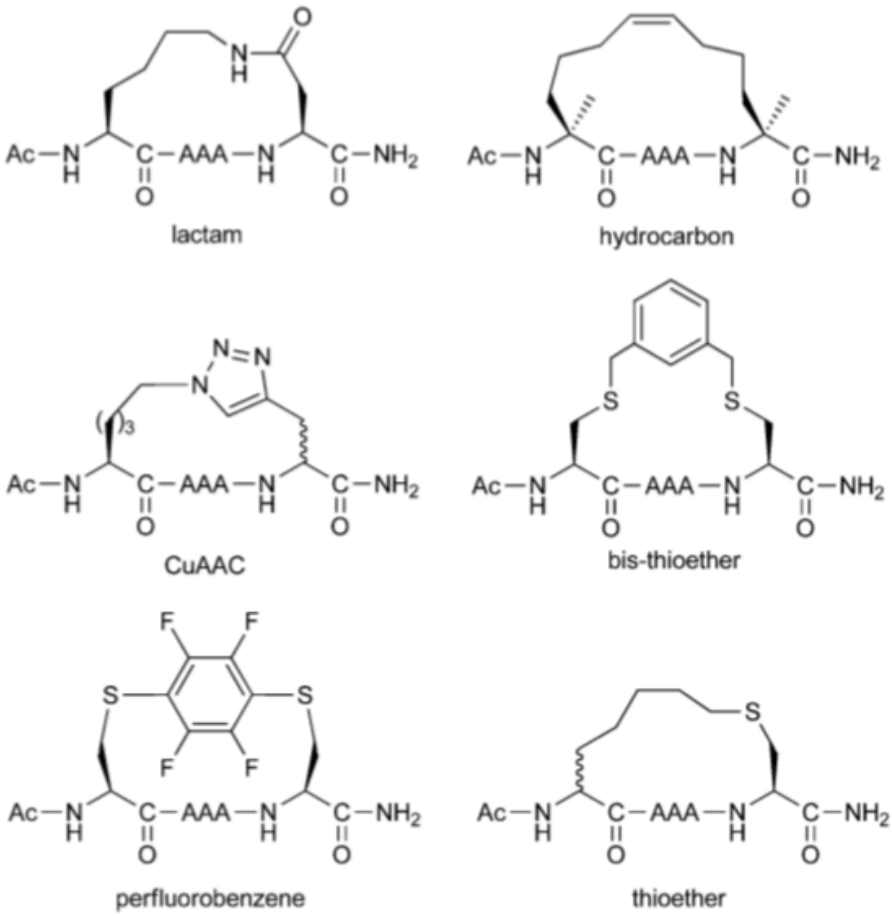

Figure 2. Comparison of different stapling chemistries on model pentapeptides. Reproduced from Ref. ## with permission from The Royal Society of Chemistry.

Side chain cross-linking results in the stabilization of protein structure—typically α-helices—and is often referred to as "peptide stapling."[13]

The diversity of naturally occurring protein side chains allows for a variety of cross-linking approaches. The earliest example of cross-linking in protein chemical synthesis involved the direct intramolecular cyclization of an amine (lysine) with a carboxylic acid (aspartic or glutamic acid) to form a lactam cyclized bioactive analog of human growth hormone-releasing factor.[14] Another area of cross-linking research introduces a molecule that acts as a bifunctional linker between pre-existing side chains.[12] For instance, work in the Pentelute lab focuses on the addition of perfluoroaryl molecules that covalently connect two cysteine side chains. Their most recent efforts resulted in cell-penetrating peptides with increased proteolytic stability attributed to perfluoroaryl cross-links.[15]

The field has now shifted focus toward chemical modification of side chains to introduce interesting novel cross-linking functionalities. For example, the Verdine group pioneered the area of hydrocarbon-stapled peptides, which can be generated from the ring-closing metathesis of side chains that display terminal alkenes.[16] A variety of chemoselective approaches can be employed to covalently cross-link protein side chains. For example, click chemistry can be used to install a triazole cross-link between side chains with terminal alkynes and azides.[17] Additionally, our group has developed oxime cross-linking, which represents another mild solution-phase approach toward covalent cross-linking.[18] Such cross-linking approaches have increased α-helix stability in many protein systems, resulting in effective protein-protein interaction mimics and peptide therapeutics.[19] Though the field has speculated as to the cause of structural stability increases,[20] no work before ours (Chapter 3) had reported direct evidence bearing on this issue.

1.3 BACKBONE MODIFICATION AND FOLDAMERS

Recently, a subset of protein modification research has focused on altering protein backbones. Protein backbone modification is often employed to advance our understanding of nature.[21] Such examples include the use of backbone modification to probe bioactive structures of interleukin-8,[22] and to provide insight into controlling the dynamics of protein folding.[23] Furthermore, judicious backbone modifications can be used to improve upon nature, resulting in proteins with enhanced folded[24] and proteolytic stabilities.[25] Modifications made to the backbones of individual amino acids generate so-called "unnatural" amino acids.[21] The term "foldamer" refers to an oligomer of unnatural amino acids that folds into a discrete, compact structure reminiscent of a protein.[26] In addition to recreating the structure of their natural counterparts, foldamers often exhibit functional benefits, including increased resistance to degradation by enzymes.[1, 25] Foldamers can be categorized by the diversity of their constituent building blocks. While homogeneous-backbone foldamers contain only one type of unnatural amino acid, their heterogeneous-backbone counterparts are comprised of an interspersed mixture of both unnatural and natural (i.e. L-α-) amino acids (**Figure 3**).[27]

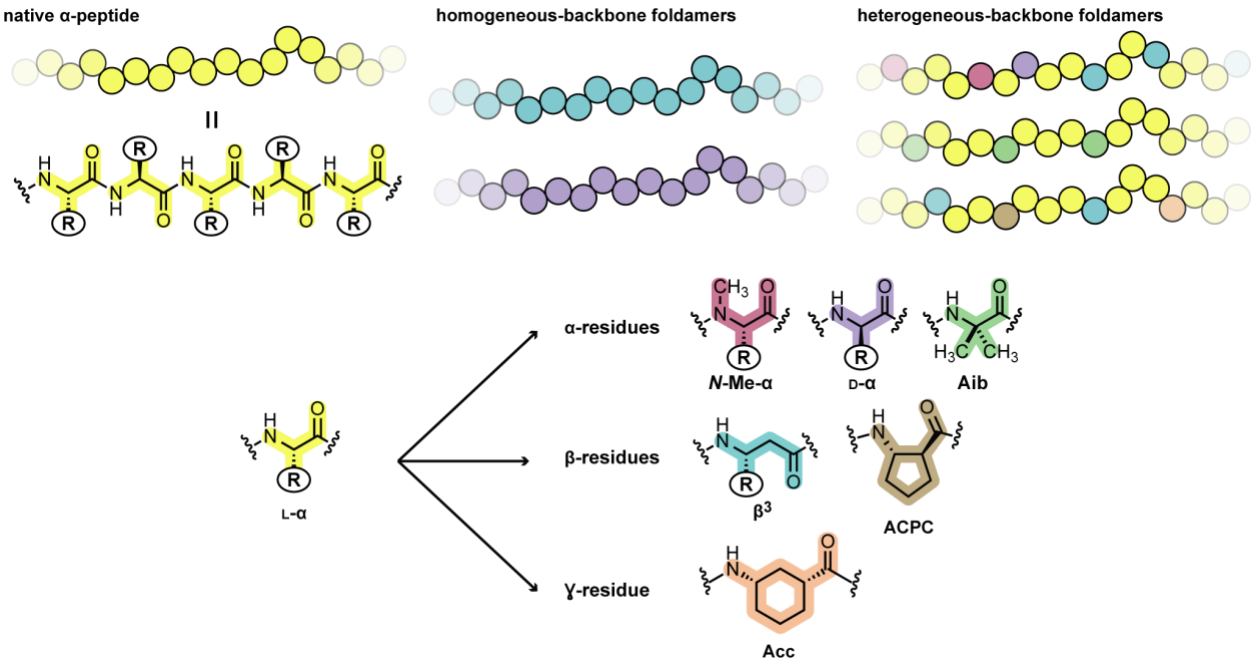

Figure 3. Chain compositions of naturally occurring α-peptides and proteins, homogeneous-backbone foldamers, and heterogeneous-backbone foldamers.

Among homogeneous-backbone foldamers, most work has investigated the interesting properties of β-peptides[28-29] and the applications of "mirror image proteins", which contain exclusively D-α-residues.[30] Interestingly, foldamers are not limited to amino acid-like building blocks. A significant subset of foldamer research studies aromatic monomers that can produce protein-like folds in their oligomeric states.[31]

A broad field of research has demonstrated that unnatural backbone analogues of α-peptides can adopt similar folds while resisting enzymatic degradation. Among the many backbones explored in this context, chains that blend α-amino acid residues with β-amino acid residues (α/β-peptides) have emerged as an important and well-studied class of heterogeneous backbone foldamers.[1] α/β-peptides of a moderate length can show biological function resulting from binding to a natural protein receptor (**Table 1**).

Table 1. Bioactive α/β-peptides with therapeutic potential.

α-Peptide Prototype	Length	β-Residue Content	Secondary Structure	Receptor	Function (Implication)
BH3 domains	26-mer	27%	α-helix	Bcl-x_L, Mcl-1	Apoptosis regulation (cancer)
gp41 (CHR domain)	38-mer	29%	α-helix	gp41 (NHR domain)	Viral cell entry (HIV)
Neuropeptide Y	12-mer	17%	α-helix	Y_4R	Gastrointestinal regulation (various)
PTH_{1-34}	34-mer	18%	α-helix	PTH1R	Calcium regulation (osteoporosis)
GLP-1	31-mer	16%	α-helix	GLP1R	Glucose regulation (diabetes)
VEGF	19-mer	32%	non-regular[a]	VEGFR	Angiogenesis (cancer, diseases of the eye)
Anginex	34-mer	9%	β-sheet	Gal-1	Angiogenesis, (cancer, diseases of the eye)
ZVEGF	39-mer	15%[a]	helix-turn-helix[a]	VEGFR	Angiogenesis, (cancer, diseases of the eye)

[a] Cyclized via a disulfide bond. This table is adapted from ref. [1] with permission from Elsevier Publishing Company.

β-Residues are among the most common building blocks in foldamer research, and a number of interesting biological activities have been reported for appropriately designed β-peptides. Although β-residues are structurally diverse, those found in bioactive α/β-peptides generally fall into one of two categories (**Figure 4**): β^3 or β^{cyc}.

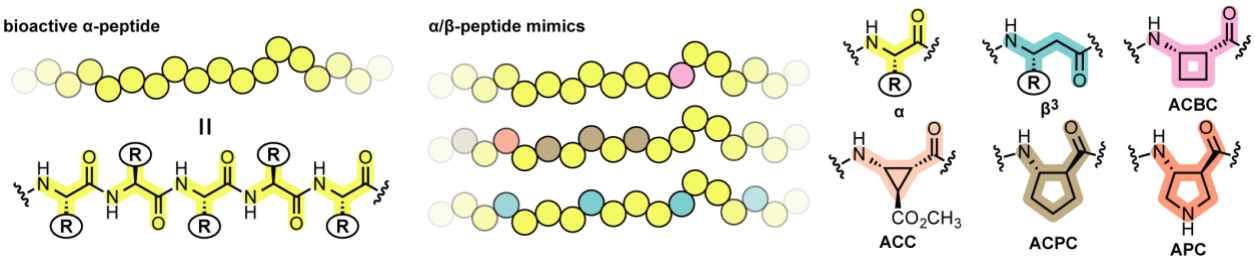

Figure 4. An α-peptide, example α/β-peptides, and their constituent residue structures. Replacing one or more α-amino acid residues in a biologically active α-peptide sequence with β-residues can lead to heterogeneous-backbone α/β-peptides with native-like function and improved biostability. Chemical structures and abbreviations are shown for a natural α-residue alongside those of the β-residues This figure is adapted from ref. [1] with permission from Elsevier Publishing Company.

β^3-Residues are backbone-homologated variants of α-residues. In α/β-peptides, β^3-residues offer the advantage of retaining protein-like side chain functionality while increasing backbone flexibility with an additional rotatable bond. In β^{cyc}-residues (e.g., ACBC, ACC, ACPC, APC), one of the backbone torsions is constrained by a carbocyclic or heterocyclic ring. This offers the advantage of exerting control over folding behavior of the β-residue based on selection of ring size and stereochemistry.

Successfully modifying the backbone of a natural protein is not trivial. Even an ostensibly minor modification can cause unexpected and detrimental consequences to the folding of a well-ordered sequence. This highlights the need to develop effective design strategies for the generation of foldamers and other backbone-modified proteins.

1.3.1 Foldamer Design Strategies

Early work on foldamer mimicry of the BH3 domain helps define two paradigms for the development of chemically modified proteins: structure- vs. sequence-based design. BH3

domains are conserved pro-apoptotic regions of the Bcl-2 protein family, which are crucial regulators of apoptosis.[32] Pioneering structural studies elucidated several helical folding patterns available to α/β-peptides with an alternating 1:1 backbone repeat, and one of these scaffolds was used to develop an α/β-peptide BH3 domain mimic.[33] Structure-guided introduction of side chains on the foldamer scaffold based on the known structure of the Bak/Bcl-x_L interface resulted in an α/β-peptide that bound Bcl-x_L, albeit with affinity much weaker than the prototype α-peptide BH3 domain. Replacement of the C-terminal half of the alternating α/β-peptide with a pure α-peptide backbone resulted in a chimeric oligomer with tight binding affinity for Bcl-x_L as well as the ability to induce release of mitochondrial cytochrome C in cancer cell lysates. Unfortunately, the α-residue rich portion of the chimera proved highly susceptible to proteolytic degradation.

Shortly after the work on chimeric α/β-peptide BH3 mimetics, an alternate design approach was developed. Starting from the BH3 domain of Bcl-2 family member Puma, a series of α/β-peptide variants were examined in which the side chain sequence of the natural ligand was displayed on all possible α/β^3-peptide backbones with an ααβαααβ repeat. This "sequence-guided" residue replacement strategy was inspired by findings that such modification can generate α/β-peptides with complex helix-bundle folding patterns.[34] Screening seven oligomers based on the Puma BH3 domain yielded an α/β-peptide with Bcl-x_L binding affinity indistinguishable from the natural α-peptide and significantly improved proteolytic stability. Later structural studies confirmed the binding mode of the Puma-based α/β-peptide with Bcl-x_L was identical to that of natural BH3 domains.[35] An important difference between the Puma α-peptide and its α/β-peptide mimic was that the unnatural backbone lost the capacity to bind tightly to the anti-apoptotic Bcl-2 family protein Mcl-1; however, structure-guided side-chain

modification was able to restore this function.[36] The development of α/β-peptides capable of modulating apoptotic signaling in the Bcl-2 protein family is an important early example of sequence-based backbone modification as a strategy for generating bioactive and protease-resistant oligomers.

The rapid success of sequence-based design as a strategy to generate α/β-peptide mimics of BH3 domains suggested it might be applicable to other prototype α-peptide sequences. Parathyroid hormone (PTH) is an 84-residue protein GPCR ligand that helps to regulate blood calcium levels. The 34-residue N-terminal peptide from PTH ($PTH_{1\text{-}34}$) has the same activity as the full length protein and is a clinically used drug for the treatment of osteoporosis.[37] Structural studies on the interaction of PTH with its receptor (PTH1R) suggest that residues 15-34 fold to form an α-helix that binds with high affinity to the GPCR extracellular domain, while the N-terminal region contacts the transmembrane domain and is responsible for signaling.[38] Sequence-guided $\alpha \rightarrow \beta^3$ residue replacement in an ααaβ pattern generated an α/β-peptide $PTH_{1\text{-}34}$ analogue with comparable receptor binding affinity *in vitro* and agonist activity in cell-based assays (**Figure 5**).[39]

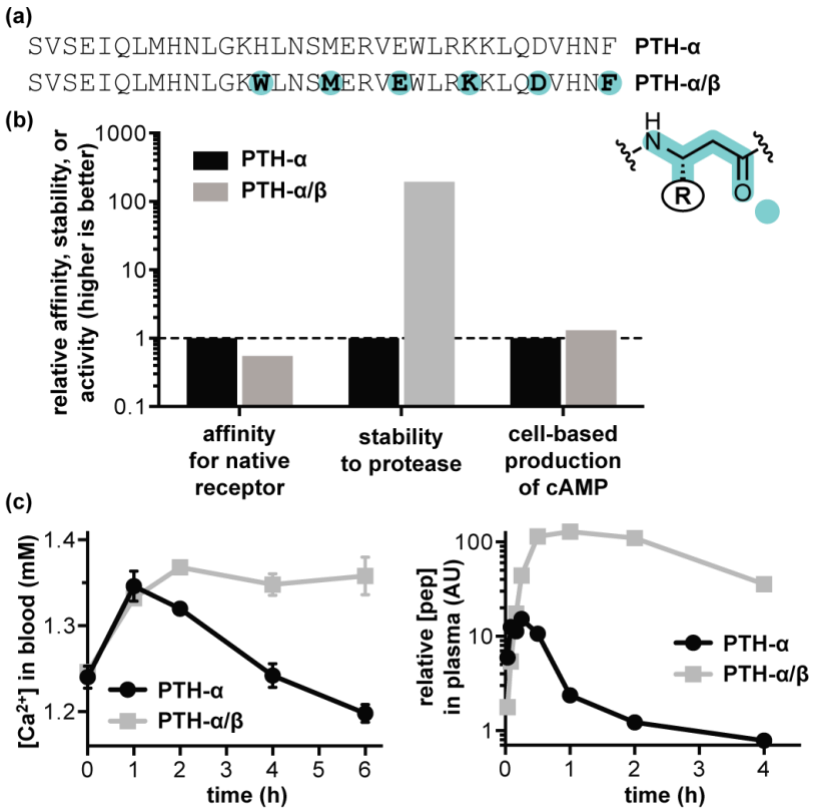

Figure 5. Design of α/β-peptide mimics of the α-peptide GPCR ligand parathyroid hormone (PTH). (a) Sequences of the prototype α-peptide PTH-α, residues 1–34 of the native hormone, and its α/β-peptide mimic PTH-α/β. (b) Comparison of in vitro bioactivity data for PTH-α and PTH-α/β: relative association affinity for parathyroid hormone receptor-1, relative half-life to proteolytic degradation by the enzyme trypsin, and relative activity in a cell-based assay of cyclic adenosine monophosphate (cAMP) production. (c) Summary of key *in vivo* data obtained for PTH-α and PTH-α/β in mice: blood calcium levels after treatment with the indicated peptide at a dose of 20 nmol/kg and relative concentration of peptide remaining in serum as a function of time after treatment. This figure is adapted from ref. [1] with permission from Elsevier Publishing Company.

A particularly significant result of this work was the demonstration that α/β-peptide mimicry of the α-peptide prototype translated from *in vitro* experiments to an *in vivo* context. Mice treated with $PTH_{1\text{-}34}$ or an α/β-peptide analogue showed identical initial spikes in blood calcium levels; however, a dramatic difference was observed in the duration of the effect. The α/β-peptide was able to sustain increased blood calcium several hours after levels in mice treated with the α-peptide had returned to baseline. Quantification of peptide in serum suggested that this effect results from enhanced stability of the α/β-peptide to proteolytic degradation. The development of α/β-peptide mimics of parathyroid hormone is the first example of sequence-guided backbone alteration leading to an agent with biological efficacy *in vivo*. The α/β-peptide showed longer circulation times and increased duration of effect compared to the α-peptide administered at the same dose.

Recent sequence-based designs of foldamers have branched out beyond β-residue incorporation alone, increasing the heterogeneity of protein backbones. Work in our group has produced heterogeneous-backbone foldamer mimics of GB1[40] and zinc finger sp1-3[24] that contain Aib, *N*-Me-, and D-residues in addition to β-residues. From the Gellman lab, sequence-guided $\alpha \rightarrow \beta^3$ residue replacement in a two-helix VEGF-binding α-peptide, along with incorporation of β^{cyc}-residues and Aib, generated a heterogeneous-backbone foldamer mimic with identical affinity for VEGF (**Figure 6**). [41]

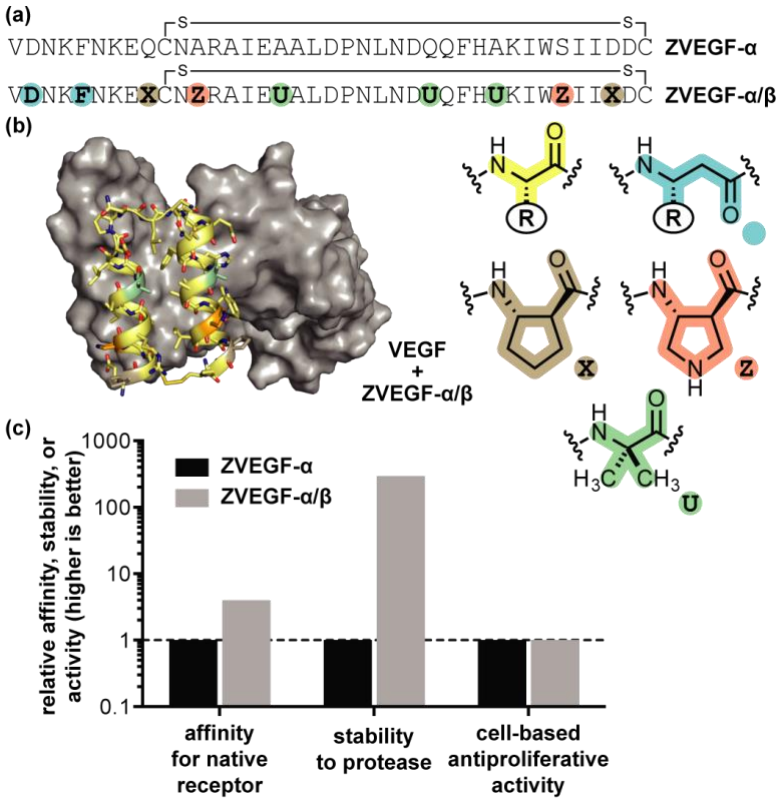

Figure 6. Design of a heterogeneous-backbone foldamer mimic of a phage-derived α-peptide that inhibits the interaction between VEGF and its receptors. (a) Sequences of the prototype VEGF-binding α-peptide ZVEGF-α and its heterogeneous-backbone foldamer mimic ZVEGF-α/β. (b) Crystal structure of ZVEGF-α/β bound to VEGF (PDB: 4WPB). (c) Comparison of in vitro bioactivity data for ZVEGF-α and ZVEGF-α/β: relative association affinity for VEGF, relative half-life to proteolytic degradation by the enzyme proteinase K, and relative activity in a cell-based assay of VEGF-induced proliferation. This figure is adapted from ref. [1] with permission from Elsevier Publishing Company.

Notably, the foldamer showed improved stability to proteolytic degradation *in vitro* and was able to inhibit VEGF-induced proliferation in cell-based assays. Despite these promising results, sequence-based design is not yet a perfected approach. For example, sequence-based $\alpha \rightarrow \beta^3$ substitutions, quite successful in the PTH analogues described above, were not tolerated in GLP-1; incorporation of just three β^3-residues in the 30mer abolished agonist activity entirely.[42] The use of β^{cyc}-residues proved much more effective; receptor binding affinity was retained in an analogue with five $\alpha \rightarrow \beta^{cyc}$ replacements in an ααααβ pattern. Interestingly, the 12-residue N-terminal segment of GLP-1 proved quite sensitive to backbone alteration; however, this problem was solved by the judicious use of two α-aminoisobutyric acid residues to block known proteolytic cleavage sites near the N-terminus. These optimized heterogeneous-backbone analogues of GLP-1, similar to PTH(1-34), were found to have enhanced *in vivo* efficacy. These advances highlight the utility of various unnatural amino acids in the sequence-based design of heterogeneous-backbone foldamers.

Heterogeneous-backbone foldamers are a class of molecules with significant therapeutic potential, especially in cases where the biological target is an extended protein surface. While early studies on modified backbones focused heavily on the mimicry of natural protein structure, more recent work has shifted toward the functional mimicry of bioactive α-peptides. These studies have shown that heterogeneous-backbone foldamers can be generated with biological properties identical to a prototype α-peptide, but with increased stability to degradation by proteases in serum. Examples of heterogeneous-backbone foldamers with long *in vivo* lifetimes represent a significant milestone toward improving bioavailability, a major limitation of current α-peptide pharmaceuticals. Although questions of potential toxicity and immunogenicity remain

areas for further investigation, heterogeneous-backbone foldamers already show tremendous promise as therapeutic agents and appear to be on a trajectory toward potential clinical use.

1.4 GOALS OF THIS WORK

While impactful findings have advanced the field of protein and peptide modification over the last 30 years, many open questions remain. Heterogeneous-backbone foldamers regularly show increased resistance to proteases; however, their proteolytic stability is often examined after the fact rather than a consideration at the outset of foldamer design. In a protein backbone interspersed with natural and unnatural residues, what is the most effective unnatural residue substitution strategy to achieve maximal protease protection with minimal artificial building block content? We investigate this question by undertaking a quantitative comparison of backbone-modified peptide proteolysis in Chapter 2. From this work, we propose that proteolytic stability be considered at the outset of foldamer design. Design considerations like these have the potential to yield heterogeneous-backbone mimics of natural proteins with predictable proteolytic stability.

The ability of side chain cross-links to stabilize protein structures, particularly α-helices, has long been appreciated in the study of intrinsically disordered proteins. The origin of this stabilizing effect is thought to be the result of backbone preorganization; however, no data bearing on this hypothesis has been reported. Can this hypothesis be corroborated? What thermodynamic variables are significant during the folding events of proteins with sidechain cross-links? We use a rigorous thermodynamic analysis of three common cross-link moieties to

address these questions in Chapter 3. We hope our results will inform the usage of sidechain cross-linking in the stabilization of α-helices.

Finally, the peptidomimetics community would greatly benefit from a set of rational design principles for heterogeneous-backbone foldamers. Our group has been working toward generating such principles through foldamer mimicry of protein GB1 and zinc finger sp1-3. We have successfully recreated these tertiary structures on heterogeneous-backbones; however, our efforts were limited by our synthetic approach. How can we target heterogeneous-backbone foldamers larger than 50 residues? Can our current design principles be applied to protein targets of increased structural and functional complexity? In Chapter 4, we examine these questions through the synthesis, structural characterization, and functional analysis of a heterogeneous-backbone ubiquitin library. Applying our design principles to ubiquitin has not only allowed for their refinement, it has resulted in the largest known heterogeneous-backbone foldamer with significant function.

2.0 PEPTIDE BACKBONE COMPOSITION AND PROTEASE SUSCEPTIBILITY: IMPACT OF MODIFICATION TYPE, POSITION, AND TANDEM SUBSTITUTION

Note: This work was published as H.M. Werner, C.C. Cabalteja, W.S. Horne* "Peptide backbone composition and proteolytic susceptibility: Impact of modification type, position, and tandem substitution." *ChemBioChem* **2016**, *17*, 712-718. It is reproduced from reference [25] with permission from John Wiley and Sons Publishing Company.

The clinical utility of peptides is limited by their rapid degradation by endogenous proteases. Modification of the peptide backbone can generate functional analogues with enhanced proteolytic stability. Existing principles for the design of such oligomers have focused primarily on effective structural mimicry. A more robust strategy would incorporate a rational approach for engineering maximal proteolytic stability with minimal unnatural residue content. Thus, we performed a systematic comparison of the proteolytic resistance imparted by four backbone modifications commonly employed in the design of protease-stable analogues of peptides with complex folding patterns. The degree of protection was quantified as a function of modification type, position, and tandem substitution in the context of a long, unstructured host sequence and a canonical serine protease. These results promise to inform ongoing work to develop biostable mimics of increasingly complex peptides and proteins.

2.1 INTRODUCTION

The involvement of proteins in human pathology is of significant research interest, and pharmaceuticals that target proteins are in high demand. While small molecules can effectively bind to pockets that natively recognize small ligands, disrupting protein-protein interactions (PPIs) involving extended interfaces remains a substantial challenge.[43-44] One solution to this problem is the use of larger peptide and protein based scaffolds, which have shown the unique ability to inhibit certain PPIs where small molecules have failed.[45] The promise of peptide therapeutics is attenuated in part by poor oral bioavailability,[46-48] often necessitating administration by invasive and inconvenient parenteral methods.[46-47, 49-51] A significant contributor to poor peptide bioavailability is rapid degradation by endogenous proteases, which can result in very short *in vivo* lifetimes.[46-48, 50-52]

Alterations to the chemical connectivity of the L-α-peptide backbone can be a useful means to improve proteolytic stability, and targeted backbone modification in short peptides has a rich history in the field of peptidomimetics research.[53] More recent work has explored modified backbones in the context of larger oligomers, seeking to recreate complex functions of diverse bioactive peptides and proteins on protease-resistant scaffolds. Found at one end of the spectrum of such efforts is the introduction of one or two unnatural building blocks in a natural α-peptide to improve efficacy or stability.[54-56] This tactic offers the advantage of employing a biological sequence as the prototype, and even limited unnatural backbone content, strategically placed, can lead to dramatically altered properties. At the other extreme are highly unnatural oligomeric backbones with protein-like folds and functions, often termed "foldamers."[26] Foldamers comprised entirely of a single type of unnatural monomer are inert to proteases and can show

interesting biological activities;[29, 57-60] however, the design of completely unnatural sequences that effectively mimic natural peptides can be challenging.

Recent results suggest significant potential for oligomers in which ~20-30% of the α-residues in a bioactive sequence are replaced by some unnatural analogue.[1, 21] Such backbone heterogeneity takes on another dimension when many classes of unnatural building blocks are incorporated alongside α-residues in a single chain. The use of heterogeneous-backbone foldamers over their homogeneous-backbone counterparts has the advantage of drawing from the wellspring of natural peptides for the design of unnatural analogues. In most examples of heterogeneous-backbone foldamer design, α-residue replacements are made in a manner guided primarily by structural considerations (e.g., maintaining local folding pattern and key interactions for receptor binding). While structural considerations alone can generate adequate proteolytic stability for biological applications, it would be valuable to additionally elucidate and employ an understanding of the relationship between proteolytic resistance and unnatural analogues. A combined approach including this consideration would enable the construction of oligomers where proteolytic protection is considered alongside structural issues at the outset.

Considering this approach, we pursued a systematic examination of the proteolytic protection imparted by four of the most common modifications employed in the design of heterogeneous-backbone foldamers (**Figure 7**): *N*-Me-α-residues, the C_α-methylated α-residue Aib, D-α-residues, and β^3-residues.

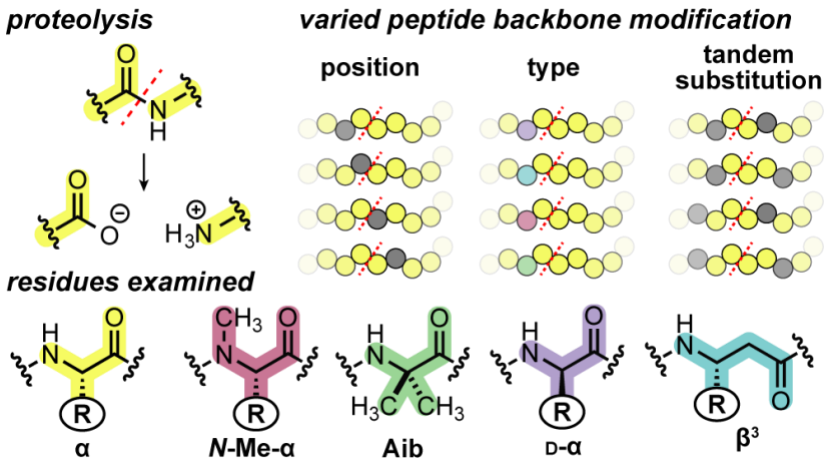

Figure 7. Chemical structures of the protease susceptible amide bond in a peptide, and the natural or unnatural residues examined. Systematic backbone modification patterns varying unnatural residue types, sequence positions, and tandem substitution. This figure is adapted from reference [25] with permission from John Wiley and Sons Publishing Company.

N-methylation in peptides and proteins has long been significant to medicinal and biological chemistry.[61-62] N-methylated analogs of substance P,[63] LH-RH,[64] β-amyloid peptide,[65-67] somatostatin,[68] G protein ligands,[56] endothelin-A/-B antagonists,[69] $\alpha v\beta^3$ receptor inhibitors,[70] and Mcl-1 inhibitors[71] have been generated, all exhibiting proteolytic stability greater than their non-methylated counterparts. While the proteolytic stability of Aib can be traced back to the mid 1930s,[72] its resistance to enzyme degradation did not gain much attention until the 90s. Aib residue substitutions in p53,[73] cell-penetrating peptide model amphipathic peptide (MAP),[74] and antimicrobial peptide lipopeptaibol trichogin GA IV[75] have proven effective in conferring proteolytic stability. D-α-amino acids, the enantiomers of natural L-α-amino acids, came under scrutiny during the mid-20th century, directly resulting from Krebs' discovery of D-amino acid oxidase;[76] however, the incorporation of D-amino acids in an effort to prevent enzymatic degradation was not envisioned until the early 1970s. Since then, the proteolytic stability

afforded by D-residues has been studied in proteins such as luteinizing hormone releasing factor,[77-78] MUC2,[79] magainin,[80] Src kinase (SH3)[25] and amyloid peptide Aβ(1-42).[81-82] β^3-residue inclusion in biologically relevant molecules has surfaced over the last few decades, including work with bradykinin,[83-84] the major histocompatibility complex (MHC),[85-87] BH3-domains,[27, 88] gp41 of HIV,[89] and most notably, an *in vivo* application in Teriparatide.[39] Combinations of these unnatural amino acids in a single peptide are scarce. Work in our group has utilized Aib, D-, N-methylated, and β^3-amino acid substitutions in the protein GB1, successfully achieving protein-like tertiary folding behavior similar to that of wild type.[40] While the half-life of the mutant GB1 was not increased, mass spectrometry analyses showed that large peptide fragments remained intact in the presence of the promiscuous proteinase K.

Although each of these building blocks has been extensively studied in isolation,[62, 74, 79, 90] no prior report has sought to compare their effectiveness at shielding a substrate from proteolytic hydrolysis. Motivated by this gap in knowledge, we sought to address a number of open questions: (1) How do the variables of backbone modification type and position relative to a cleavage site affect protease efficiency? (2) What are the molecular mechanisms by which various modified backbones exert proteolytic protection? (3) How do multiple backbone modifications work in concert to protect a peptide from hydrolysis? Gaining a deeper understanding of these issues promises new design strategies for achieving maximal proteolytic protection in heterogeneous-backbone foldamers with minimal unnatural residue content.

2.2 HOST PEPTIDE SEQUENCE AND EXPERIMENTAL DESIGN

As outlined above, the primary goals at the outset of the present work were to gain new insights into the relationship between peptide backbone composition and proteolytic susceptibility, as well as the molecular origins of observed trends. To this end, we chose to carry out *in vitro* studies with an isolated sequence-specific protease rather than a promiscuous enzyme or whole serum. Chymotrypsin is the type example of the largest subfamily of serine proteases, which account for ~1/3 of total proteases in humans.[91] Its prevalence has led to a robust literature on structure, mechanism, and substrate recognition behavior (spanning well beyond the primary cleavage site).[92-93] While chymotrypsin substrate scope is well studied, the vast majority of that work has focused on short peptides, many of which contain unnatural leaving groups to facilitate spectroscopic analysis. We sought a host sequence for backbone modification that was more analogous to what the enzyme might encounter in the context of a larger bioactive peptide or protein.

2.2.1 Investigation of Potential Host Sequences

Our original concept was of an α-peptide that would: 1) be accessible by solid-phase peptide synthesis (SPPS), 2) contain no appreciable secondary structure, 3) be easily recognized and cleaved by chymotrypsin, and 4) yield digestion products visible by MALDI-TOF MS. We examined an initial set of three peptides in an effort to satisfy these requirements. α-peptides **A**, **B**, and **C** were derived from the C-terminal heptad repeat of gp41-5,[94] the Z domain of Staphylococcal Protein A,[95] and a subunit derived from the coiled coil GCN4-p1[96] (**Figure 8**).

α–peptide	Sequence
	....|....|....|....|....
A	TEETDKEINKY|TKLIHKLIRE
B	TTEILHLPNW|NEEQRNAE
C	KKKLQALKKKNAQLKW|KLQALKKK

Figure 8. Sequences of α-peptides **A-C**. Putative cleavage sites are marked with a vertical red line.

All three peptides were successfully synthesized by SPPS and appeared unfolded by circular dichroism spectroscopy (**Figure 9**).

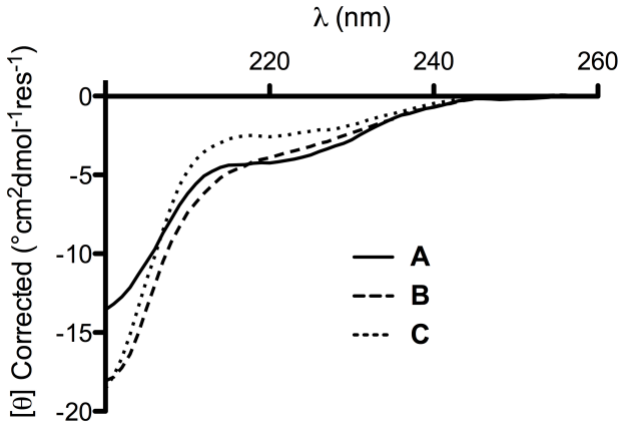

Figure 9. Circular dichroism spectra of peptides **A-C**.

Although no peptide met all original criteria, we gleaned some important perspectives on our experimental design from this set of experiments. There were immediate complications with two of the three peptides. The digestion of peptide **B** was inefficient, as it required a working enzyme concentration nearly ten times higher than previous experiments, and we abandoned it in an effort to utilize enzyme frugally. The proteolysis of peptide **C** halted at roughly 50% peptide remaining. By HPLC, this looked like the result of secondary proteolysis, in which the digested peptide fragments have a higher affinity for chymotrypsin than did the parent peptide. While

peptide **A** initially looked promising, other cleavage sites were revealed upon initial efforts of unnatural amino acid incorporation.

After discovering that chymotrypsin was hydrolyzing peptide bonds C-terminal to unexpected residues—namely, leucine, glutamic acid, and threonine—in all three of our initial peptides, we decided that a slight modification of our design was needed. Quantitative comparisons of protection would only be valid if we were monitoring a single cleavage site. If another peptide bond were easily cleaved once the initial site was protected, then the calculated half-life would be an underestimation of the true protection being afforded by the unnatural residue. Thus, we rigidified the third criterion for the host peptide to 3) be easily recognized and cleaved by chymotrypsin at a single cleavage site.

2.2.2 Final Host Peptide Design and Backbone Modifications

We loosely based the host peptide on a recently reported sequence motif selected by phage display for high inherent resistance to intestinal proteases, including chymotrypsin.[97] We fused two of these motifs in a single chain and introduced a defined chymotrypsin-specific cleavage site (AY↓K)[92] at the center to generate 21-residue α-peptide **2.1** (**Figure 10**).

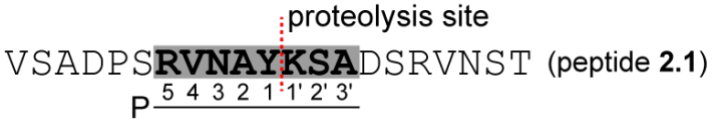

Figure 10. Prototype α-peptide **2.1** with putative site of proteolysis (dashed line) and corresponding Schechter-Berger nomenclature. Positions of unnatural residue substitution are highlighted in gray. This figure is adapted from reference [25] with permission from John Wiley and Sons Publishing Company.

Peptide residues in gray are labeled according to Schechter-Berger nomenclature as "Pn"; n increases with distance away from the cleavage site, unprimed toward the N-terminus and primed toward the C-terminus. Peptide **2.1** is processed cleanly by chymotrypsin, resulting in two products observed by MALDI-TOF-MS from hydrolysis of the amide between residues Tyr11 and Lys12. Monitoring the reaction time course by HPLC reveals a single-phase exponential decay with a half-life of 8 min for 200 μM peptide in the presence of 0.25 μM chymotrypsin (**Figure 11**, left). As expected, we did not observe significant cleavage of the Y11A mutant over several days (**Figure 11**, right).

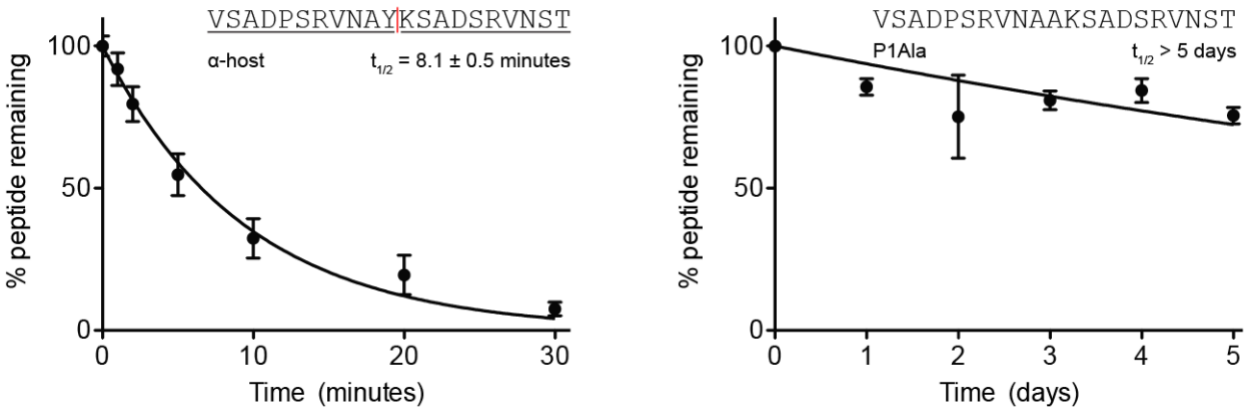

Figure 11. Sequences, full progress degradation curves, and calculated half-lives of peptide **2.1** and Y11A. Observed proteolysis products (horizontal black lines) and corresponding cleavage sites (vertical red lines) for each peptide are indicated in its sequence. Data points represent at least two replicate proteolysis experiments, while error bars represent the SEM for each timepoint. Full digestion curves are modeled by a one-phase decay fit: $Y = (Y_0)\, e^{-kx}$ (solid curve).

To explore the effect of backbone modification on proteolytic stability, we synthesized a library comprising 32 analogues of peptide **2.1** in which individual α-residues in the prototype were replaced by one of four unnatural analogues: *N*-Me-α-residues, the C_α-Me-α-residue Aib,

D-α-residues, or β^3-residues (**Figure 7**). These four classes of backbone modification were each scanned across eight positions surrounding the cleavage site (Arg7 to Ala14, P5 to P3' in the Schechter and Berger nomenclature).[98] In cases where the α-residue was replaced by *N*-Me-α-, D-α-, or β^3-residues, the side chain from the prototype sequence was retained after backbone modification. In contrast, α→Aib substitution involves the loss of a side chain functional group. We therefore synthesized a set of alanine mutants of the parent sequence to isolate the effects of Cα-methylation from any potential change in proteolytic susceptibility resulting from the removal of a side chain. As expected, with the exception of Y11A, these alanine mutants were digested by chymotrypsin at rates comparable to that of peptide **2.1** (**Figure 12**).

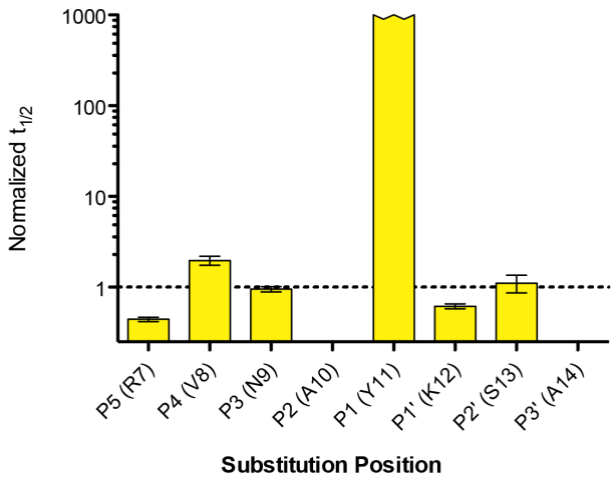

Figure 12. Normalized peptide half-lives for Xxx→Ala mutants of peptide **2.**1 in the presence of α-chymotrypsin. Half-lives are normalized to the half-life of peptide **2.1** (dotted line). Error bars represent the error in the fit of the full progress curve.

Peptide **2.1** is highly resistant to cleavage by the enzyme outside the engineered hydrolysis site; the Y11A mutant showed no apparent digestion at the engineered cleavage site up to 5 days under the same conditions (**Figure 11**, right). α-Peptide **2.1** and its Aib- and D-residue-modified counterparts lack any measurable secondary structure by circular dichroism (CD) spectroscopy (**Figure 13**).

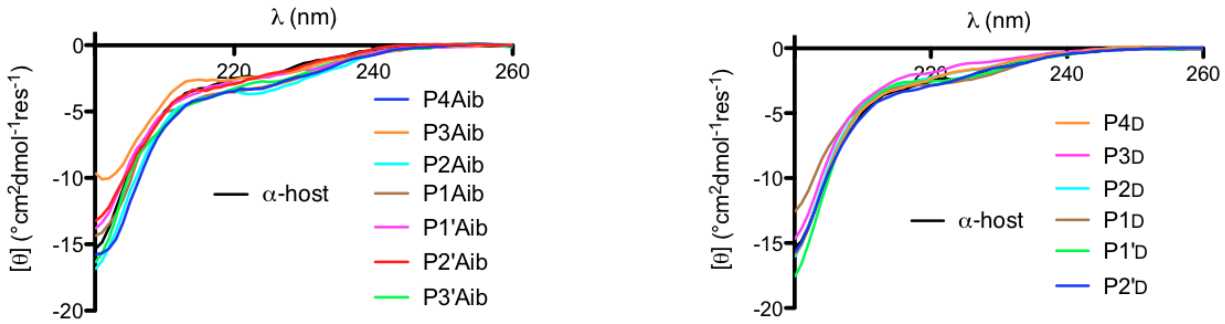

Figure 13. Circular dichroism (CD) scan spectra of α-host peptide compared with Aib (left) and D-residue (right) substituted peptides. This figure is adapted from reference [25] with permission from John Wiley and Sons Publishing Company.

This is an important feature as it enables the attribution of protection afforded by various modifications to changes in backbone chemical connectivity rather than changes in the folded state.

Each of the peptides described above was synthesized by Fmoc solid phase methods and purified by preparative reverse phase HPLC; the identity and purity of the final products were assessed by MALDI-TOF-MS and analytical HPLC, respectively. After synthesis and purification, each peptide was subjected to proteolysis under identical experimental conditions (50 nM chymotrypsin, 160 μM peptide, 50 mM TBS buffer pH 7.5) and the reactions were

monitored over time by analytical HPLC and MALDI-TOF-MS. Some peptides exhibited digestion profiles that plateaued at a non-zero value (**Figure 14**).

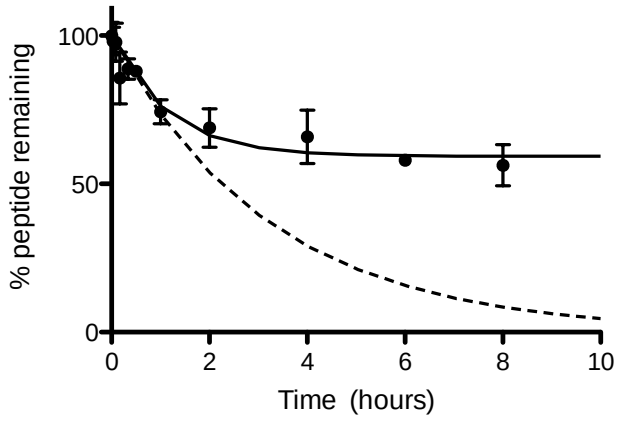

Figure 14. Representative example of halted proteolysis. In these cases, half-lives were calculated from the extrapolated full progress curve (dotted line).

This has previously been observed during proteolysis of backbone-modified peptides.[56, 99-101] We attribute these observations to enzyme inactivation,[102] which we investigated further in unpublished work. While enzyme inactivation is an indirect form of proteolytic protection, the focus of the present study is on the inherent susceptibility of a particular backbone. Thus, we treated these data by extrapolating a full progress digestion curve from the time points collected before product inhibition. Assuming that under different circumstances the initial rate of proteolysis could be sustained, this treatment of the data provides the most conservative estimate of the degree of protection that could be afforded by a particular backbone modification.

The resulting dataset for single residue substitutions is summarized as a set of normalized half-life values for degradation as a function of backbone modification type and position (**Figure 15**).

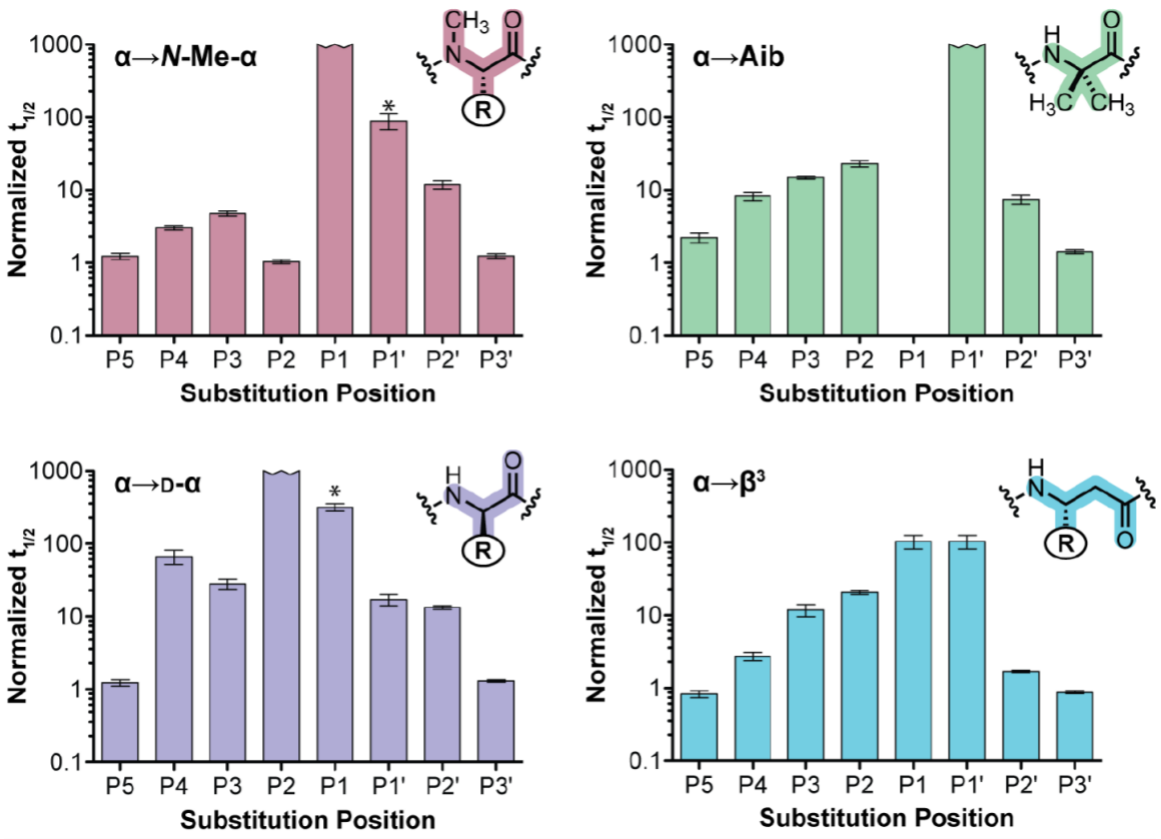

Figure 15. Normalized peptide half-lives as a function of substitution type and position. α→Aib half-lives are normalized to the corresponding Ala mutants of peptide **2.1**. All others are normalized to the half-life of peptide **2.1**. Error bars represent the error in the fit of the full progress curve. An asterisk over a bar indicates that proteolysis was observed outside of the putative site. This figure is adapted from reference [25] with permission from John Wiley and Sons Publishing Company.

2.3 DISCUSSION OF BACKBONE MODIFICATION IMPACT

2.3.1 Single Substitution by Type and Position

Predictably, modification of the backbone at the primary specificity site P1 (i.e., Tyr11) resulted in significant protection (100-1000 fold increased half-life). The more intriguing aspect of the data were trends in the moderate changes in proteolytic susceptibility observed upon substitution near, but not at, the chymotrypsin cleavage site. Here both the magnitude and profile of protection differed for each backbone modification type. A summary of the key observations for each class of unnatural monomer is provided in the following section, along with interpretation of some results in terms of potential molecular mechanisms of protection.

In general, *N*-Me-α-residue incorporation provided the smallest degree of proteolytic protection among the unnatural monomer types examined. Only three positions clustered directly around the cleavage site (P1-P2′) gave rise to >10-fold improvement in stability relative to the prototype α-peptide. This result is not surprising, given that *N*-Me-α-residues are also most similar among the modified backbones examined to natural α-residues in folding propensity and structural properties. We propose that the positional dependence of *N*-Me-α-residue incorporation can be interpreted based on putative enzyme–substrate hydrogen bonds. Like most proteases, chymotrypsin recognizes substrates in an extended conformation, resulting in hydrogen bonds to alternating residues at sites P3, P1, and P2′ (**Figure 16**).[92]

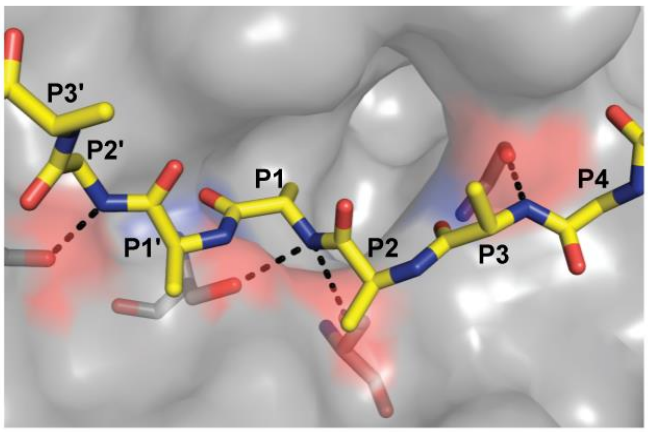

Figure 16. Proposed mode of protection for *N*-Me-residues: chymotrypsin (surface) complexed with a representative non-covalent inhibitor (PDB: 1GL0). Amide protons of residues P3, P1, and P2' are hydrogen bonded (hashed black lines) to chymotrypsin. This figure is adapted from reference [25] with permission from John Wiley and Sons Publishing Company.

Since amide methylation replaces a hydrogen-bond donor with a potential steric clash, it would be expected to provide protection only when incorporated on the face of substrate that engages the enzyme binding pocket. This hypothesis is supported by the observation that α→*N*-Me-α replacement at P1 or P3 results in strong to moderate proteolytic protection, while the same modification at P2 leads to no change in susceptibility relative to the parent α-peptide (**Figure 15**). The proteolytic resistance imparted by P1′ *N*-methylation is likely the result of a steric clash during formation of the acylenzyme intermediate.[103]

C_α-methylation through incorporation of Aib provided protection over a wider range from the cleavage site relative to α→*N*-Me-α substitution; >10-fold protection was observed from P3-P2′ and near 10-fold protection at P4 and P2′. Interestingly, >2-fold protection was observed as far as from the cleavage site as position P5, where all other backbone modifications examined had no effect. The complete protection observed upon substitution at P1 is unsurprising, given the loss of the key Tyr side chain. In order to focus analysis of data from the other peptides in the

Aib series on the contribution of backbone methylation, we normalized the half-life of each to the corresponding Ala mutant of prototype α-peptide **2.1**. The strong protection conferred by C_α-methylation at P1′ likely results from a steric clash around the scissile amide bond; however, the behavior of the remaining Aib mutants is more readily interpreted as a result of altered conformational preferences.

Compared to L-α-residues, Aib has a more constrained range of accessible backbone conformations, favoring α-helical secondary structure.[104] An induced folded structure in the substrate would certainly alter proteolytic processing; however, analyses of the Aib series by CD indicated no measurable change to the random coil signature observed for the prototype peptide (**Figure 13**). We reasoned that Aib, although not inducing a particular folded state, may be altering the denatured ensemble to disfavor chymotrypsin recognition of the substrate. Support for this hypothesis can be found in the analysis of 11 published crystal structures of the enzyme in complex with inhibitors that mimic natural substrate recognition.[105-110] A Ramachandran plot comparing the average backbone conformation observed at substrate positions P4-P2′ to a previously calculated profile for Aib shows that the conformation necessary for effective recognition by the enzyme falls in a disallowed region for the unnatural residue (**Figure 17**).[111-112]

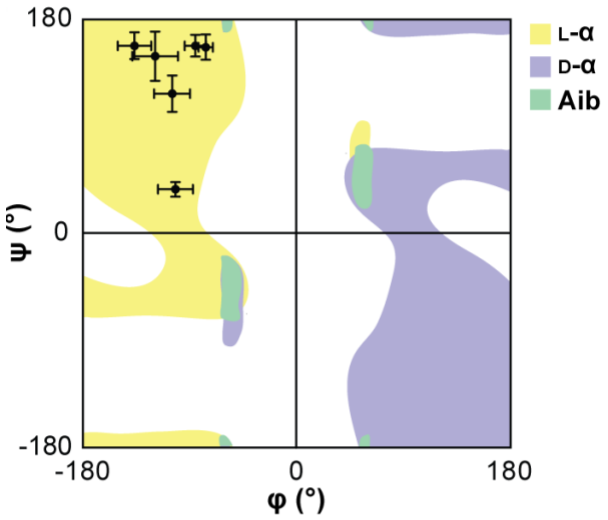

Figure 17. Proposed mode of protection for D-/Aib residues: Overlaid Ramachandran plots of L-α-residues, D-α-residues, and Aib. The average dihedral angles observed at each inhibitor residue (P4-P2') are represented by a black point. This figure is adapted from reference [25] with permission from John Wiley and Sons Publishing Company.

Among the backbone modification types examined, alteration of C_α stereochemistry through single incorporation of D-α-residues resulted in the greatest degree of protection over the widest range. >10-fold increases in half-life were observed after incorporation of a D-residue at any of six positions surrounding the cleavage site (P4-P2′). Known features of chymotrypsin stereospecificity explain some aspects of the data;[113-114] however, the dramatic protection resulting from D-residue incorporation at remote sites was surprising. Literature precedent suggests the S3 site of chymotrypsin is not particularly stereospecific,[92, 115] but these conclusions were based on analysis of short 4-5 residue substrates. Our results show that, in a more native-like extended oligomer, D-residues impart strong protection as far from the cleavage site as P4. As with C_α-methylation, the impact of D-residue incorporation on proteolytic susceptibility can be most readily interpreted in terms of an altered ensemble constituting the unfolded state. As

with Aib, the typical substrate conformation at residues P4-P2′ falls in the disallowed region of the D-residue Ramachandran plot (**Figure 17**).

Peptides containing α→β^3 substitutions showed a moderate degree of protection from degradation by chymotrypsin. Substitution adjacent to the site of hydrolysis (P1 or P1′) resulted in only a 100-fold improvement in proteolytic stability (compared to >1000-fold for Aib), and the range of >10-fold protection only extended over four residues (P3-P1′). Although the extra methylene unit relative to an α-residue leads to additional conformational flexibility, β^3-residues have been shown capable of recreating protein-like helix, sheet, loop, and turn secondary structures when incorporated into α/β-peptides.[21] Thus, the majority of proteolytic protection afforded by α→β^3 residue substitution is not likely the result of the inability of the modified peptide to adopt a native-like conformation. The extra backbone methylene unit may interfere sterically by changing the spacing of side chains distributed along the substrate. Alternatively, β-residue incorporation may disrupt chymotrypsin-substrate interactions by inverting the display of side chains along the extended strand.[116]

2.3.2 Impact of Tandem Backbone Modifications

The above data provided insights into the role of backbone modification type and position in determining susceptibility of a given amide bond to hydrolysis by chymotrypsin; however, open questions remained. In the design of heterogeneous-backbone foldamers that mimic larger peptides and proteins, there are many potential cleavage sites, the identities of which are often not known *a priori*. Efforts to generate stable analogues are characterized by two opposing trends. The proteolytic stability of a backbone is generally positively associated with its unnatural content; completely unnatural backbones (e.g., β-peptides, D-α-peptides) are inert, and

the stability of heterogeneous backbones will improve with increasing unnatural content. Activity and modification are often negatively associated; the more a backbone is modified, the less likely it is to maintain a native-like folding pattern and function. When the entire peptide backbone is considered protease susceptible, evenly spaced modification along a sequence is the most efficient means to achieve maximal biostability with minimal chemical alteration. Thus, we sought to determine the optimal density of modification and how it varies with the type of unnatural monomer employed.

In an effort to address this issue, we synthesized and characterized a series of additional peptides bearing two substitutions flanking the cleavage site. Comparing their degradation rates to the corresponding singly substituted analogues provided insights into synergistic effects of backbone modification on proteolytic protection. Due to the prevalence of bioactive α/β-peptides in the recent heterogeneous-backbone foldamer literature,[1] we focused attention initially on tandem β^3-residue substitutions. Five peptides were prepared and characterized, each bearing two $\alpha \rightarrow \beta^3$ substitutions separated by two to six α-residues surrounding the cleavage site (**Figure 18**).

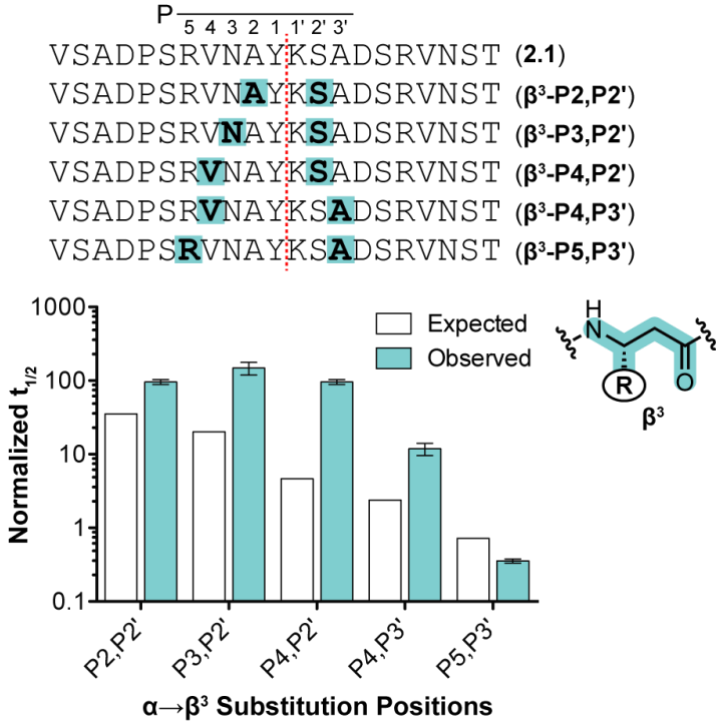

Figure 18. Prototype α-peptide and tandem β^3-residue substituted sequences with putative site of proteolysis (red hashed line) and corresponding residue nomenclature. Positions of β^3-residue substitution are highlighted cyan. Normalized peptide half-lives as a function of tandem β^3-residue substitution position. Half-lives were normalized to the half-life of peptide **2.1**. Error bars represent the error in the fit of the full progress curve. This figure is adapted from reference [25] with permission from John Wiley and Sons Publishing Company.

We expected the half-life of a tandemly-substituted peptide to be predictable from our single-substitution data. Briefly, we assumed that the proteolysis of a peptide with two substitutions would equal the sum of the activation energies from the constituent single-substitution proteolysis reactions. Because the half-life ($t_{1/2}$) of proteolysis is logarithmically related to activation energy, we calculated the expected half-lives of tandem substitutions by adding the natural logs of the corresponding single substitution half-lives.

Surprisingly, multiple α→β^3 substitutions appeared to be synergistic; their observed half-life was greater than expected. Tandem mutants bearing β-residues separated by two, three, or four α-residues (βα↓αβ, βαα↓αβ, βααα↓αβ) showed a degree of protection that was comparable to β^3-residue substitution directly at the cleavage site. This observation suggests there may be a maximum achievable stability conferred by a particular type backbone modification. Increasing the spacing between substitutions α-residues (βααα↓ααβ) resulted in a half-life that was lower, albeit still greater than predicted from the single substitutions. Interestingly, incorporation of two β^3-residues separated by six α-residues (βαααα↓ααβ) led to a tandem mutant that was significantly less stable than any of the single β^3 substitutions and even more susceptible to chymotrypsin than the host α-peptide. This result demonstrates that combined backbone modifications can have a negative synergistic effect, and the correlation between unnatural residue density and proteolytic stability is not necessarily direct.

The trends observed in the tandem β^3-residue mutants prompted us to investigate potential synergistic effects of incorporating the other monomer types. Thus, N-Me-α, Aib, and D-α-residues were incorporated in combination in a fixed pattern (Xααα↓ααX) where β^3-residue incorporation led to only a modest improvement in proteolytic stability (**Figure 19**).

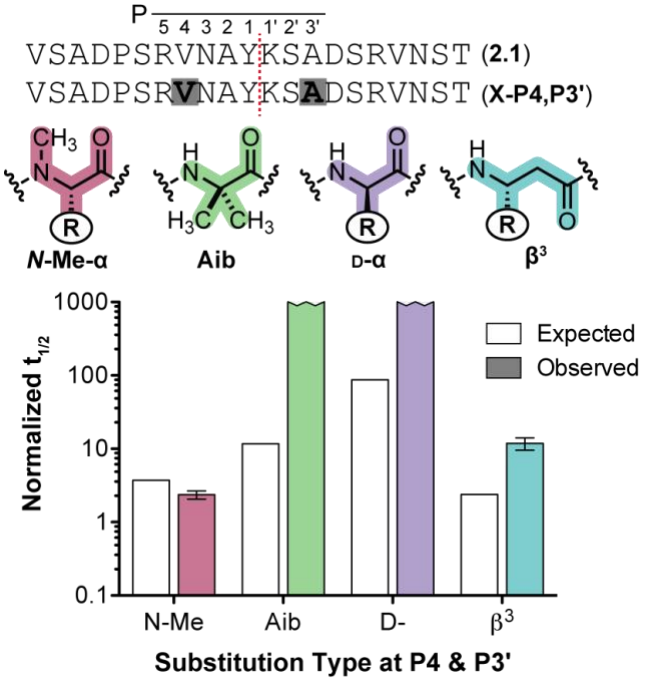

Figure 19. Prototype α-peptide and various tandem substituted sequences with putative site of proteolysis (red hashed line) and corresponding residue nomenclature. Positions of unnatural substitution are highlighted gray. Normalized peptide half-lives are shown as a function of unnatural residue substitution type at sequence positions P4 and P3'. The half-life of the tandem Aib substituted peptide is normalized to the corresponding Ala mutants. All others are normalized to the half-life of peptide **2.1**. Error bars represent the error in the fit of the full progress curve. This figure is adapted from reference [25] with permission from John Wiley and Sons Publishing Company.

Backbone modifications that alter local folding propensity (D-α, Cα-Me-α) had strong positive synergistic effects on proteolytic stability when combined in a single chain. In contrast, combining N-Me-α residues led to a degree of protection no different than predicted from the corresponding single substitutions. This further supports our hypothesis that N-Me-α-residues confer proteolytic resistance by disrupting specific enzyme–substrate interactions rather than by affecting local folding.

2.4 SUMMARY AND FUTURE DIRECTIONS

In summary, we compared the proteolytic protection afforded by four building blocks commonly used in heterogeneous-backbone foldamers. Systematic examination of the variables of backbone modification type and position in the context of a long unstructured host α-peptide and the canonical serine protease chymotrypsin reveal some clear trends. In terms of isolated α-residue replacement, the degree of protection imparted as a function of modification type follows as D-α > C_α-Me-α > β^3 > *N*-Me-α. Differences are most apparent at sites 2-4 residues removed from the scissile amide bond. The proposed modes by which the unnatural residues exert protection fall under two broad categories: (1) interference with specific enzyme-substrate contacts (local effects), and (2) alteration of the denatured ensemble of the unstructured host peptide (global effects).

D-α and C_α-Me-α residues likely impart proteolytic stability by shifting the denatured ensemble away from conformers effectively recognized by the enzyme. As a result, the protection they exert from proteolysis is large in magnitude, wide-ranging, and synergistic when substitutions are combined in a single chain. *N*-Me-α-residues appear to influence proteolytic

susceptibility primarily through disruption of discrete enzyme–substrate contacts, making their effects modest in magnitude, short-range, and simply additive when combined. Among the residue types examined, the behavior of β^3-residues was most complex. The protection afforded was modest in magnitude yet somewhat wide-ranging, and the molecular origins are difficult to unambiguously define. The effects of combined backbone $\alpha \rightarrow \beta^3$ replacements can be synergistic; however, the density of β^3-residues is not directly correlated to proteolytic resistance.

Although the scope of the present findings is limited by involving only a single protease, they generate a number of clear hypotheses for future work on the development of agents that recreate natural peptides and protein function on biostable scaffolds. Considerations for effective structural mimicry are now well defined for many systems, and we can begin to develop design principles for achieving maximal proteolytic stability at minimal unnatural backbone content. For example, both Aib and β^3-residues can be readily incorporated into peptide and protein helices.[117] β^3-Residues have the functional advantage of retaining native side chains, but our data suggest Aib may impart a greater degree of proteolytic protection at lower substitution density. Taken together, these observations suggest that chiral Cα-methylated amino acids bearing protein-derived side chains may be superior to both Aib and β^3-residues as building blocks in heterogeneous-backbone foldamers. As another example of a new design insight, the folding propensity of D-α-residues differs greatly from their L-α counterparts, but they are quite effective turn inducers.[118] Given the far-ranging proteolytic protection provided by even limited backbone stereochemical alteration, our data suggest D-residues as an ideal backbone modification in situations where they would be structurally accommodated.

It is our hope that these and other aspects of the present study will inform ongoing work on the design of heterogeneous-backbone foldamers and prompt further investigation into the

mechanisms by which unnatural amino acids impart proteolytic stability. Areas of particular interest include how backbone alteration influences the structure of the denatured ensemble[119] as well as the detailed kinetics (i.e., k_{cat}, K_m) for the enzymatic degradation of modified substrates. Finally, while unexpected, the enzyme inactivation observed during this work highlights the potential relevance of these results to informing the design of protease inhibitors.

2.5 EXPERIMENTAL

2.5.1 Materials

2-(6-Chloro-1H-benzotriazole-1-yl)-1,1,3,3-tetramethylaminium hexafluorophosphate (HCTU), Fmoc-D-Val-OH, Fmoc-D-Lys(Boc)-OH, Fmoc-D-Arg(Pbf)-OH, Fmoc-β^3-HAsn(Trt)-OH, Fmoc-β^3-HArg(Pbf)-OH, and Fmoc-N-Me-Asn(Trt)-OH were purchased from AAPPTec. Fmoc-D-Asn(Trt)-OH, Fmoc-D-Ala-OH, Fmoc-D-Tyr(tBu)-OH, Fmoc-D-Ser(tBu)-OH, Fmoc-β^3-HVal-OH, Fmoc-β^3-HAla-OH, Fmoc-β^3-HTyr(tBu)-OH, Fmoc-β^3-HLys(Boc)-OH, Fmoc-β^3-HSer(tBu)-OH, Fmoc-N-Me-Val-OH, Fmoc-N-Me-Ala-OH, Fmoc-N-Me-Tyr(tBu)-OH, and Fmoc-N-Me-Ser(tBu)-OH were purchased from Chem-Impex International. Fmoc-N-Me-Arg(Pbf)-OH was purchased from ChemPep. NovaPEG Rink Amide resin and Fmoc-protected α-amino acids were purchased from Novabiochem. Fmoc-α-Me-Ala-OH, Fmoc-N-Me-Lys(Boc)-OH, N,N-diisopropylethylamine (DIEA), and bovine α-chymotrypsin were purchased from Sigma–Aldrich. All other reagents were purchased from Acros Organics, Fisher Scientific, JT Baker, and Sigma–Aldrich.

2.5.2 Peptide Synthesis and Characterization

Peptides were synthesized using microwave-assisted (CEM MARS) Fmoc-solid-phase synthesis techniques. All peptides were prepared as the C-terminal carboxamide using NovaPEG Rink Amide resin (0.025 mmol scale). Fmoc protected amino acids (0.1 mmol) were coupled to the growing peptide chain with HCTU (0.1 mmol) and DIEA (0.15 mmol) in NMP (1 mL) for 2 minutes after a 1.5-minute ramp to 90 °C. Double couplings were performed at hindered amine nucleophiles (i.e. proline or *N*-methylated residues). Fmoc groups were removed with 4-methylpiperidine in DMF (20% v/v) for 1 minute after a 1.5-minute ramp up to 90 °C. The resin was washed three times with DMF after each reaction. After the final deprotection, the resin was rinsed three times each with DMF, dichloromethane, and methanol, and then dried. Peptides were cleaved from resin using a solution of TFA/H_2O/TIS (95%/2.5%/2.5%) for 3 hours. After precipitation in cold diethyl ether, the solutions were centrifuged, and the pelleted solids were dissolved in mixtures of 0.1% TFA in H_2O and 0.1% TFA in acetonitrile. Peptides were purified by preparative RP-HPLC on a Phenomenex Luna C18 column using gradients between 0.1% TFA in H_2O and 0.1% TFA in acetonitrile. Peptide identity and purity were determined by mass spectrometry (Voyager DE Pro MALDI-TOF, **Table 2**) and analytical RP-HPLC (**Figures 20-24**), respectively.

Table 2. MALDI-TOF data for all peptides.

Peptide	$[M+H]^+$ *m/z*	
	Expected	Observed
α-host (**2.1**)	2223.1	2223.4
P5Ala	2138.0	2137.6
P4Ala	2195.1	2194.8
P3Ala	2180.1	2179.9
P1Ala	2131.1	2131.4
P1'Ala	2166.1	2165.8
P2'Ala	2207.1	2205.9
P5D	2223.1	2221.2
P4D	2223.1	2222.5
P3D	2223.1	2222.3
P2D	2223.1	2223.1
P1D	2223.1	2221.9
P1'D	2223.1	2223.5
P2'D	2223.1	2223.1
P3'D	2223.1	2221.5
P5*N*-Me	2237.1	2236.8
P4*N*-Me	2237.1	2236.3
P3*N*-Me	2237.1	2236.7
P2*N*-Me	2237.1	2237.5
P1*N*-Me	2237.1	2236.6
P1'*N*-Me	2237.1	2237.4
P2'*N*-Me	2237.1	2236.4
P3'*N*-Me	2237.1	2237.0
P5β^3	2237.1	2236.8
P4β^3	2237.1	2236.9
P3β^3	2237.1	2236.8
P2β^3	2237.1	2236.1
P1β^3	2237.1	2237.1
P1'β^3	2237.1	2237.4
P2'β^3	2237.1	2237.0
P3'β^3	2237.1	2236.0
P5Aib	2152.1	2151.8
P4Aib	2209.1	2208.6
P3Aib	2194.1	2193.9
P2Aib	2237.1	2237.3
P1Aib	2145.1	2143.6
P1'Aib	2180.1	2179.6
P2'Aib	2221.1	2220.8
P3'Aib	2237.1	2236.6
P2-P2'β^3	2251.1	2249.4
P3-P2'β^3	2251.1	2250.1
P4-P2'β^3	2251.1	2250.9
P4-P3'β^3	2251.1	2250.0
P5-P3'β^3	2251.1	2250.6
P4-P3'D	2223.1	2223.1
P4-P3'*N*-Me	2251.1	2250.9
P4-P3'Aib	2223.1	2222.7

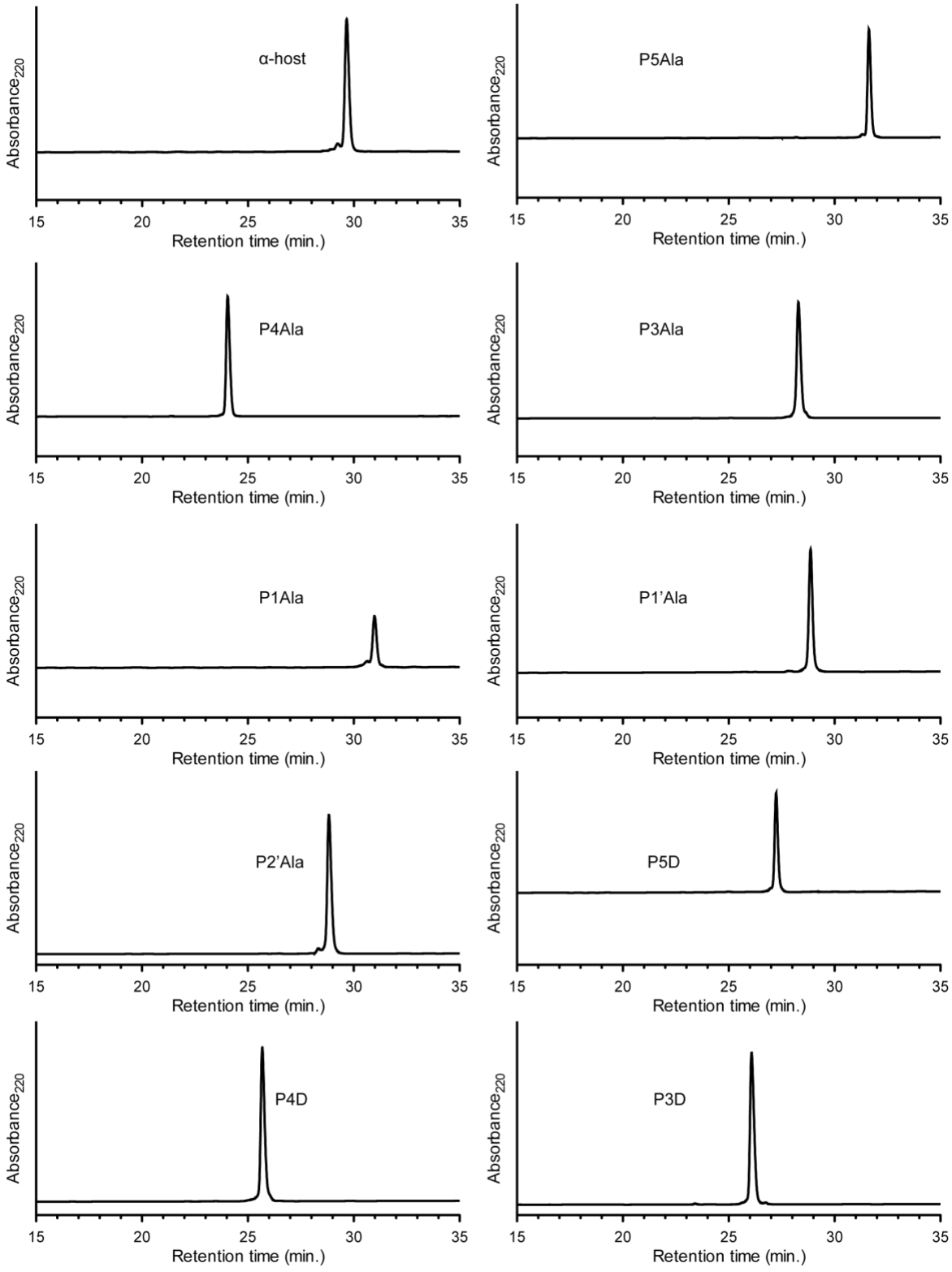

Figure 20. HPLC chromatograms of purified peptides.

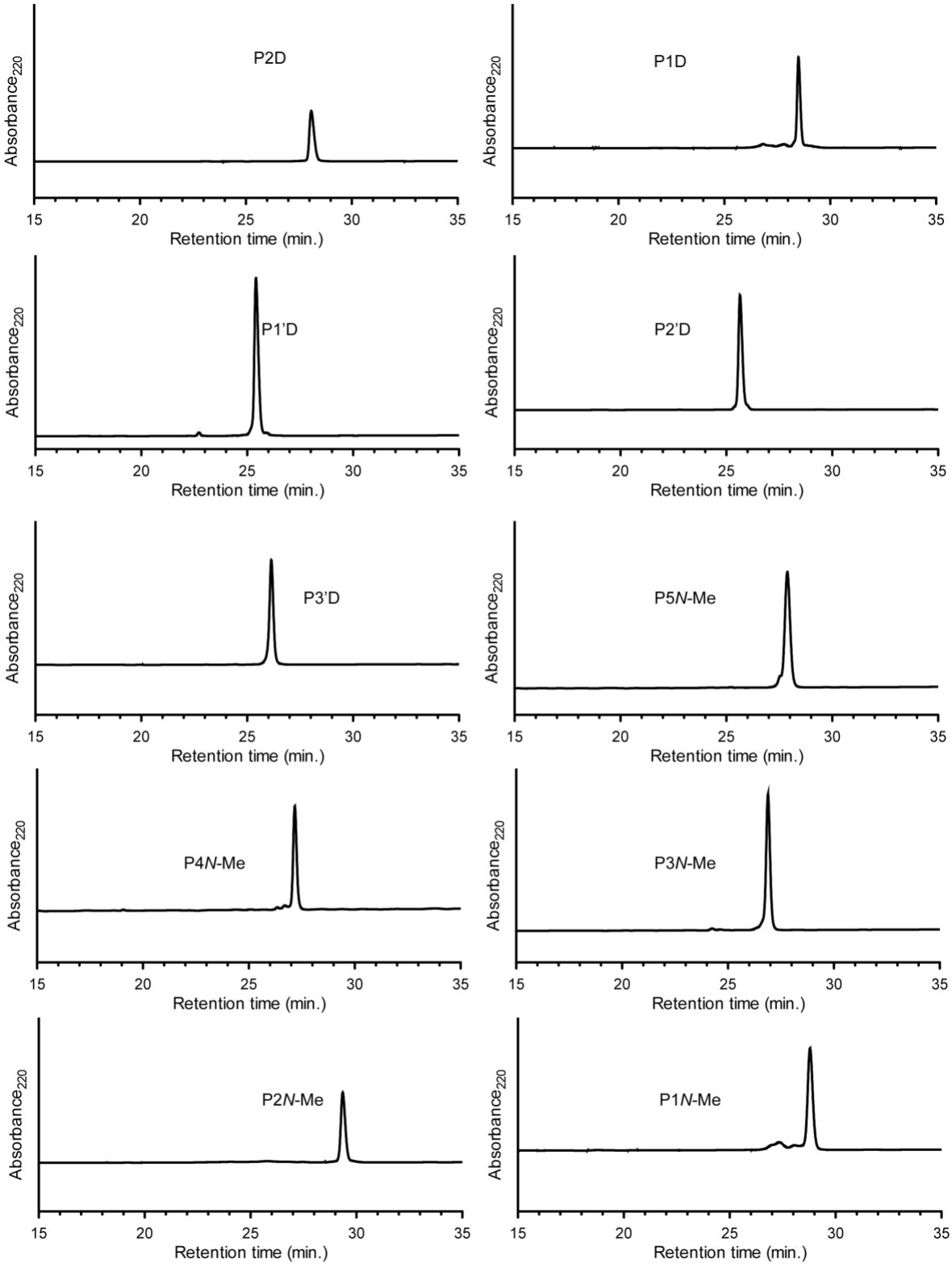

Figure 21. HPLC chromatograms of purified peptides.

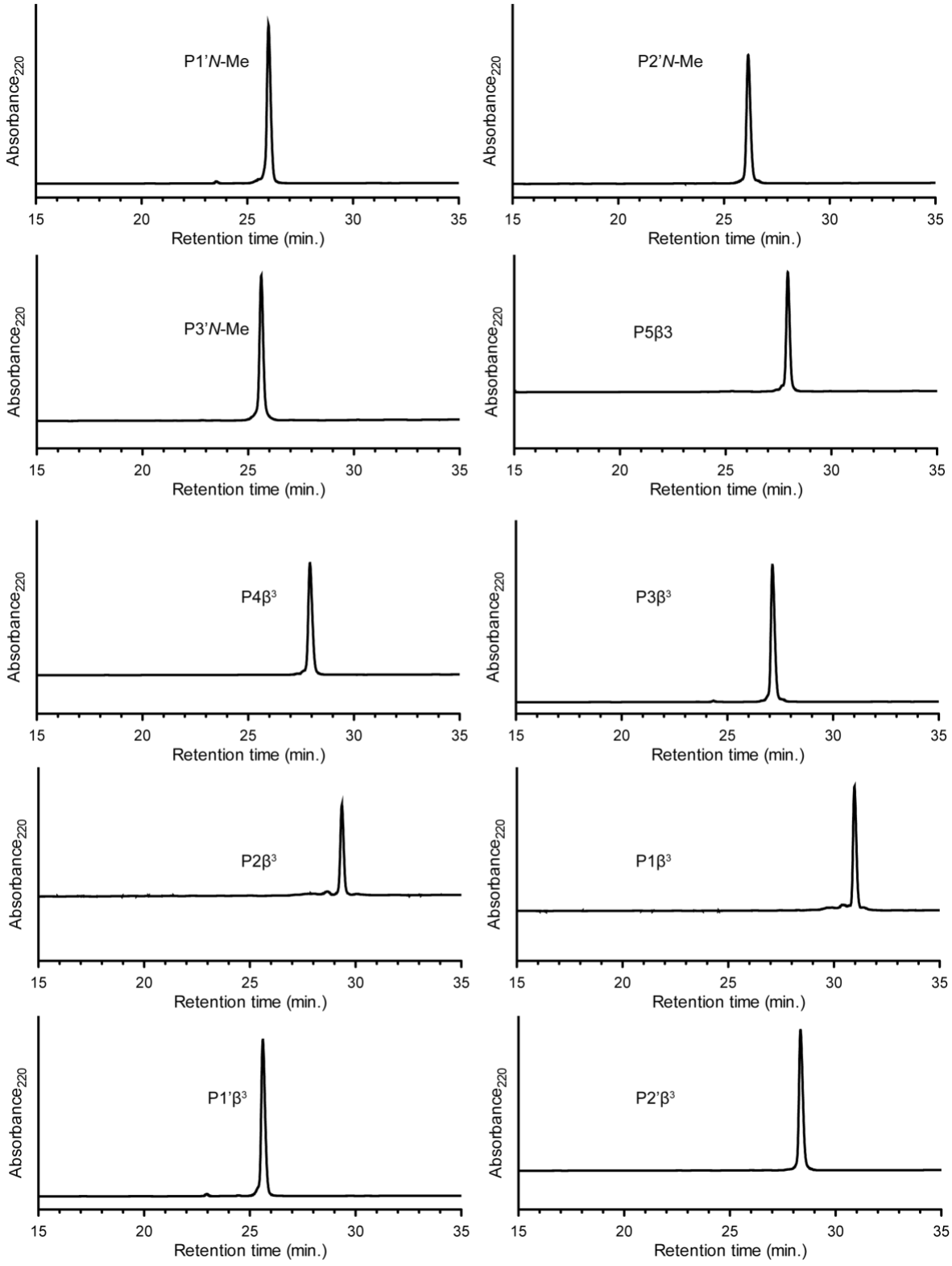

Figure 22. HPLC chromatograms of purified peptides.

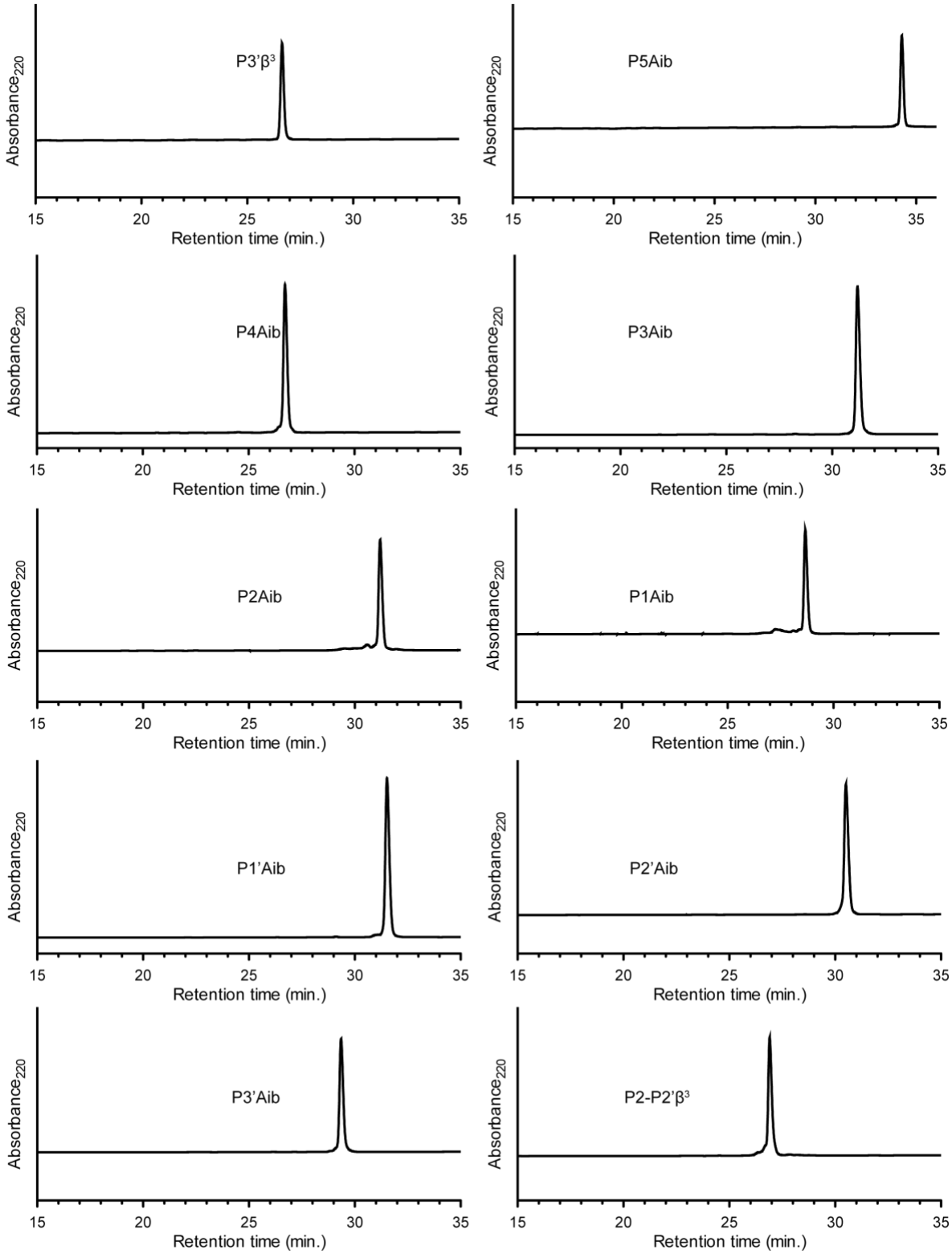

Figure 23. HPLC chromatograms of purified peptides.

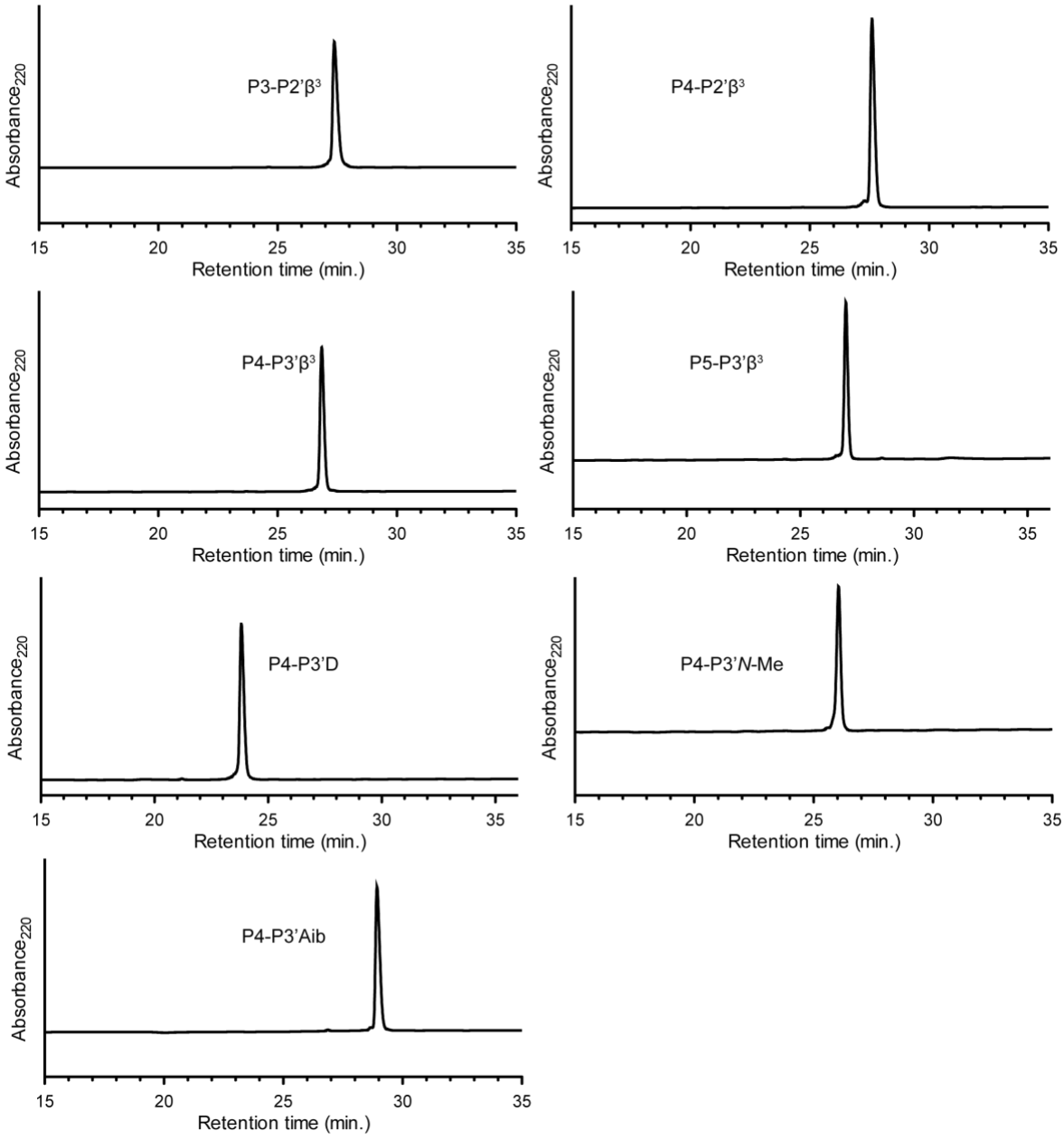

Figure 24. HPLC chromatograms of purified peptides.

Peptide stock concentrations were quantified by UV spectroscopy (ε_{280} = 1280 M^{-1} cm^{-1}). Stock concentrations for peptides lacking a chromophoric residue (Y11A, Y11Aib) were estimated by weight to volume.

2.5.3 Circular Dichroism Spectroscopy

Solutions of 40 μM peptide in 20 mM sodium phosphate buffer (pH 6.9) were subjected to CD scans using an Olis DSM17 circular dichroism spectrophotometer. Scans were performed at 20 °C from λ 200 – 260 nm with 1 nm step size, 2 nm bandwidth, and 5 s integration time at each wavelength. All measurements were baseline corrected against a buffer blank measured in the same cell. Scans were smoothed by the Savitzky-Golay method[120] using GraphPad Prism.

2.5.4 Proteolysis Reactions

The concentrations of bovine α-chymotrypsin stock solutions were quantified by UV spectroscopy (ε_{280} = 51,240 M^{-1} cm^{-1}). Aliquots of 0.25 μM chymotrypsin in TBS (50 mM Tris, 150 mM NaCl, pH 7.5) were made and frozen. Each proteolysis reaction was initiated by the addition of chymotrypsin from a freshly thawed aliquot to a 200 μM solution of peptide in water, giving a final sample composition of 160 μM peptide, 50 nM chymotrypsin, 50 mM Tris, 150 mM NaCl, pH 7.5. For each time point, a 50 μL portion of the reaction was removed and quenched with 0.5% (v/v) trifluoroacetic acid (40 μL). Quenched samples were analyzed by analytical RP-HPLC (90 μL injection), and the undigested peptide remaining was quantified by integration of the corresponding chromatogram peak. MALDI-MS was also performed at each time point to identify the sites of enzymatic hydrolysis. A plot of percent peptide remaining vs.

time was generated, and the data was fit to a one-phase exponential decay using GraphPad Prism to generate a calculated half-life (**Figures 25-32**).

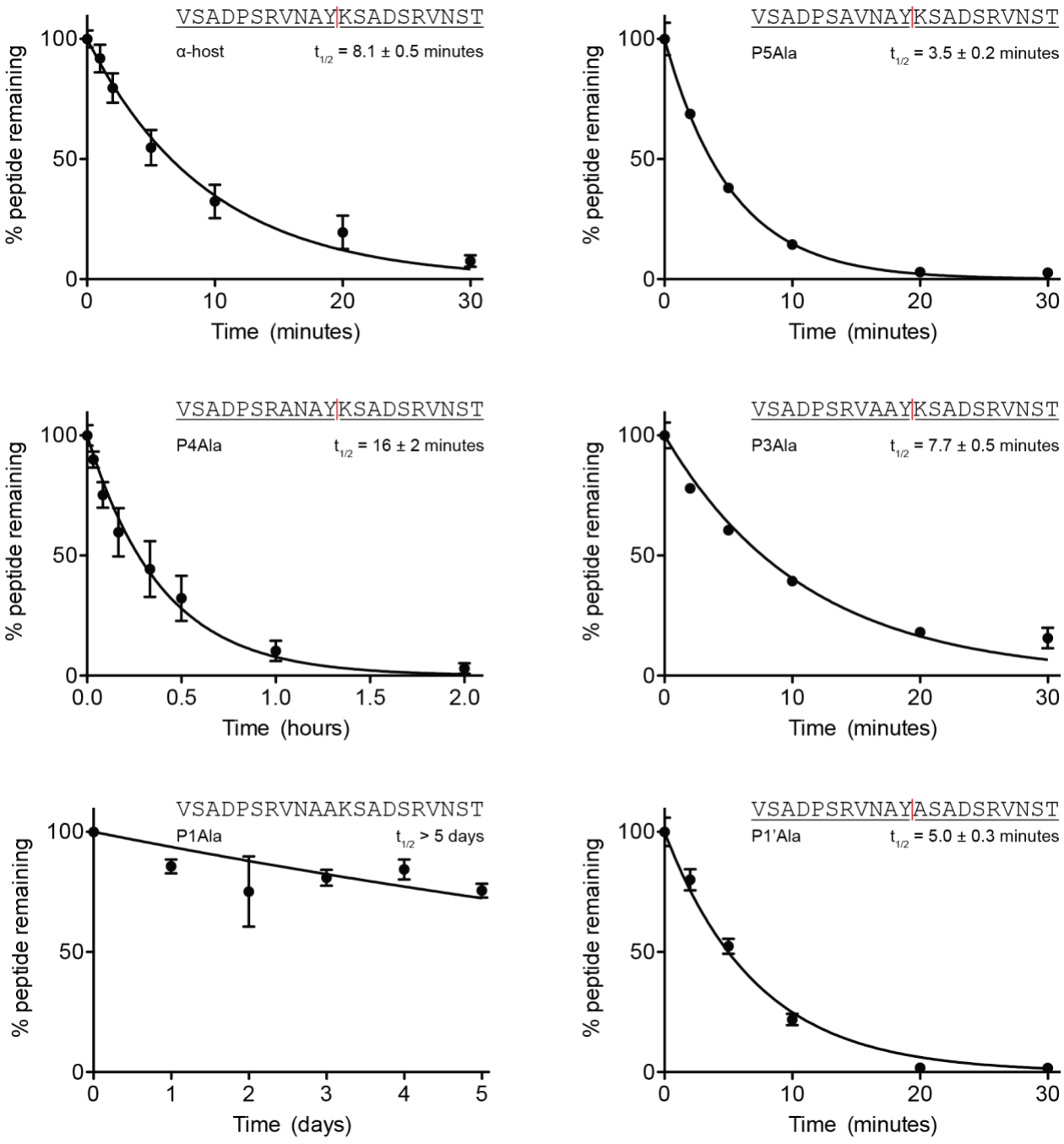

Figure 25. Full progress degradation curves and calculated half-lives of various peptides. Observed proteolysis products (horizontal black lines) and corresponding cleavage sites (vertical red lines) for each peptide are indicated in its sequence. Data points represent at least two replicate proteolysis experiments, while error bars represent the SEM for each timepoint. Full digestion curves are modeled by a one-phase decay fit with a variable plateau value $Y = (Y_0 - Y_P)\, e^{-kx} + Y_P$ (solid curve).

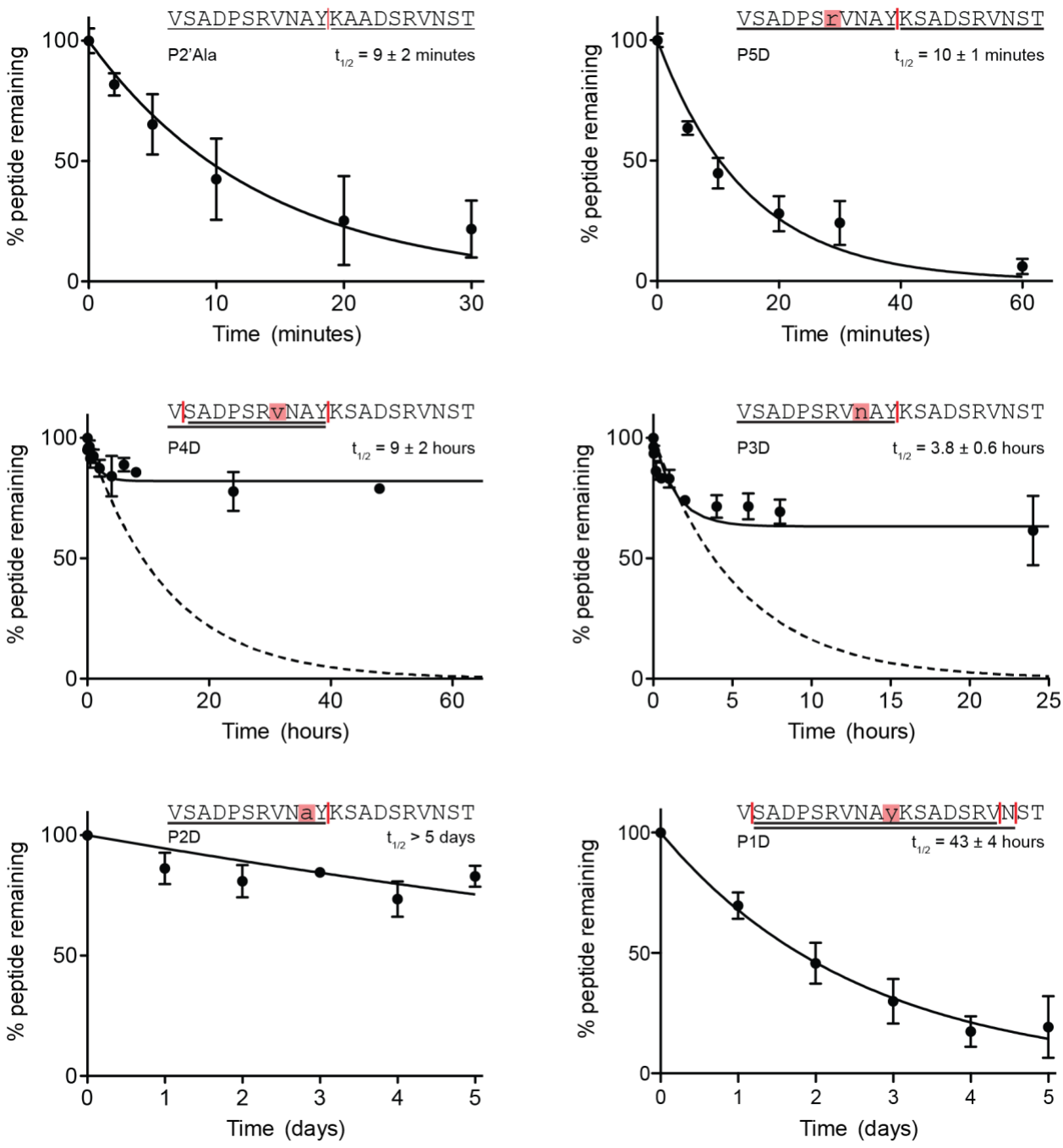

Figure 26. Full progress degradation curves and calculated half-lives of various peptides. Observed proteolysis products (horizontal black lines) and corresponding cleavage sites (vertical red lines) for each peptide are indicated in its sequence. Data points represent at least two replicate proteolysis experiments, while error bars represent the SEM for each timepoint. Full digestion curves are modeled by a one-phase decay fit with a variable plateau value $Y = (Y_0 - Y_P)\, e^{-kx} + Y_P$ (solid curve). For peptides that did not degrade fully, the earliest data points are modeled by a one-phase decay model with a plateau constrained to zero $Y = (Y_0)\, e^{-kx}$ (hashed curve).

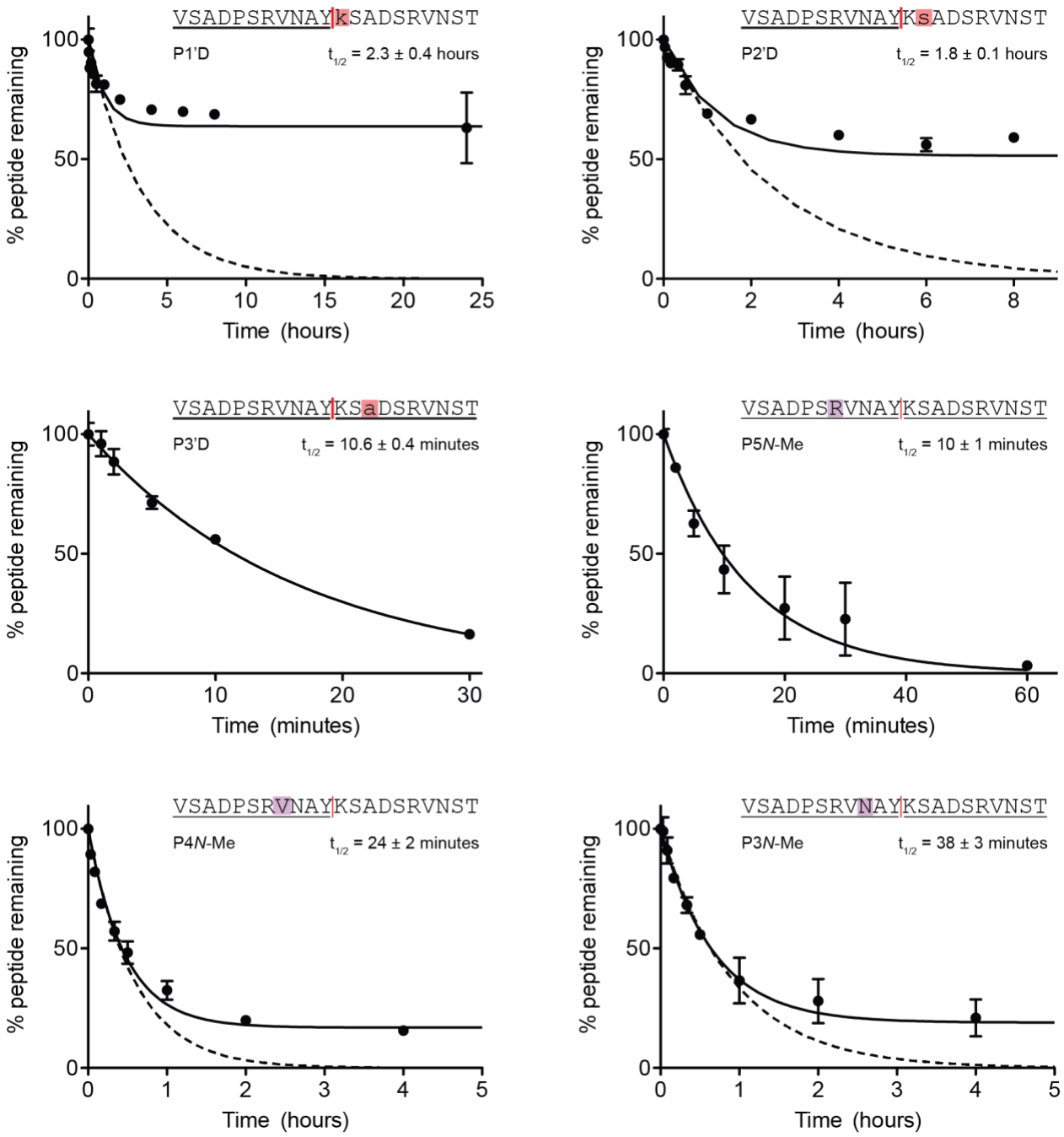

Figure 27. Full progress degradation curves and calculated half-lives of various peptides. Observed proteolysis products (horizontal black lines) and corresponding cleavage sites (vertical red lines) for each peptide are indicated in its sequence. Data points represent at least two replicate proteolysis experiments, while error bars represent the SEM for each timepoint. Full digestion curves are modeled by a one-phase decay fit with a variable plateau value $Y = (Y_0 - Y_P)\, e^{-kx} + Y_P$ (solid curve). For peptides that did not degrade fully, the earliest data points are modeled by a one-phase decay model with a plateau constrained to zero $Y = (Y_0)\, e^{-kx}$ (hashed curve).

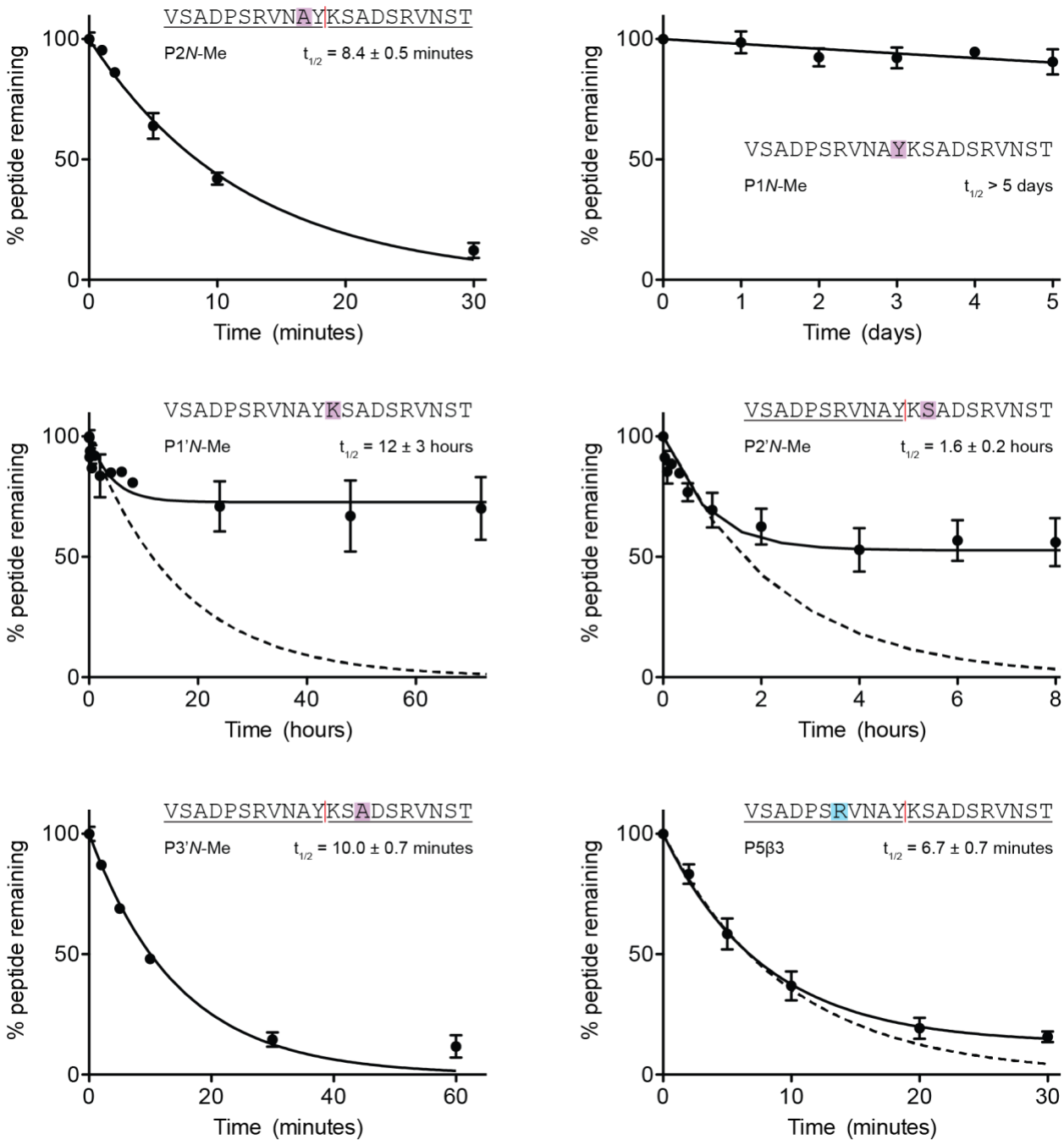

Figure 28. Full progress degradation curves and calculated half-lives of various peptides. Observed proteolysis products (horizontal black lines) and corresponding cleavage sites (vertical red lines) for each peptide are indicated in its sequence. Data points represent at least two replicate proteolysis experiments, while error bars represent the SEM for each timepoint. Full digestion curves are modeled by a one-phase decay fit with a variable plateau value $Y = (Y_0 - Y_P)\, e^{-kx} + Y_P$ (solid curve). For peptides that did not degrade fully, the earliest data points are modeled by a one-phase decay model with a plateau constrained to zero $Y = (Y_0)\, e^{-kx}$ (hashed curve).

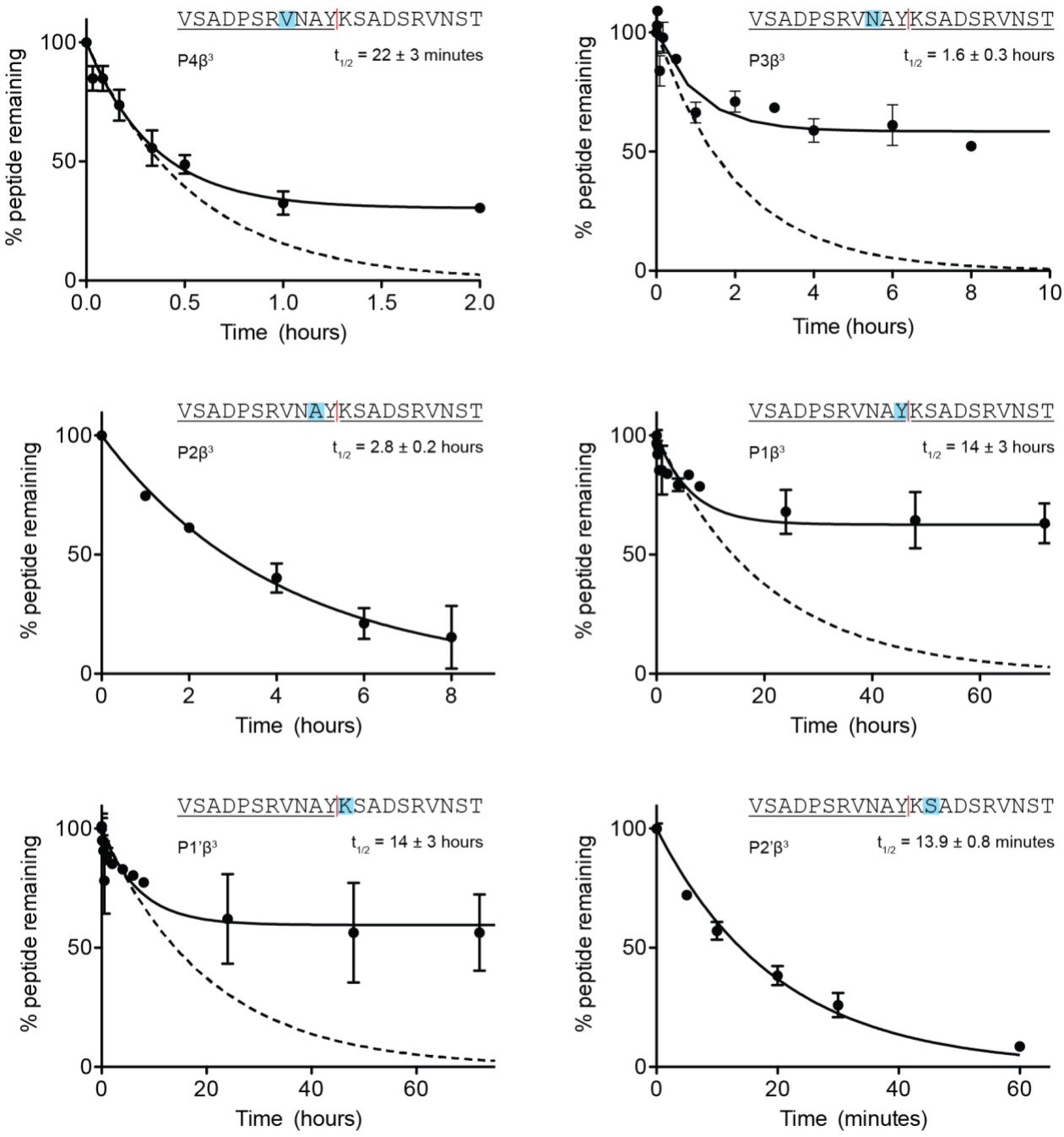

Figure 29. Full progress degradation curves and calculated half-lives of various peptides. Observed proteolysis products (horizontal black lines) and corresponding cleavage sites (vertical red lines) for each peptide are indicated in its sequence. Data points represent at least two replicate proteolysis experiments, while error bars represent the SEM for each timepoint. Full digestion curves are modeled by a one-phase decay fit with a variable plateau value $Y = (Y_0 - Y_P)\, e^{-kx} + Y_P$ (solid curve). For peptides that did not degrade fully, the earliest data points are modeled by a one-phase decay model with a plateau constrained to zero $Y = (Y_0)\, e^{-kx}$ (hashed curve).

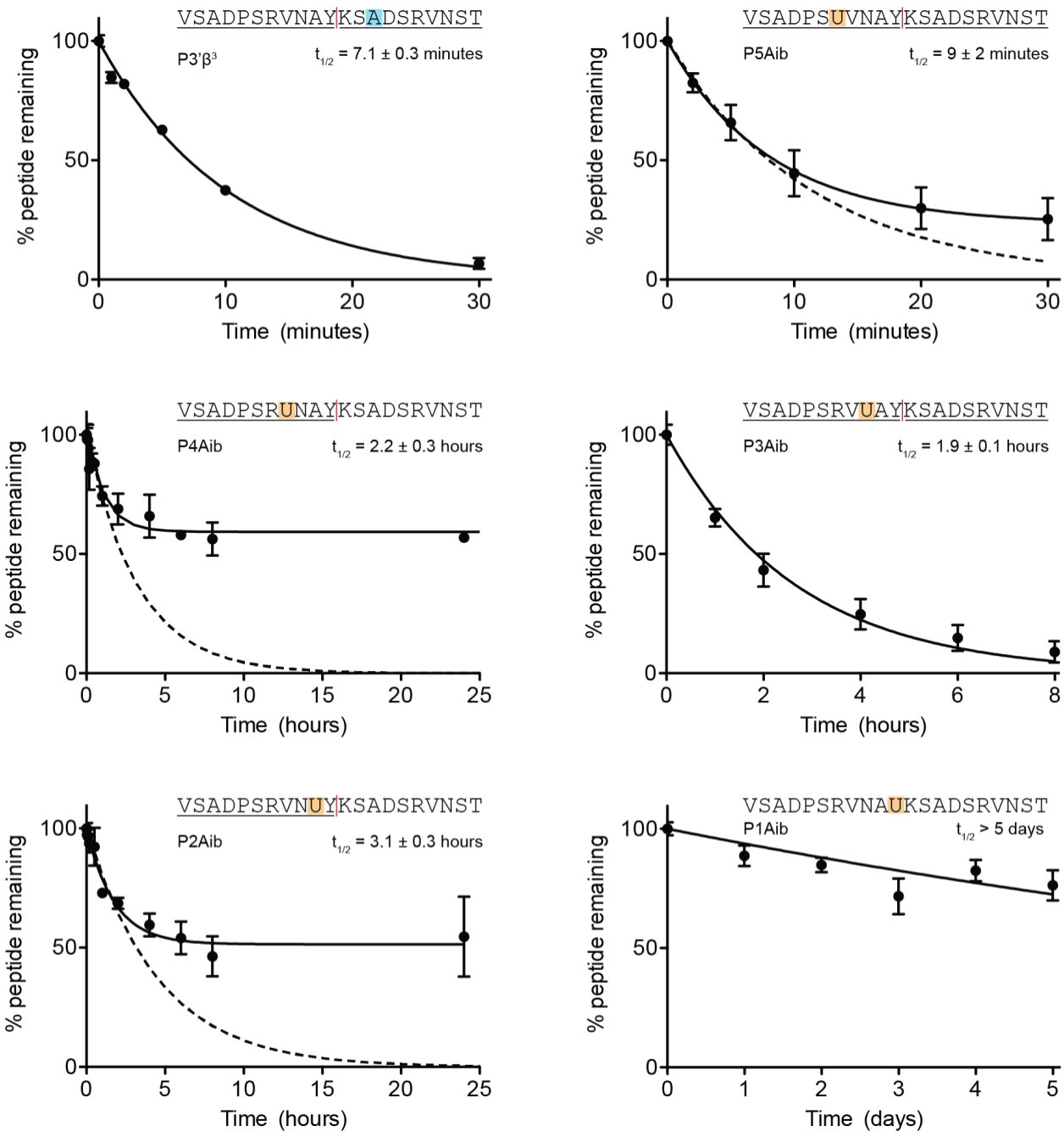

Figure 30. Full progress degradation curves and calculated half-lives of various peptides. Observed proteolysis products (horizontal black lines) and corresponding cleavage sites (vertical red lines) for each peptide are indicated in its sequence. Data points represent at least two replicate proteolysis experiments, while error bars represent the SEM for each timepoint. Full digestion curves are modeled by a one-phase decay fit with a variable plateau value $Y = (Y_0 - Y_P)\, e^{-kx} + Y_P$ (solid curve). For peptides that did not degrade fully, the earliest data points are modeled by a one-phase decay model with a plateau constrained to zero $Y = (Y_0)\, e^{-kx}$ (hashed curve).

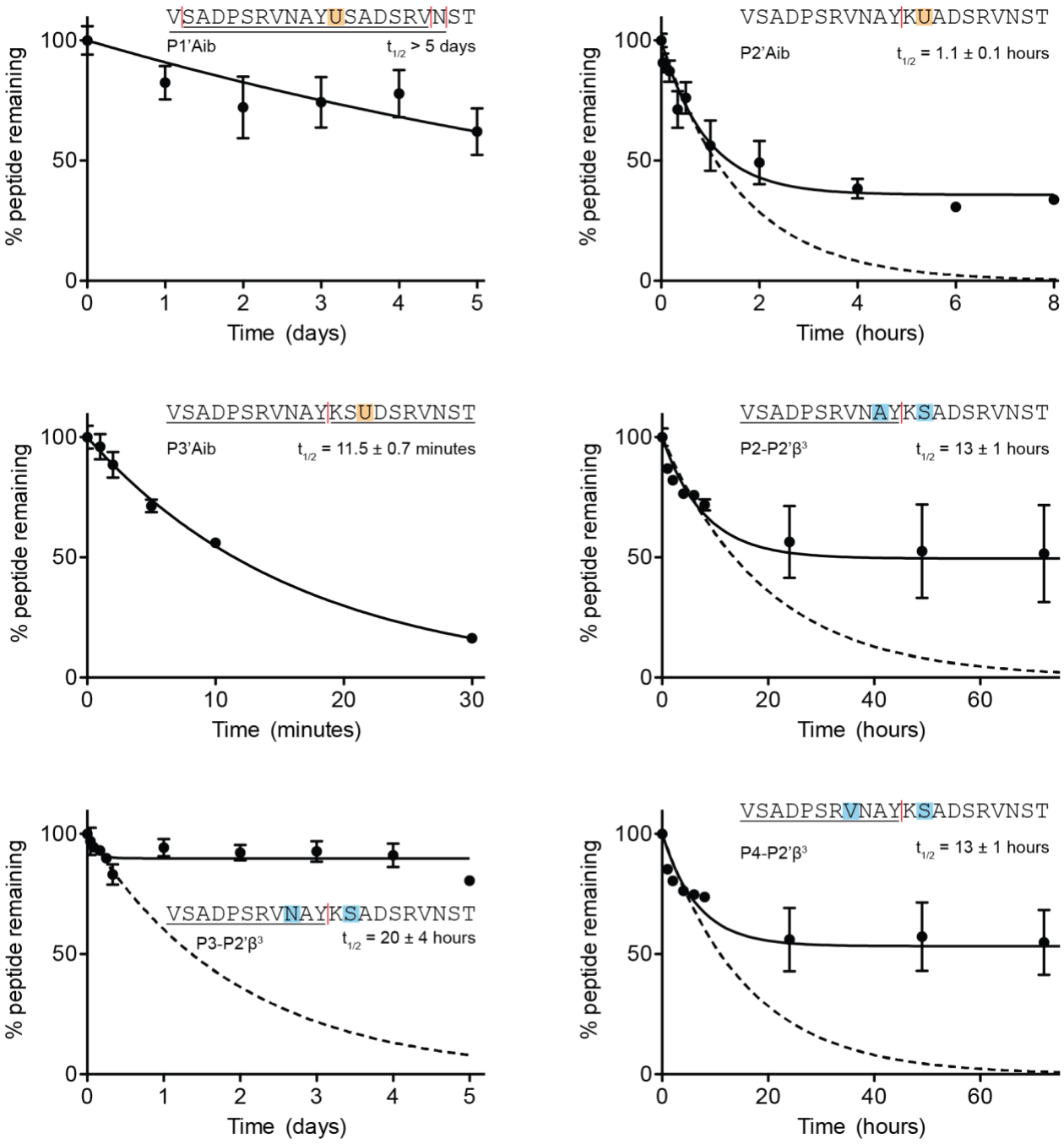

Figure 31. Full progress degradation curves and calculated half-lives of various peptides. Observed proteolysis products (horizontal black lines) and corresponding cleavage sites (vertical red lines) for each peptide are indicated in its sequence. Data points represent at least two replicate proteolysis experiments, while error bars represent the SEM for each timepoint. Full digestion curves are modeled by a one-phase decay fit with a variable plateau value $Y = (Y_0 - Y_P)\, e^{-kx} + Y_P$ (solid curve). For peptides that did not degrade fully, the earliest data points are modeled by a one-phase decay model with a plateau constrained to zero $Y = (Y_0)\, e^{-kx}$ (hashed curve).

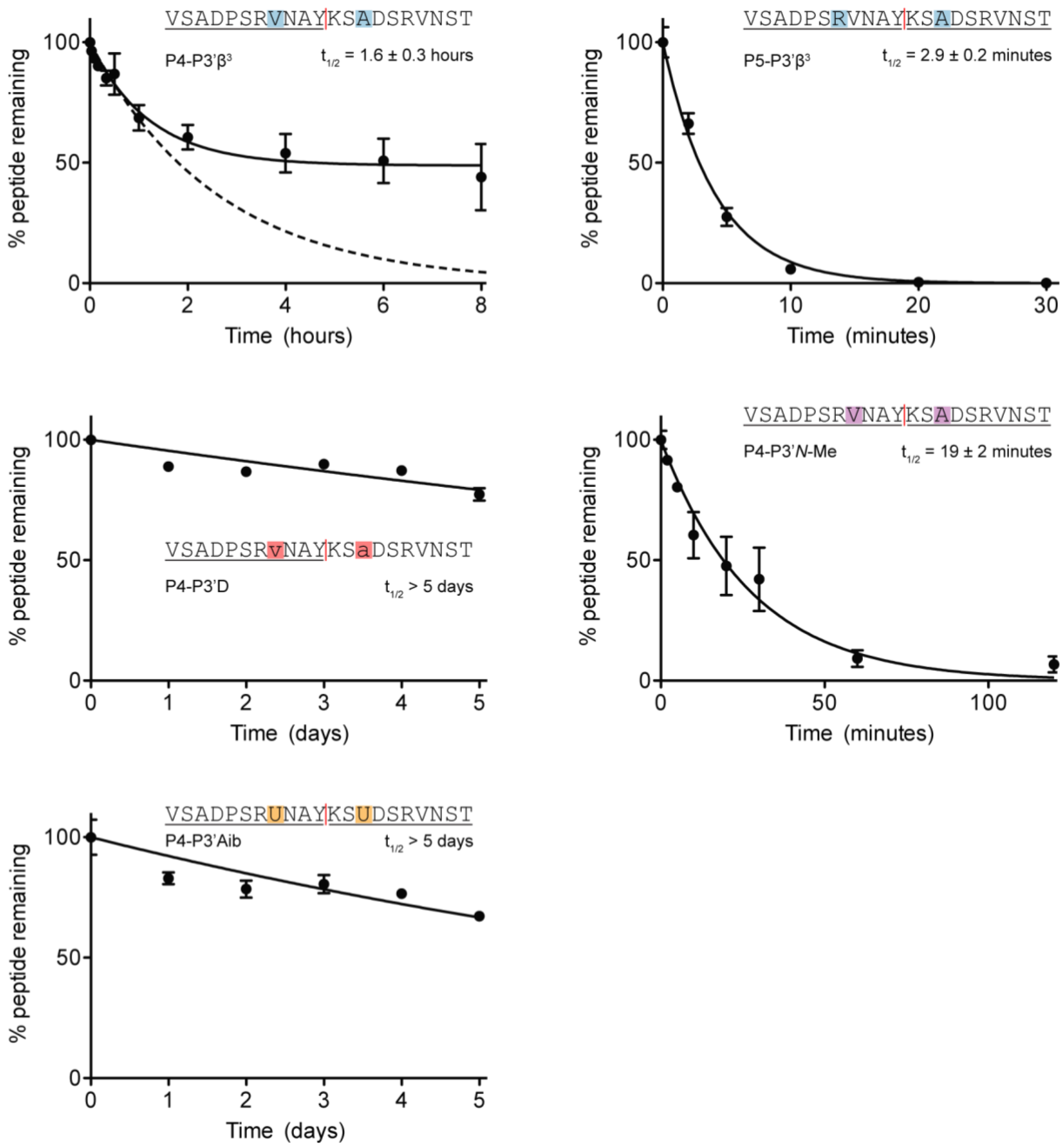

Figure 32. Full progress degradation curves and calculated half-lives of various peptides. Observed proteolysis products (horizontal black lines) and corresponding cleavage sites (vertical red lines) for each peptide are indicated in its sequence. Data points represent at least two replicate proteolysis experiments, while error bars represent the SEM for each timepoint. Full digestion curves are modeled by a one-phase decay fit with a variable plateau value $Y = (Y_0 - Y_P)\, e^{-kx} + Y_P$ (solid curve). For peptides that did not degrade fully, the earliest data points are modeled by a one-phase decay model with a plateau constrained to zero $Y = (Y_0)\, e^{-kx}$ (hashed curve).

3.0 THERMODYNAMIC ORIGIN OF α-HELIX STABILIZATION BY SIDE-CHAIN CROSS-LINKS IN A SMALL PROTEIN

Note: This work was published as C.M. Haney‡, H.M. Werner‡, J.J. McKay, W.S. Horne* "Thermodynamic origin of α-helix stabilization by side-chain cross-links in a small protein." *Org. Biomol. Chem.* **2016**, *14*, 5768-5773. It is reproduced from ref. [121] with permission from The Royal Society of Chemistry.

Peptide cross-linking has been widely explored as a means of constraining short sequences into stable folded conformations, most commonly α-helices. The prevailing hypothesis for the origin of helix stabilization is an entropic effect resulting from backbone pre-organization; however, obtaining direct evidence bearing on this hypothesis is challenging. Here, we compared the folding thermodynamics of a small helix-rich protein domain and analogues containing one of three common cross-linking motifs. Analysis of the folding free energy landscapes of linear vs. cyclized species reveal consistent trends in the effect of cyclization on folding energetics, as well as subtle differences based on the chemistry of the cross link. Stabilization in all three systems arises entirely from a reduction in the entropic penalty of folding that more than compensates for an enthalpic destabilization of the folded state.

3.1 INTRODUCTION

The importance of protein-protein interactions (PPIs) in pathology has made specific binders of protein surfaces an important goal in biomedical research.[44, 122] Due to the inability to target most PPIs with small molecules, considerable effort has been invested in the generation of peptide-based agents that can engage larger binding surfaces and show enhanced inhibitory efficacy.[123-124] However, a lack of well-folded structure in short peptide sequences can diminish potency and specificity as well as contribute to rapid proteolytic degradation. In order to address these issues, researchers have explored the use of protease-resistant backbones[1, 53] as well as constraint of natural backbones by covalent bonds.[12] The prevalence of α-helices in PPIs[125] has encouraged particular interest in mimics of helical peptides,[118, 126] though covalent constraint of other secondary structures has also been examined.[118, 127]

A variety of methods have been developed for the generation of covalently constrained peptides. Some approaches employ bimolecular cyclization by reaction of a peptide chain with an exogenous linking molecule.[12, 20, 128] However, the most common strategies are based on direct intramolecular cyclization via peptide side-chains. Such side-chain to side-chain cyclization, often termed "cross-linking" or "stapling," has relied on both natural (e.g. Asp, Lys)[129] and unnatural (e.g. olefin-functionalized)[16] amino-acid pairs. Many cross-linking methods require significant on-resin manipulation during solid-phase peptide synthesis to introduce the macrocycle, but we and others have described alternative strategies which can be performed using fully unprotected substrates.[18, 130-133] In addition to side-chain cross-linking, prior work has shown helix stabilization can also be achieved through covalent constraint of backbone atoms.[134-135]

The stabilization of helices by cross-linking is thought to arise primarily from a reduction in backbone conformational freedom; however, direct evidence bearing on this hypothesis is limited.[20] Prior work has compared various cross-link types for their ability to stabilize short α-helices,[136] as well as the effect of residue spacing and macrocycle size.[133, 137-140] A more complete understanding of the physical basis for the stabilization of folded states requires examination of folding thermodynamics. Analysis of thermodynamic changes is challenging for short sequences due to the lack of a fully folded structure or well-defined folding transition. Accordingly, prior work seeking the thermodynamics associated with α-helix cross-linking has taken place primarily in the context of peptide-peptide and peptide-protein complexes.[138, 141-144] Data from such systems are valuable; however, interpretation with respect to the molecular origins of helix stabilization is difficult when the process of folding and assembly are inseparable.

Determination of the thermodynamic impact of cross-link formation on helical folding in the absence of quaternary contacts requires a well-folded unimolecular motif that undergoes a simple two-state unfolding transition. Here, we apply three established cross-linking methods in such a system—a small helix-rich protein with a compact tertiary fold. Examination of folding thermodynamics for each cyclized species compared to its linear counterpart reveal consistent perturbations to the overall energy landscape of folding. These perturbations shed light on the molecular mechanisms by which side-chain cyclization stabilizes α-helices. Subtle differences observed in the side-by-side comparison of three established cyclization chemistries provide data bearing on their relative effectiveness as α-helix stabilizers.

3.2 RESULTS AND DISCUSSION

In selecting a host peptide for our studies, a sequence with the following characteristics was sought: (1) a monomeric and stable folded structure in aqueous solution, (2) one or more α-helices in which to insert a cross-link, and (3) a length amenable to preparation by solid-phase synthesis and post-synthetic manipulations associated with cross-link formation. Based on these considerations, we chose the villin headpiece (VHP) domain for our work (**Figure 33**).

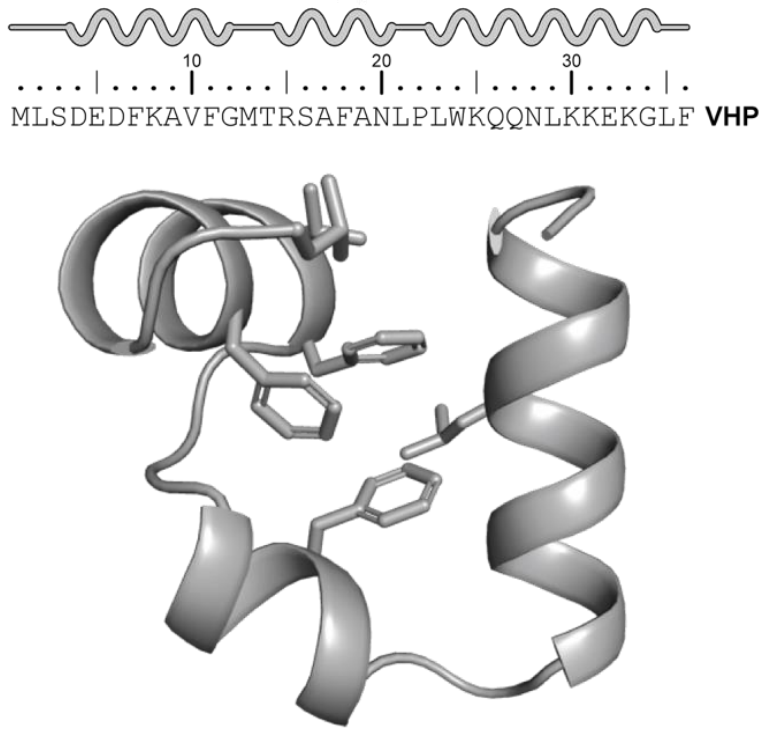

Figure 33. Sequence and crystal structure of the villin headpiece (VHP) domain (PDB 3TRW).

The 36-residue VHP sequence folds into a compact tertiary structure consisting of three α-helices that pack to form a defined hydrophobic core (**Figure 33**).[145-146] VHP is a widely used model system in the study of folding kinetics and thermodynamics in short, fast-folding sequences.[147-153]

To avoid complications from methionine oxidation during synthesis and biophysical analysis, we replaced the two Met residues in VHP with hydrocarbon isostere norleucine to generate sequence **3.1** (**Figure 34**).

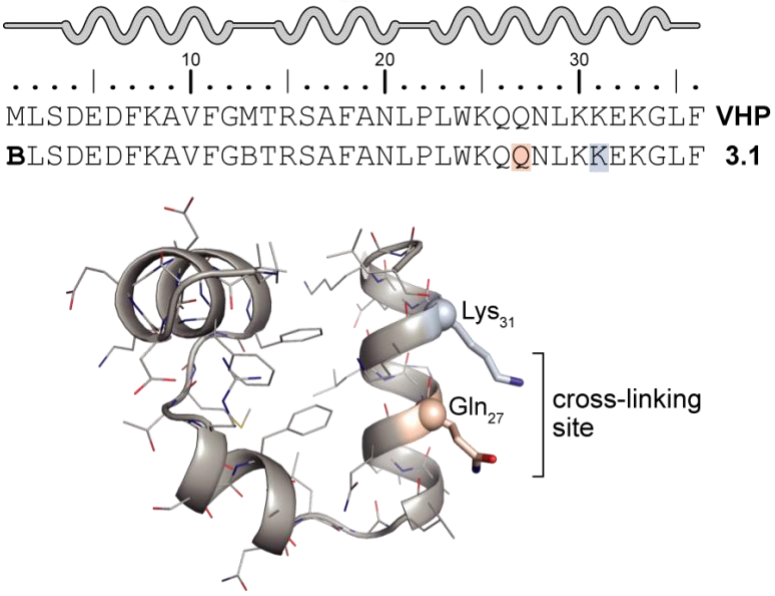

Figure 34. Sequence and crystal structure of the VHP domain, linear mutant **3.1** with cross-linking site indicated (PDB 3TRW). B = norleucine. This figure is adapted from ref. [121] with permission from The Royal Society of Chemistry.

Circular dichroism (CD) spectroscopy and thermal denaturation experiments indicate **3.1** has a tertiary folding pattern and stability similar to the native VHP sequence (T_m = 65 °C for **3.1** vs. 70 °C for wild-type VHP).[154-155] Having established **3.1** as a suitable host sequence, we next

designed and prepared three mutants (**3.2a**-**3.4a**) containing amino acids suitable for cross-link formation, and three corresponding cyclized variants (**3.2b**-**3.4b**). In each case, the cross-link is installed at the same site, between positions 27 and 31 on the C-terminal VHP helix (**Figure 35**).

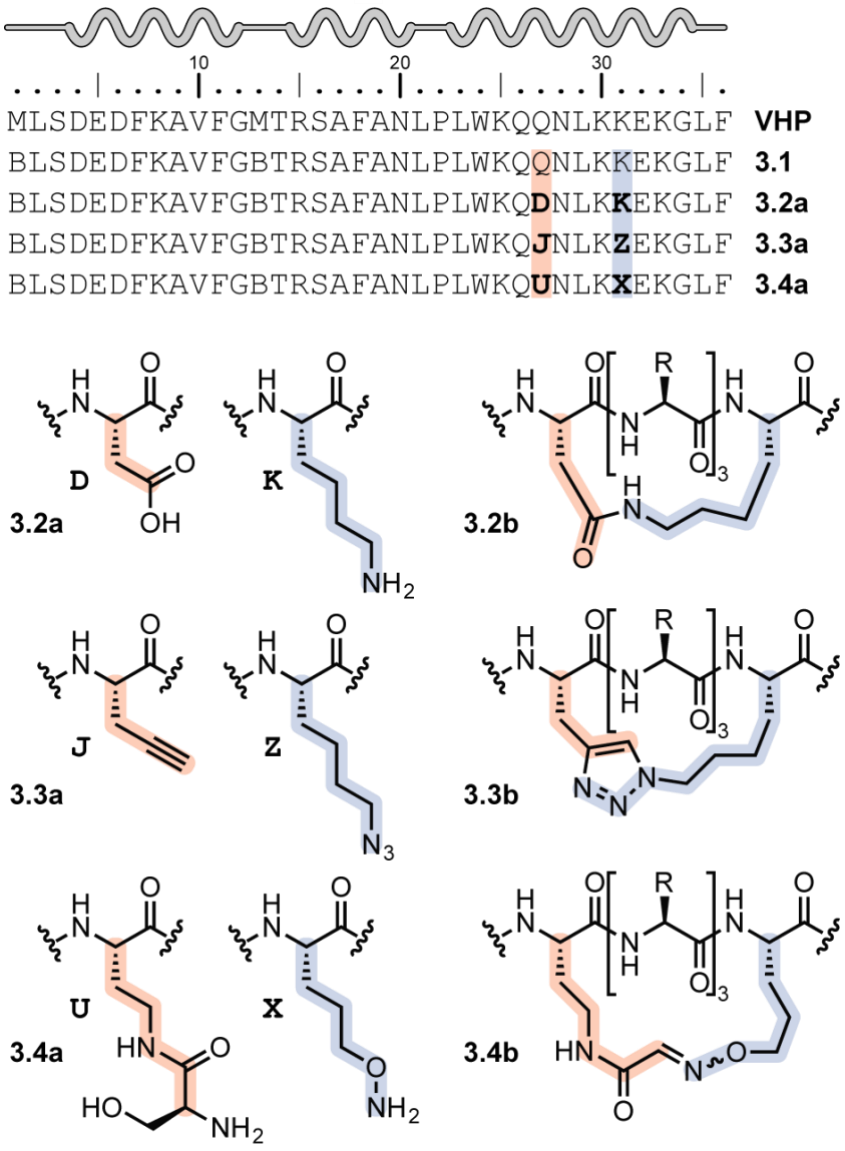

Figure 35. Sequence of the VHP domain, linear mutants **3.1** and **3.2a-3.4a**, and cyclized variants **3.2b-3.4b**. B = norleucine. This figure is adapted from ref. [121] with permission from The Royal Society of Chemistry.

We reasoned substitution at this solvent-exposed position would minimize the impact of each cross-link on the packing interactions involved in folding and enable the thermodynamic analysis to inform maximally on the effect of cyclization on helix folding propensity. The $i \rightarrow i+4$ spacing for each cross-linking moiety (**Figure 35**) was selected based on prior work suggesting this is optimal for stabilizing an α-helical fold for macrocycle sizes in the range we examine here.[18, 133, 137]

VHP variants **3.2b-3.4b** represent three established methods for helix stabilization by side-chain to side-chain cross linking: lactam (**3.2b**),[156] triazole (**3.3b**),[157] and oxime (**3.4b**).[18] We chose these three motifs based on their ease of introduction synthetically and high degree of similarity in terms of structure and polarity (**Figure 36**).

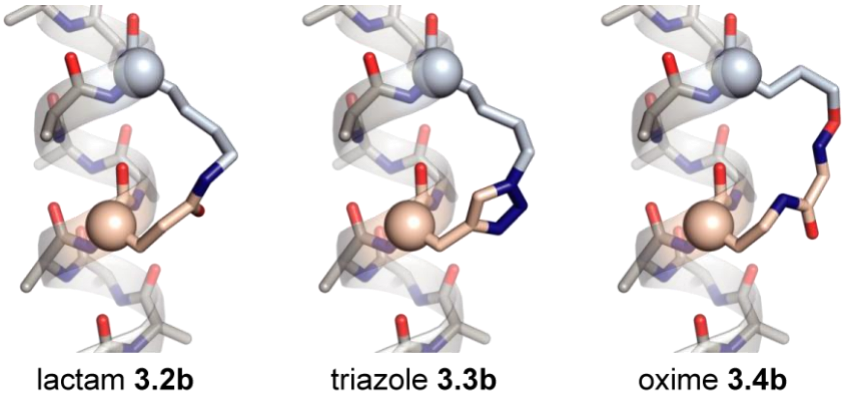

Figure 36. Molecular models of lactam, triazole, and oxime cyclized helices. This figure is adapted from ref. [121] with permission from The Royal Society of Chemistry.

In each case Lys_{31} is replaced by an isosteric or nearly isosteric analogue, and Gln_{27} is replaced with an appropriate moiety to enable cyclization on resin or in solution. The resulting cross-links among **3.2b-3.4b** vary only slightly in overall macrocycle size as well as placement of non-rotatable bonds relative to the backbone.

Linear peptides **3.1** and **3.2a-3.4a** were prepared by Fmoc solid-phase methods. The lactam in cyclic peptide **3.2b** was installed on-resin after revealing Lys_{31} and Asp_{27} side chains masked with 4-methyltrityl and phenylisopropyl groups, respectively (**Figure 37**).[156]

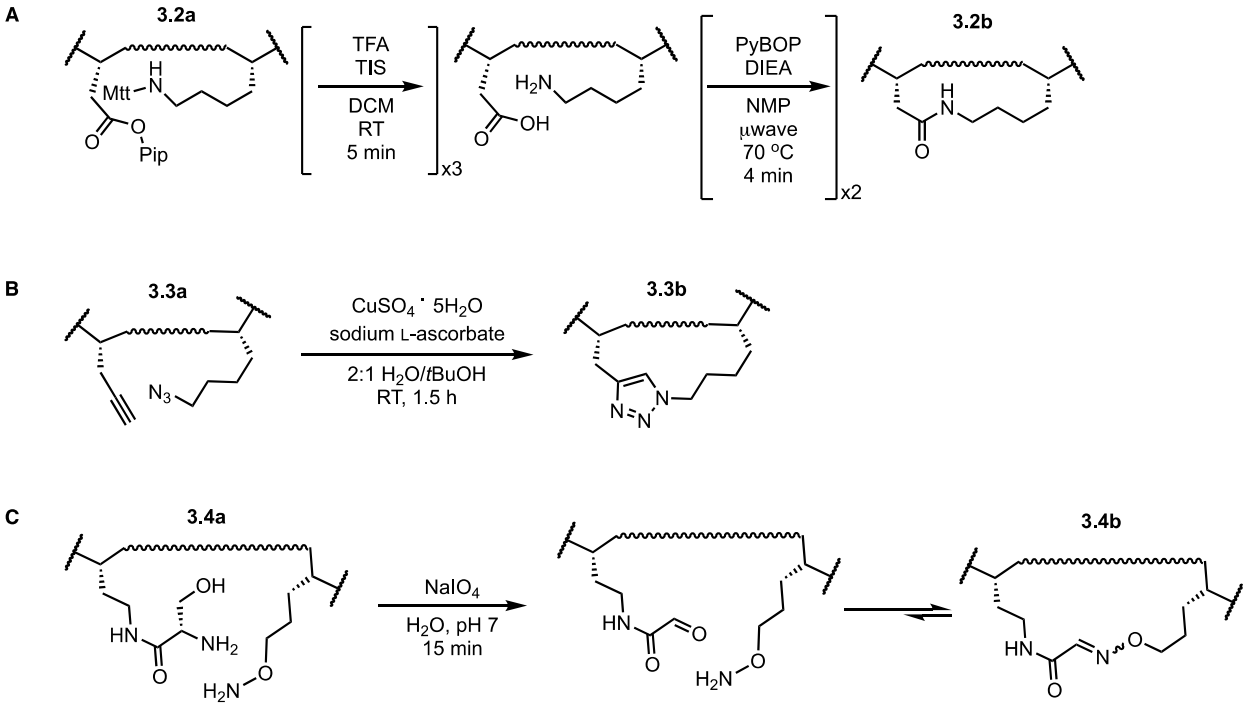

Figure 37. Synthesis of cyclic peptides from their linear precursors: A) on-resin cyclization of **3.2a** to generate **3.2b**, B) solution phase cyclization of **3.3a** to generate **3.3b** and C) solution phase cyclization of **3.4a** to generate **3.4b**.

Triazole peptide **3.3b** was prepared by the chemoselective cyclization of precursor **3.3a** in solution through the copper(I)-mediated dipolar cycloaddition between alkyne-functionalized residue J and azide-functionalized residue Z (**Figure 35**).[133] Oxime peptide **3.4b** was prepared by the solution cyclization of **3.4a**; periodate-mediated cleavage of the vicinal amino alcohol in the U residue unmasks a glyoxylic aldehyde that subsequently reacts with the nearby aminooxy X residue to form the oxime (**Figure 35**).[18] Each synthetic VHP variant was purified by preparative reverse-phase HPLC and its identity was confirmed by MALDI-MS prior to further analysis.

We first sought to determine any effect side-chain substitutions in linear sequences **3.2a-3.4a** had on folding relative to **3.1**. CD scans (**Figure 38**) suggested no impact on the folded state resulting from the mutations necessary for cross-link introduction.

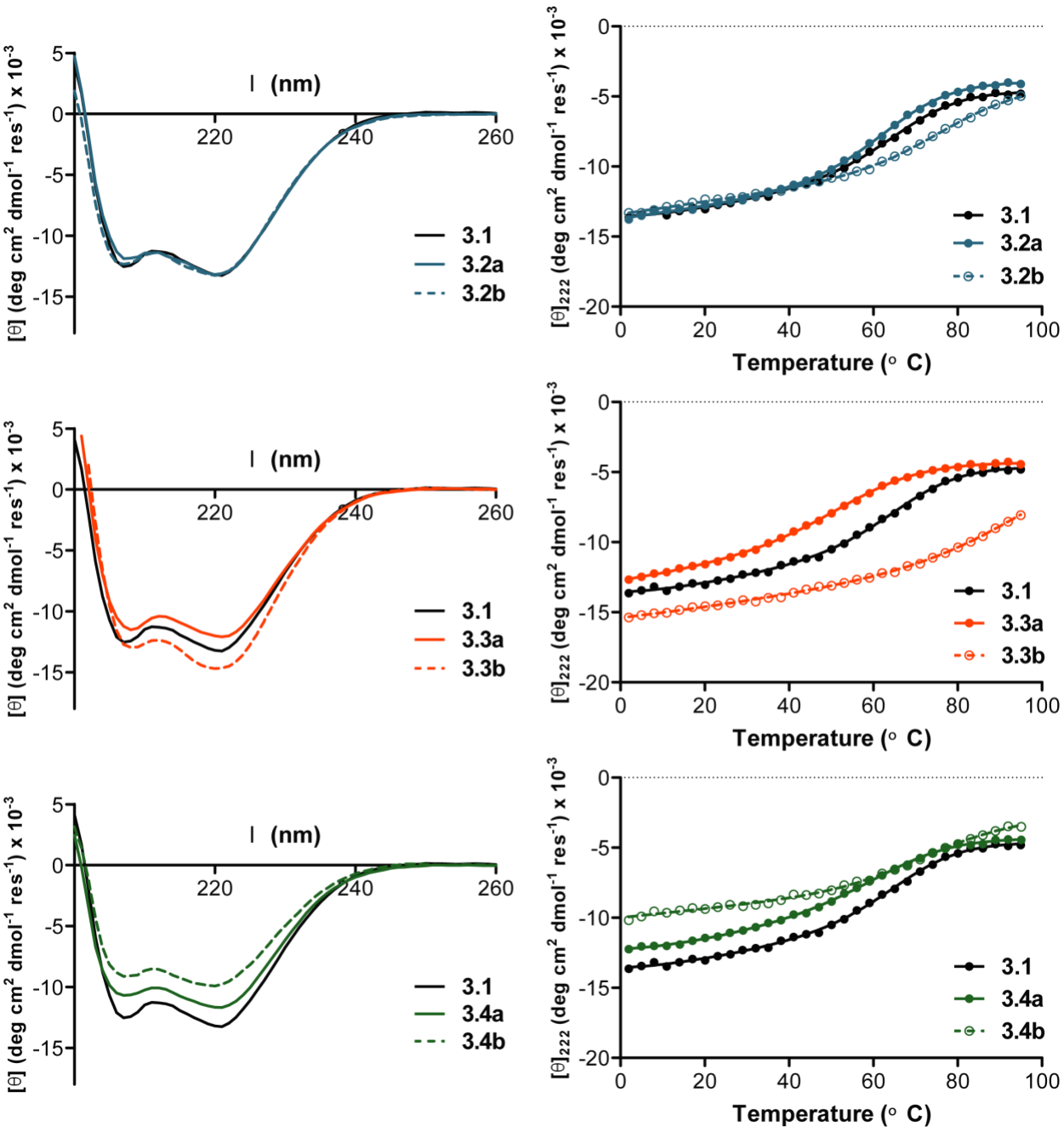

Figure 38. Circular dichroism (CD) data for peptides **3.1, 3.2a-3.4a** and **3.2b-3.4b** at 50 μM concentration. Left: CD scans acquired at 20 °C. Right: CD thermal melts obtained by monitoring molar ellipticity at 222 nm as a function of temperature; circles represent measured ellipticity values, while dashed or solid lines represent the nonlinear fit to a two-state thermal denaturation model. This figure is adapted from ref. [121] with permission from The Royal Society of Chemistry.

In thermal denaturation experiments, **3.2a** and **3.4a** exhibited two-state unfolding transitions, with minimal change in the observed T_m relative to **3.1** (**Table 3**, **Figure 38**). Two-state unfolding transitions were modeled with seven parameters related by **Equations 1-3**.

$$\Delta G = \Delta H\left(1 - \frac{x + 273}{T_m + 273}\right) + \Delta C_P\left[((x + 273) - (T_m + 273)) - (x + 273)\ln\left(\frac{x + 273}{T_m + 273}\right)\right]$$

Equation 1. Relationship between free energy of unfolding (ΔG), melting temperature in ^oC (T_m), enthalpy of unfolding at T_m (ΔH), change in heat capacity during unfolding (ΔC_p), and temperature in ^oC (x).

$$f(x) = \frac{e^{\frac{\Delta G}{0.00198721558(x+273)}}}{1 - e^{\frac{\Delta G}{0.00198721558(x+273)}}}$$

Equation 2. Function representing the fraction of molecules in the denatured state at a given temperature in ^oC (x).

$$Y = f(x)[\theta_U + M_U x] + [1 - f(x)][\theta_F + M_F x]$$

Equation 3. Ellipticity (Y) as a function of temperature (x) with parameters representing the ellipticity of the unfolded state at 273K (θ_U), slope of the unfolded baseline (M_U), ellipticity of the folded state at 273K (θ_F), and slope of the folded baseline (M_F).

Table 3. Thermodynamic parameters for folding at 293 K for VHP domain **3.1**, linear mutants **3.2a-3.4a**, and cyclized variants **3.2b-3.4b**.

Peptide	Macrocycle size	$[\theta]_{222}$ (deg cm^2 dmol^{-1} res^{-1})[a]	T_m (°C)[b]	ΔH (kcal mol^{-1})[c]	TΔS (cal mol^{-1})[c]	ΔC_p (kcal mol^{-1} K^{-1})[c]	*m* (kcal mol^{-1} M^{-1})[c]	ΔG (kcal mol^{-1})[d]
3.1	-	-12,900	65 ± 1	-7.9 ± 0.4	-6.2 ± 0.3	-0.29 ± 0.03	0.58 ± 0.04	-1.7
3.2a	-	-12,900	63 ± 1	-10.6 ± 0.5	-8.4 ± 0.4	-0.36 ± 0.03	0.74 ± 0.04	-2.2
3.2b	20	-12,900	80 ± 0.5	-9.6 ± 0.2	-6.6 ± 0.2	-0.32 ± 0.01	0.66 ± 0.02	-3.0
3.3a	-	-12,000	52 ± 2	-9.2 ± 0.2	-7.5 ± 0.2	-0.29 ± 0.01	0.73 ± 0.02	-1.7
3.3b	21	-14,600	95 ± 0.6	-7.9 ± 0.3	-4.6 ± 0.2	-0.31 ± 0.02	0.57 ± 0.03	-3.3
3.4a	-	-11,400	60 ± 2	-9.3 ± 0.5	-7.2 ± 0.4	-0.32 ± 0.03	0.69 ± 0.04	-2.1
3.4b	23	-9,500	77 ± 7	-7.7 ± 0.6	-5.3 ± 0.5	-0.31 ± 0.05	0.58 ± 0.06	-2.3

[a] Mean residue molar ellipticity at 222 nm from a CD scan carried out at 20 °C. [b] Midpoint of the thermal unfolding transition in the absence of chemical denaturant as determined by a fit of simple CD melts to a two-state thermal denaturation model; error represents the parameter uncertainty from the fit. [c] Parameters obtained from fitting coupled thermal-chemical denaturation experiments to the Gibb-Helmholtz equation; error shown is the parameter uncertainty from the fit. [d] Calculated from ΔH and TΔS.

In contrast, linear peptide **3.3a** proved to be somewhat destabilized relative to the parent sequence ($\Delta T_m \approx$ -13 °C). This may result from replacing the solvent-exposed polar Lys_{31} and Gln_{27} in **3.1** with more hydrophobic residues J and Z.

We next assessed the impact of cross-link formation on folding and thermal stability by comparing CD data for linear peptides **3.2a-3.4a** and their cyclic counterparts **3.2b-3.4b**. Consistent with expectation based on precedent for the known cross-linking chemistries examined, cyclization had minimal effect on the helical signature observed in CD scans but led to improved resistance to denaturation (**Figure 38**). Lactam peptide **3.2b**, triazole **3.3b**, and oxime **3.4b** all showed significantly greater thermal stability relative to their linear counterparts and did not reach a clear fully unfolded state by the highest temperature measured (95 °C). Interestingly, the unfolding transitions were slightly shallower for the cyclic series, suggesting the possibility of altered folding landscapes.

In order to rigorously examine the folding thermodynamics before and after cross-link formation, we performed thermal-chemical denaturation experiments monitored by CD, a method previously applied to explore protein folding energetics in a variety of natural and unnatural systems.[119, 158-159] Analysis of the resulting data provides the changes to free energy (ΔG), enthalpy (ΔH), entropy (ΔS), and heat capacity (ΔC_p) accompanying the folding process, as well as the dependence on the folding free energy on denaturant concentration (*m*). We subjected VHP peptide **3.1**, linear mutants **3.2a-3.4a**, and cyclized variants **3.2b-3.4b** to this experiment (**Figure 39**, **Table 3**).

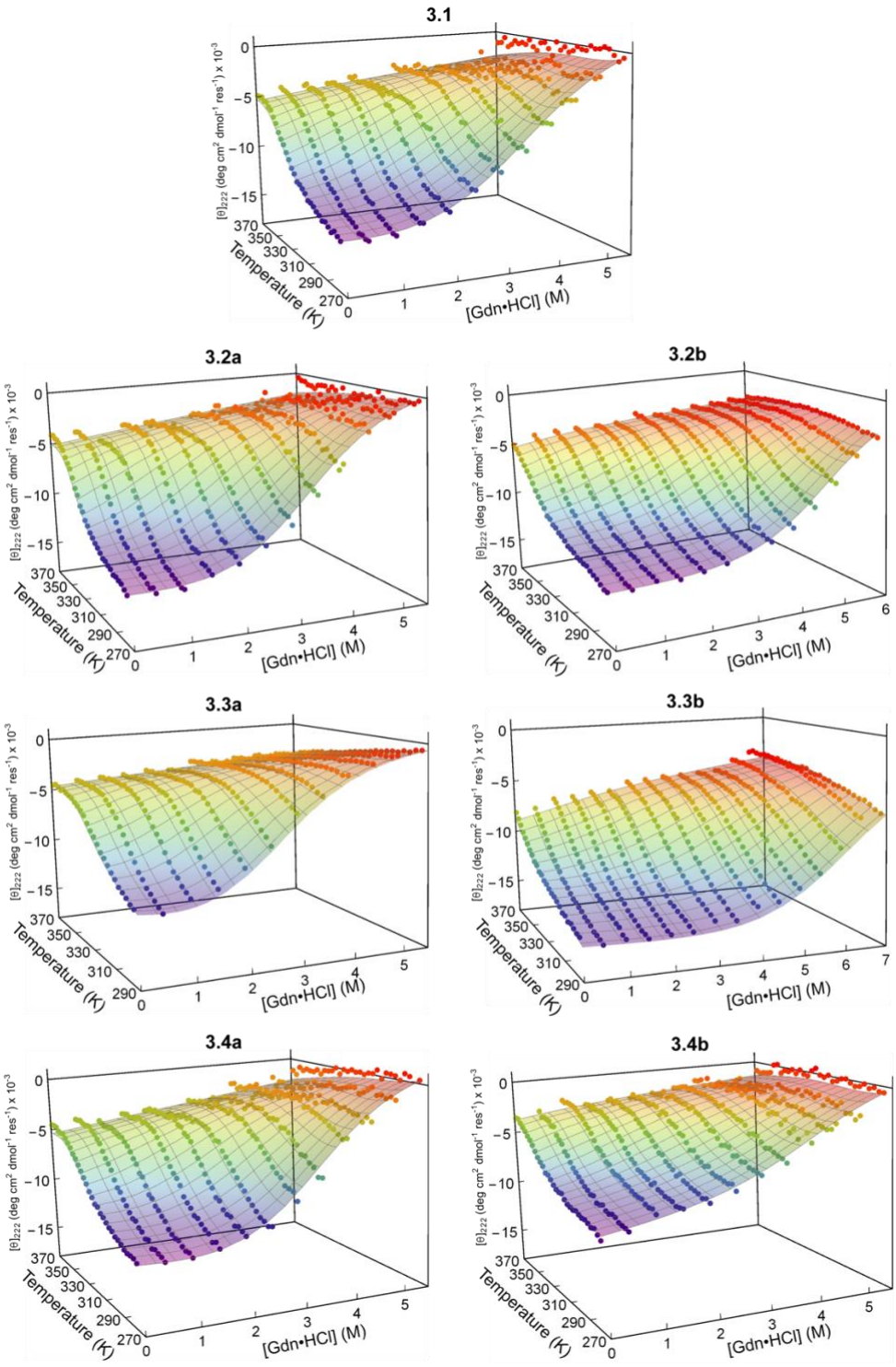

Figure 39. Thermal-chemical denaturation plots for peptides **3.1**, **3.2a-3.4a** and **3.2b-3.4b** as indicated above each plot. Helicity at 222 nm is monitored as both temperature and denaturant concentration vary. Raw data (points) are fit (surface) to extract thermodynamic parameters for the folding equilibrium. This figure is adapted from ref. [121] with permission from The Royal Society of Chemistry.

Data for **3.1** and **3.2a-3.4a** revealed measurable changes to folding thermodynamics among the series despite the conservative nature of the mutations (**Figure 40**, **Table 3**).

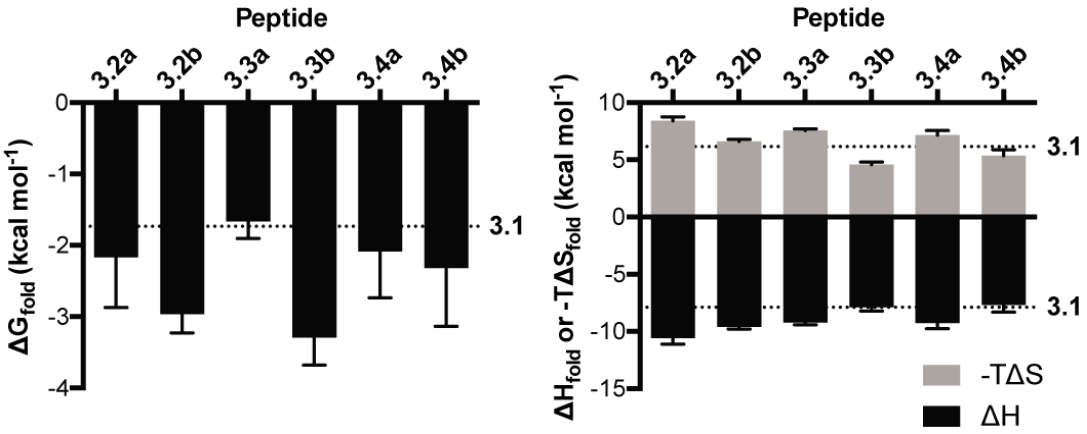

Figure 40. Free energy, enthalpy, and entropy of folding for VHP domain **3.1**, linear mutants **3.2a-3.4a**, and cyclic variants **3.2b-3. 4b**. All thermodynamic parameters are reported at 293 K. This figure is adapted from ref. [121] with permission from The Royal Society of Chemistry.

In all cases, an unfavorable change in the entropy of folding (ΔS_{fold}) was observed, accompanied by an increase in susceptibility to chemical denaturant (*m*). Peptide **3.2a** showed a favorable change in folding enthalpy (ΔH_{fold}) relative to **3.1**, which we attribute to the ability of Lys_{31} to form a salt bridge with newly introduced Asp_{27} in **3.2a**. These data suggest that VHP is somewhat sensitive to sequence alterations even at solvent-exposed sites, consistent with prior studies showing how mutations can change the thermodynamics and/or kinetics of VHP folding.[147-148, 155, 160]

In order to isolate the effects of cyclization from the side-chain alterations necessary to introduce a given type of cross-link, we compared the thermodynamic parameters of folding for each cyclized peptide to those for its corresponding linear precursor. In terms of folding free energy, cyclization had a consistently favorable effect, with the magnitude of stabilization

varying from 0.2-1.6 kcal mol^{-1} at 293 K. The improvement in stability as a function of cross-link chemistry followed the trend triazole > lactam > oxime. The stabilization upon cyclization was entirely entropic in origin for all three cases ($T\Delta\Delta S$ 1.8-3.0 kcal mol^{-1} at 293 K). This provides direct thermodynamic evidence supporting the hypothesis that backbone preorganization is a general mechanism by which side-chain to side-chain cross links stabilize folded α-helices. Intriguingly, cyclization had a consistent unfavorable effect on ΔH_{fold} for all three cross-link types (**Table 3**, **Figure 40**), which partially abrogates the favorable effect on ΔS_{fold}. While the origin of the effect is not clear, we suggest that cyclization might abolish enthalpically favorable polar contacts that exist between the side-chains of the linear precursors.

The importance of backbone flexibility in the impact of cyclization on folding energetics is further supported by the changes to the sensitivity of the fold to chemical denaturant upon cyclization. The magnitude of *m* is known to correlate strongly with the change in solvent accessible surface area upon protein folding and is typically similar for proteins of similar size.[161] Assuming similar folded states among the series of VHP variants examined (supported by the CD scan results), the consistent decrease in the magnitude of *m* upon cyclization indicates the cyclized peptides are less accessible to solvent when unfolded compared to their linear counterparts. This, in turn, suggests a more compact ensemble constituting the denatured state and increased residual folded structure in the denatured ensemble due to the presence of the macrocycle; however, the data obtained does not rule out potential contributions from altered solvation of the modified protein surface.[161]

3.3 CONCLUSIONS

Significant interest in development of α-helical peptides as inhibitors of PPIs has led to diverse methods to stabilize helical conformations, and side-chain to side-chain cross-links have proven quite successful in this context. The invention of such strategies was motivated by the hypothesis that cyclization can stabilize a helical fold by reducing chain entropy in the unfolded state and promoting the desired folded conformation. This hypothesis has proven challenging to probe by direct thermodynamic analysis in a unimolecular fold. Through examination of three different $i \rightarrow i+4$ cross-linking motifs in a small protein rich in α-helical regions, we have obtained data bearing on the fundamental molecular mechanisms by which side-chain to side-chain cyclization stabilizes α-helices.

Consistent decreases in both the entropic penalty toward folding and the sensitivity of the folded state to chemical denaturant provide direct evidence supporting the hypothesis that backbone preorganization is the dominant factor, regardless of the cross-linking chemistry employed. Subtle differences are observed in the magnitude of these effects as a function of cross-link size, structure, and flexibility. Among three similar polar motifs examined, cyclization via a triazole proved best, followed by lactam, then oxime. We also note a consistent enthalpic penalty toward folding upon cyclization that works against the favorable entropic effect. This suggests that cyclization, even at solvent-exposed sites, may perturb the network of weak interatomic interactions that drive folding.

Overall, these results suggest that covalent constraint via cross-linking stabilizes α-helices by reducing the disorder of the unfolded state and altering its solvation. Further exploration of the effects of cross-link formation on the folding energy landscape and kinetics may help to guide researchers in the *a priori* selection of the optimal cross-linking strategy to

utilize in a given system in order to generate stabilized α-helical peptides for therapeutic applications.

3.4 EXPERIMENTAL

3.4.1 Materials

Solvents and reagents were purchased from Sigma Aldrich, Baker, EMD Millipore, Fisher, Acros Organics, or ChemImpex, and used as received. Fmoc-protected monomers for installation of residues X, U, and Z were synthesized as previously described.[18, 138, 162] Flash column chromatography was performed using SorbTech (60 Å, 40-63 μm) silica gel. MALDI- TOF mass spectrometry was performed on a Voyager DE Pro instrument. Circular dichroism spectra were recorded on an Olis DSM17 spectrometer equipped with a Peltier temperature controller using quartz cuvettes of 0.1 cm path length. Preparative and analytical HPLC were performed on Phenomenex Luna C18 columns using gradients between 0.1% TFA in water and 0.1% TFA in acetonitrile.

3.4.2 Peptide Synthesis, Cyclization, and Purification

Peptides **3.1**, **3.2a**, and **3.4a** were synthesized on NovaPEG Rink Amide Resin with microwave heating (MARS microwave reactor, CEM). Amino acid couplings were performed with 5 equivalents of amino acid to resin. Natural α-amino acids were preactivated with HCTU (5 equivalents to resin) and DIEA (7.5 equivalents to resin) in NMP for 2-3 minutes. Unnatural

residues were preactivated with PyBOP (5 equivalents to resin) and DIEA (7.5 equivalents to resin) in NMP for 2-3 minutes. The preactivated amino acid was then added to the resin in a reaction vessel equipped with a stir bar, and a microwave program consisting of a 2 minute ramp to 70 °C followed by a 4 minute hold at 70 °C was run. The resin was washed three times with DMF and then treated with 20% 4-methylpiperidine in DMF using a microwave deprotection program consisting of a 2 minute ramp to 80 °C followed by a 2 minute hold at 80 °C. The resin was washed with DMF, and the above cycle was repeated until the desired peptide chain was obtained. Peptides were cleaved from resin by treatment with 92.5% TFA, 3% water, 3% ethanedithiol, and 1.5% triisopropylsilane.

Peptide **3.3a** was synthesized at room temperature on NovaPEG Rink Amide Resin using a Protein Technologies, Inc. Tribute automated peptide synthesizer. The synthesis proceeded in the same couple-wash-deprotect cycle as stated above with the following exceptions. Couplings were performed for 50 minutes with 7 equivalents of amino acid relative to resin. Natural amino acids were preactivated with HCTU (7 equivalents to resin) and N-methylmorpholine (14 equivalents to resin) in DMF for 2 minutes. Unnatural residues were preactivated with PyBOP (7 equivalents to resin) and N-methylmorpholine (14 equivalents to resin) in DMF for 2 minutes. Deprotections were performed in 2 iterations of 4.5 minutes each. The peptide was cleaved from resin by treatment with 95% TFA, 2.5% water, and 2.5% triisopropylsilane.

Lactam-cyclized peptide **3.2b** was prepared via on-resin cyclization.[156] A linear precursor was assembled on resin bearing 4-methyltrityl (Mtt) group at Lys_{31} and a phenylisopropyl ester (OPip) at Asp_{27}. Following assembly of the protected chain, but prior to N-terminal Fmoc deprotection, the resin was washed five times with dichloromethane. The resin was then subjected to treatment with 3% TFA acid and 5% triisopropylsilane in dichloromethane for 5

min. The procedure was repeated three times to achieve removal of the Mtt and OPip groups. The resin was then washed three times with DMF, treated with PyBOP (1 equivalent to resin) and DIEA (1.5 equivalents to resin) in NMP and subjected to the microwave coupling program described above. This procedure was repeated twice to form the desired lactam cross-link between Asp_{27} and Lys_{31}. Following cyclization, the N-terminal Fmoc group was removed and the peptide cleaved from resin by treatment with 92.5% TFA, 3% water, 3% ethanedithiol, and 1.5% triisopropylsilane.

Following cleavage of peptides **3.1**, **3.2a-3.4a** and **3.2b** from resin, the crude peptide was precipitated in cold diethyl ether and pelleted by centrifugation. The ether was decanted, and the resulting pellet dissolved in water and acetonitrile with 0.1% TFA. Purification was performed by HPLC on a Luna C18 preparative column using gradients between 0.1% TFA in water and 0.1% TFA in acetonitrile. Peptide identity and purity were determined by MALDI-TOF mass spectrometry (**Table 4**) and analytical RP-HPLC (**Figure 41**), respectively.

Table 4. MALDI-TOF data for peptides **3.1**, **3.2a-3.4a** and **3.2b-3.4b**.

	$[M+H]^+$ (*m/z*)	
Peptide	**Calculated**	**Observed**
3.1	4151.3	4151.1
3.2a	4138.2	4138.0
3.2b	4122.7	4122.4
3.3a	4146.8	4146.0
3.3b	4146.8	4146.5
3.4a	4212.3	4212.3
3.4b	4163.2	4163.0

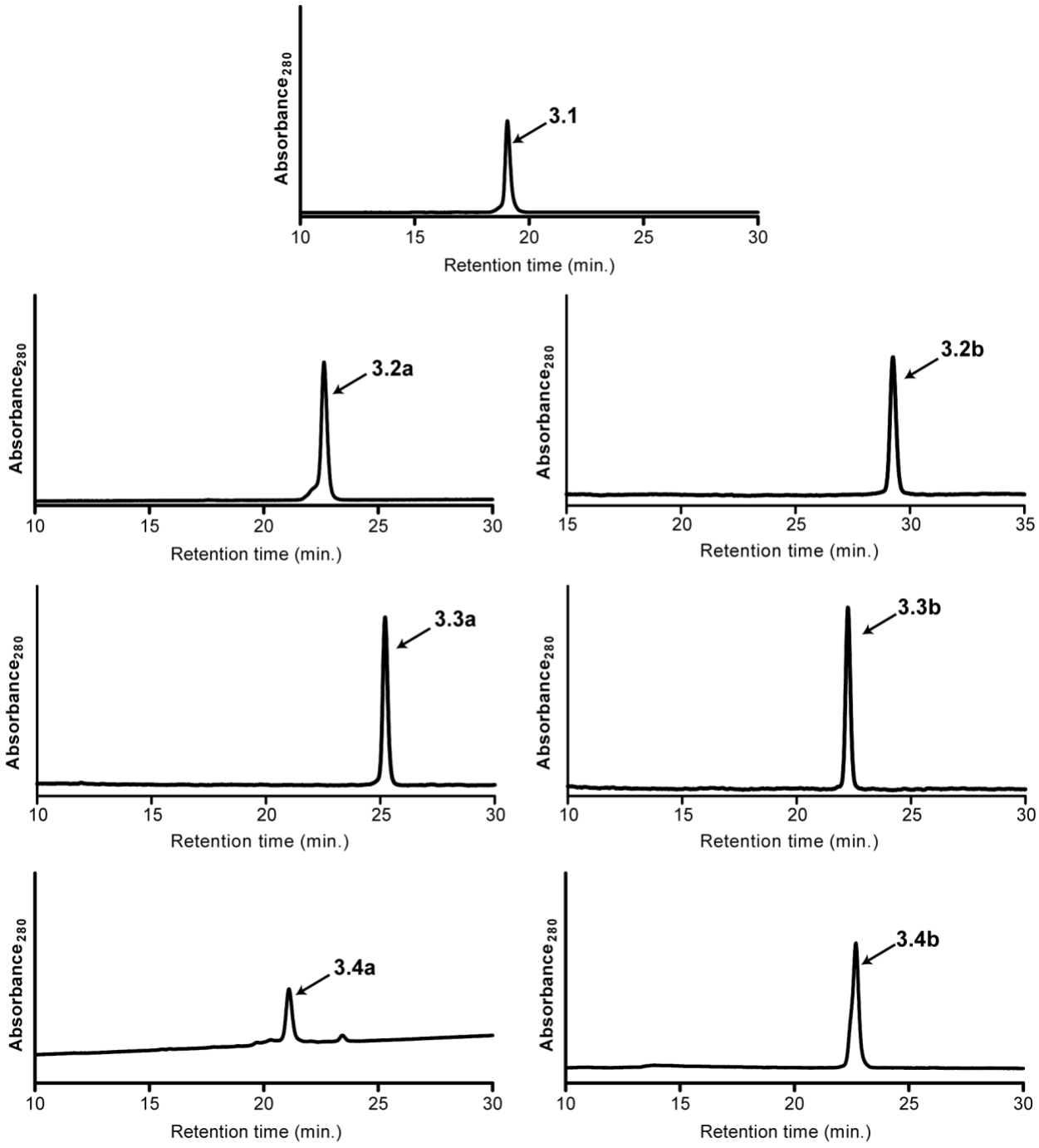

Figure 41. Analytical HPLC chromatograms of purified peptides **3.1, 3.2a-3.4a** and **3.2b-3.4b.** This figure is adapted from ref. [121] with permission from The Royal Society of Chemistry.

Triazole-cyclized peptide **3.3b** was prepared from purified peptide **3.3a** by copper(I)-mediated azide-alkyne cycloaddition in solution.[133] Pure, lyophilized **3.3a** and CuSO4•5H2O (4.4 equivalents) were dissolved in 2:1 water:tert-butanol (v/v) to give a final peptide concentration of 2 mg/mL. Sodium L-ascorbate (4.4 equivalents) dissolved in water was added in 4 portions over the course of 1 hour. The reaction was placed on a shaker at room temperature for 30 minutes following completion of ascorbate addition. Then product **3.3b** was purified by preparative HPLC. This procedure was repeated as necessary to obtain sufficient purified **3.3b** for subsequent biophysical analysis.

Oxime-cyclized peptide **3.4b** was prepared from purified **3.4a** by treatment with aqueous sodium periodate.[18, 138] Pure, lyophilized **3.4a** was dissolved in water and its concentration determined by UV-Vis spectroscopy (ε_{280} = 5690 M^{-1} cm^{-1} based on Trp absorbance).[163] A stock of sodium periodate was prepared in water and the concentration determined by UV-Vis spectroscopy (ε_{280} = 317 M^{-1} cm^{-1}).[164] Oxidation and cross-link formation was performed by dilution of the peptide stock with water, buffer, and periodate to a final concentration of 100 μM peptide in 100 mM pH 7 phosphate buffer with 1 equivalent periodate in a total volume of 2 mL. The reaction was allowed to stand for 15 minutes, then product **3.4b** was purified by preparative HPLC. This procedure was repeated to obtain sufficient purified **3.4b** for characterization.

3.4.3 Molecular Modelling

Molecular modelling of the cross-linked helices shown in **Figure 36** was carried out using Spartan'10 (Wavefunction Inc.). Coordinates for the VHP domain were obtained from a published crystal structure (PDB 3TRW).[165] The C-terminal helix was extracted from chain A in that structure (acetyl N-terminus, methyl amide C- terminus). All atoms were frozen except for

the side chains of Gln_{27} and Lys_{31}, which were deleted and rebuilt to correspond to the lactam, triazole, or oxime cross-link present in **3.2b-3.4b**. A Monte Carlo equilibrium conformation search was performed for each model with the MMFFaq force field. The lowest energy conformer obtained for each cross-link is shown in **Figure 36**.

3.4.4 Circular Dichroism Spectroscopy and Data Analysis

Stock solutions of peptides **3.1**, **3.2a-3.4a** and **3.2b-3.4b** were prepared in water, and the concentration of peptide was determined by UV-Vis spectroscopy (ε_{280} = 5690 M^{-1} cm^{-1}).[163] Samples for CD analysis were prepared by dilution of the peptide stock with water and buffer stocks to yield solutions consisting of 50 μM peptide in 50 mM pH 7 phosphate buffer with the appropriate quantity of guanidinium chloride.

CD scans were performed from 200-260 nm with 1 nm step size, 2 nm bandwidth, and 5 second integration time at each wavelength. CD melts were performed by monitoring molar ellipticity at 222 nm over the range of 2 °C to 95 °C in 3 °C increments, with a dead band of 0.5 °C and a 2 minute equilibration time at each temperature. All measurements were baseline corrected against a buffer blank measured in the same cell. Scans were smoothed by the Savitsky-Golay method using GraphPad Prism. Thermal melts of samples lacking guanidinium were fit to a two-state thermal denaturation model using GraphPad Prism to obtain T_m values.[166] Cyclic peptides **3.2b-3.4b** failed to reach a fully unfolded state over the temperature range measured. T_m values for these sequences were determined by constraining the unfolded baselines based on data for the corresponding linear sequence **3.2a-3.4a**. Raw data from thermal-chemical denaturation experiments were fit using Mathematica 8 (Wolfram) and equations reported previously.[159]

4.0 MODULAR SYNTHESIS, FOLDING, AND FUNCTION OF BACKBONE-MODIFIED UBIQUITINS

Chemical modification is a versatile tool that scientists can use to probe the structure and function of proteins. One modification approach involves the synthesis of heterogeneous-backbone foldamers, which have shown promise as structural and functional mimics of their natural protein counterparts. This approach has previously been shown to recapitulate the structures of two natural proteins; however, to date it has not been applied to design a large heterogeneous-backbone foldamer protein mimic with significant biological function. In an effort to fill this knowledge gap, we report here the design, synthesis, and functional characterization of a library of heterogeneous-backbone ubiquitin variants. Nine backbone-modified variants of the native protein were synthesized in a modular fashion through native chemical ligation and desulfurization techniques. Circular dichroism (CD) spectroscopy indicated the library of variants adopt folds similar to that of wildtype ubiquitin. In collaboration with the Brodsky lab in the Biological Sciences Department at the University of Pittsburgh, the variants were assessed for biological function. Four variants successfully ubiquitinated chaperone protein Hsc70 *in vitro* and were then subjected to a more complex ubiquitination and retrotranslocation assay. All four variants were able to ubiquitinate a transmembrane protein, and three conclusively facilitated its retrotranslocation from a biological membrane to the cytosol.

These results represent the first examples of highly-unnatural, yet functional heterogeneous-backbone foldamers larger than 50 residues.

4.1 INTRODUCTION

Proteins play a crucial role in life, and thus have sustained great interest across many fields. One approach toward understanding the folding and function of proteins is through global or localized modification of their structure to introduce artificial covalent connectivity. In addition to providing valuable insights into the protein structure-function relationship, such modification can be used to impart benefits including increased cell permeability,[167-169] resistance to proteases,[25, 170-171] structural stability,[121, 172-174] and improved bioactivity.[175-176] The degree of protein modification can vary from the replacement of a single amino acid residue,[177] to the complete stereochemical inversion of an L-protein to its D-protein counterpart.[178] A moderate approach toward modifying proteins involves blending a fraction (20-30%) of the natural L-amino acids with unnatural counterparts, which generates a "heterogeneous-backbone" foldamer.[27]

Heterogeneous-backbone foldamers, in contrast with *de novo*-designed modified proteins,[179] are derived from natural protein sequences. Through a process called sequence-based design, a portion of the L-α-amino acids in a natural sequence are replaced with unnatural amino acids. Early work focused on mimicry of isolated secondary structures such as α-helices[35, 89, 180-183] and β-hairpins,[116, 184-185] then advanced to mimicry of various secondary structures in the context of a larger tertiary fold.[117, 119, 186-187] Our group has recently achieved structural mimicry of all secondary structures in two tertiary folds: the 56-residue protein GB1,[40] and the 28-residue zinc-finger protein sp1-3.[24] Moving beyond structural mimicry, the Gellman group has reported

heterogeneous-backbone foldamers that successfully recapitulate the functions of several natural peptides and proteins smaller than 40 residues, including parathyroid hormone,[39, 188-189] a phase-derived VEGF mimic,[41, 190] and glucagon-like peptide 1.[42]

Inspired by these promising examples, our goal has been to develop a general approach for the design of heterogeneous-backbone tertiary folds with predictable structural propensities and functional properties. In pursuit of this approach, we have produced prototype principles for the sequence-based design of backbone-modified proteins that retain the structures of their natural protein counterparts.[21] However, we have not yet utilized these principles to achieve structural *and* functional mimicry of a protein larger than 56 residues. The goal of the work described in this chapter is to further develop our design principles by applying them to ubiquitin, a medium-sized protein with a complex range of functions. We employed these principles to design and synthesize a library of backbone-modified ubiquitin variants, some of which are structurally and functionally comparable to the natural protein. In addition to validating current design principles, these results are expected to guide their refinement and future application to the sequence-based backbone modification of other proteins.

4.2 SYSTEM DESIGN

We decided to target ubiquitin protein because it: 1) is of a medium-length (76 residues), 2) is amenable to preparation by total chemical synthesis,[177, 191-192] 3) adopts a complex fold with a variety of secondary structures, and 4) has many essential and diverse biological functions, some of which are measurable. First, we designed a "WT" ubiquitin (WT_{chem}) with two side-chain point mutations: Met1Nle to avoid methionine oxidation, and Phe4Tyr to facilitate chromophoric

detection. We then designed two heterogeneous-backbone ubiquitin variants—one conservatively designed, and one ambitiously designed—each containing about 15-20% unnatural residues (**Figure 42**).

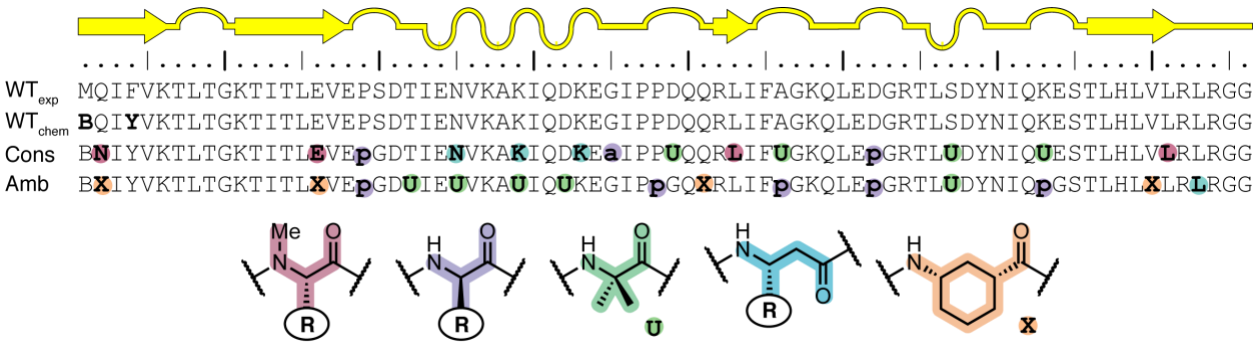

Figure 42. Secondary structure map of ubiquitin with sequences of wildtype ubiquitin (WT_{exp}), chemically synthesized ubiquitin (WT_{chem}), the conservative design variant (Cons), and the ambitious design variant (Amb). Side-chain point mutations are bolded in the WT_{chem} sequence (**B** = norleucine). Unnatural residues in the variant sequences are highlighted with circles, which are color-coded to the residue structures (below). Side-chain R groups, when present, are indicated by the single letter code of the corresponding α-amino acid.

When deciding how to modify the backbone of ubiquitin, we carefully considered several of its structural and functional features, as detailed in the following sections.

4.2.1 Structural and Functional Considerations

The tertiary structure of ubiquitin contains an α-helix, a short 3/10-helix, a 4-stranded β-sheet, and 6 β-turns; the fold is held together by a 14-residue hydrophobic core[193] and several intramolecular polar contacts (**Figure 43**).

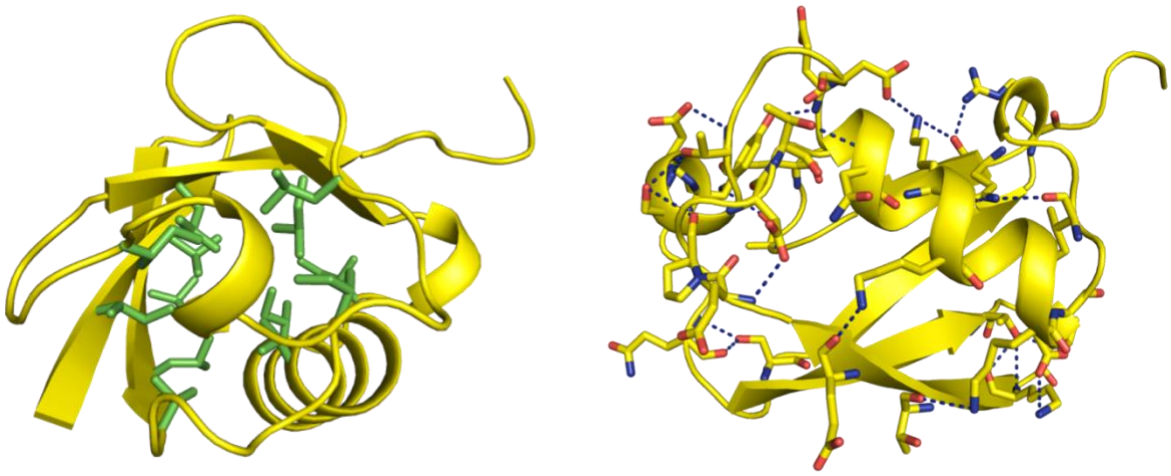

Figure 43. Hydrophobic core (left) and intramolecular polar contacts (right) present in ubiquitin. Green = hydrophobic core sidechains, red = oxygen atoms, blue = nitrogen atoms. PDB: 1UBQ.

Our first structural design consideration was to keep as many of these intramolecular interactions as possible intact, thus reducing the possibility of disrupting the native tertiary structure. Interestingly, the tertiary fold of ubiquitin is somewhat similar to protein GB1 (**Figure 44**), which our lab has mimicked successfully in previous work.[40, 117, 119, 186-187]

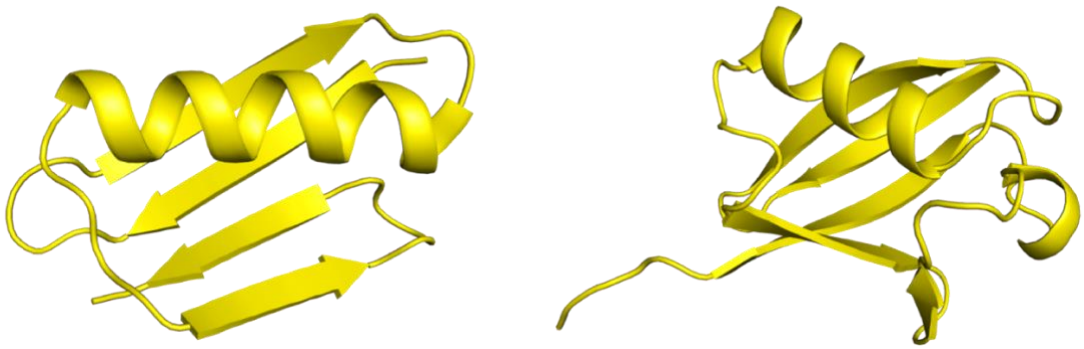

Figure 44. Tertiary fold comparison of GB1 (left, PDB: 2QMT) and Ubiquitin (right, PDB: 1UBQ).

Thus, our conservative design for ubiquitin backbone modification is based on our first successful heterogeneous-backbone mimic of GB1.[40] We decided to incorporate β^3-residues in

the α-helix in an iterative *i*→*i+4* substitution pattern, *N*-Me-residues in the sheet regions, and Aib residues or D-Pro-Gly dipeptides in the turns. Unlike GB1, ubiquitin contains a 3/10-helix, design principles for which our group has not yet established. Previous studies have shown that short peptide sequences containing Aib residues adopt 3/10-helical conformations.[194-196] Thus, after a dihedral angle analysis of the four residues in the 3/10-helix, we hypothesized that a Ser57Aib replacement would likely be accommodated.

Our design of the ambitious ubiquitin variant was derived from findings in later work on GB1 mimics. The α-helix contains Aib residues, which were previously shown to be most favorably accommodated in α-helices.[117] In other studies, our group determined that Acc, a γ_{cyc}-residue (note: this residue is distinct from the cyclic β-residue ACC in Chapter 1), was well-tolerated in a small hairpin peptide[184] and in the β-sheet of GB1.[186] Accordingly, we planned to incorporate four Acc residues into ubiquitin, one in each strand of the β-sheet. Though our group and others have previously modified tight turns in many systems,[40, 185, 197-198] generalizable design principles for the mimicry of turn secondary structures have remained elusive. Thus, the riskiest aspect of the ambitious variant design is the decision to include D-Pro-Gly in 5 of the 6 ubiquitin turns. This decision was partly inspired by a functional consideration from our earlier work (Chapter 2),[25] which suggested D-residues are most effective in preventing proteolytic digestion.

Because the primary side chain sequence of a protein dictates its folding and subsequent function, we must consider the presence or absence of side chains in the unnatural residues we are employing. *N*-Me-, D-, and β^3-residues are able to retain the native side chains of ubiquitin, but Acc residue replacement always involves the loss of a side chain. While substituting Aib for an alanine residue preserves the native methyl side chain, replacement of any other residue with

Aib will result in side chain deletion. Thus, it is important to note that our conservative and ambitious designs retain 93% and 84% of the native side chains displayed by ubiquitin, respectively. This further highlights a need for new classes of unnatural residues that are able to preserve the side chain functionalities of native sequences.

Preserving the function of ubiquitin was a priority in the design of the foldamer mimics. Ubiquitin serves an important cellular role, primarily in the tagging and degradation of misfolded proteins.[199] A trio of enzymes, the ubiquitin cascade enzymes, attach ubiquitin through its C-terminus onto misfolded or extraneous proteins (**Figure 45**).

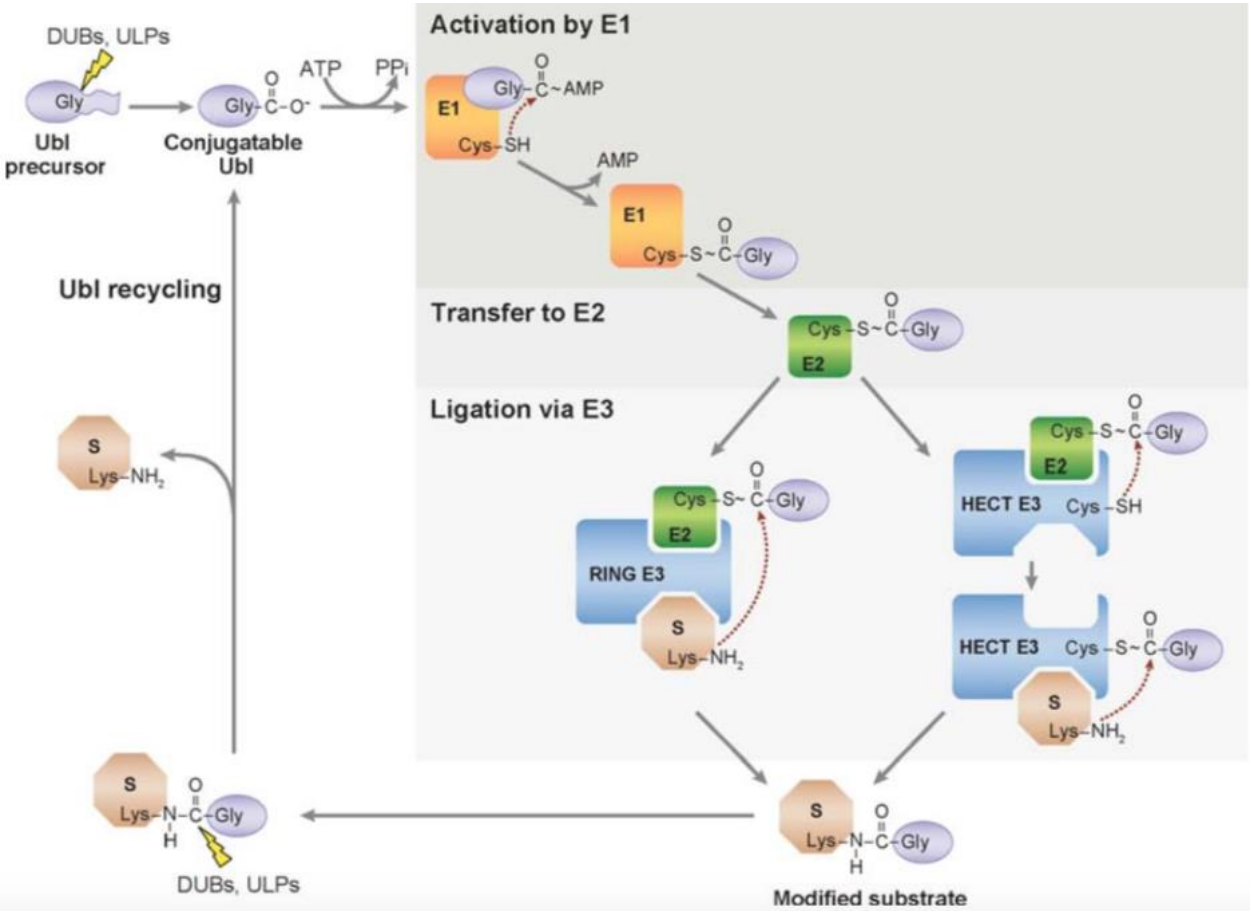

Figure 45. Ubiquitin is attached to a protein substrate by the ubiquitin cascade enzymes (E1, E2, and E3). This figure is adapted from reference [200] with permission from Annual Reviews.

First, a ubiquitin activating enzyme (E1) activates the C-terminus of ubiquitin for nucleophilic attack. A cysteine residue on a ubiquitin conjugating enzyme (E2) then forms a thioester bond with ubiquitin. Finally, a ubiquitin ligase (E3) recruits the target protein and ubiquitinates it, either alone (HECT-type), in combination with an E2 enzyme (RING-type), or through the recruitment of a multi-protein complex (ex. SCF-type). After monoubiquitination occurs, the cascade enzymes facilitate the polymerization of ubiquitin onto the substrate, termed polyubiquitination. The various functions of ubiquitin are determined by the characteristics of polyubiquitin chains (**Figure 46**), which are formed through isopeptide bonds between the C-terminus of one ubiquitin and a lysine residue (or N-terminus) of another.

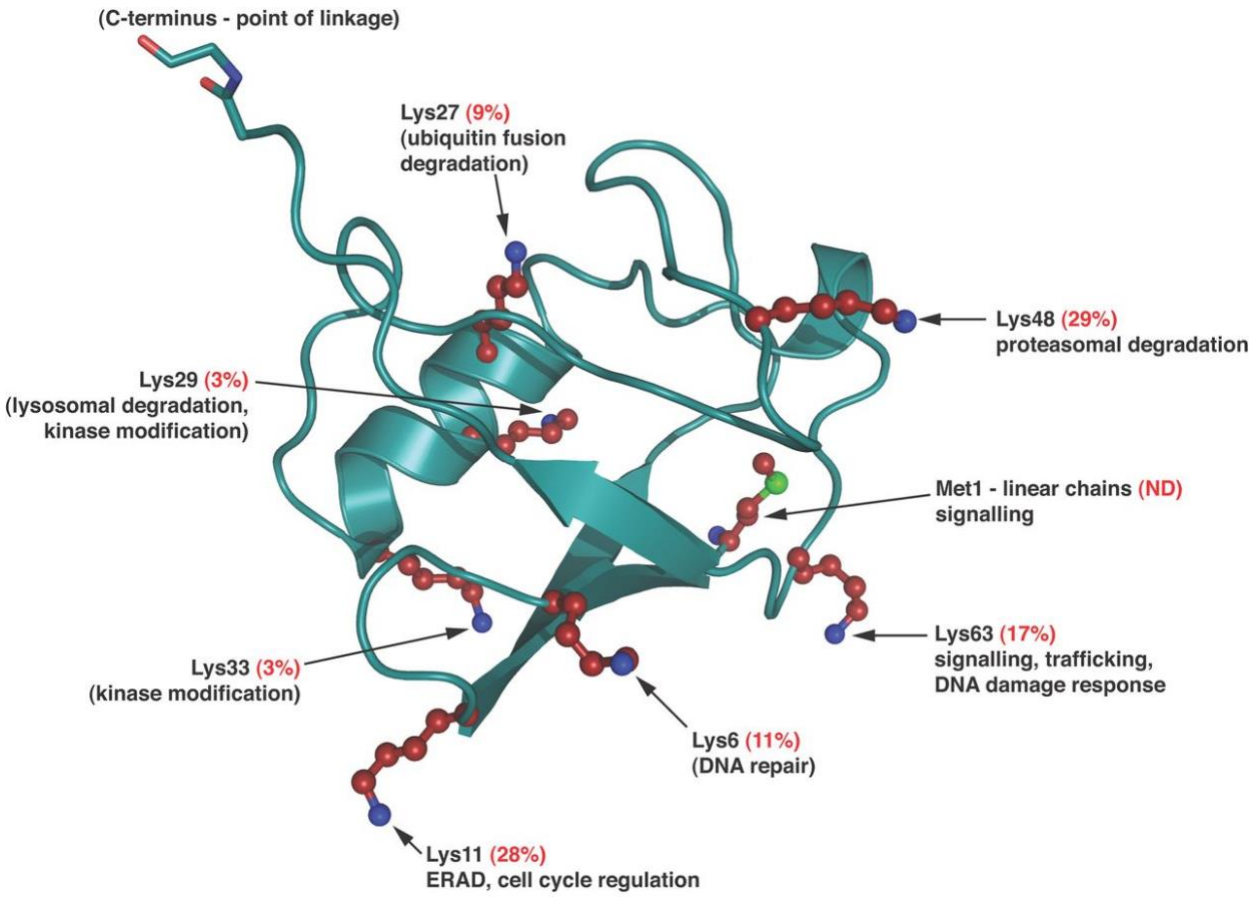

Figure 46. The function of ubiquitin is determined by the nature of its lysine-linked polyubiquitin chains. This figure is adapted from reference [201] with permission from Portland Press Publishing.

We considered these functional aspects during the design of our ubiquitin variants. We first avoided modifications at the C-terminus, where ubiquitin is attached to ubiquitin cascade enzymes as well as target proteins. To preserve the possibility for polyubiquitination, we aimed to maintain the 7 lysine sidechains in ubiquitin; however, we had to make some exceptions. First, while the β^3-residues used in helices in the conservative design retain the lysine sidechain, the Aib residues of the ambitious design do not. We attempted to mitigate this by shifting the Aib substitution pattern to avoid the lysines but were unable to avoid modifying Lys_{29}. Second, Lys_{63} exists at the center of a tight turn, which we modified in both designs. Finally, we sought to preserve the interactions that occur between ubiquitin and the enzymes that process it. Thus, we thoroughly inspected over 50 published crystal structures of complexes between ubiquitin and E1, E2, and E3 enzymes. Among these structures, we catalogued polar contacts and hydrophobic binding areas between ubiquitin and the enzymes (**Figure 47**).

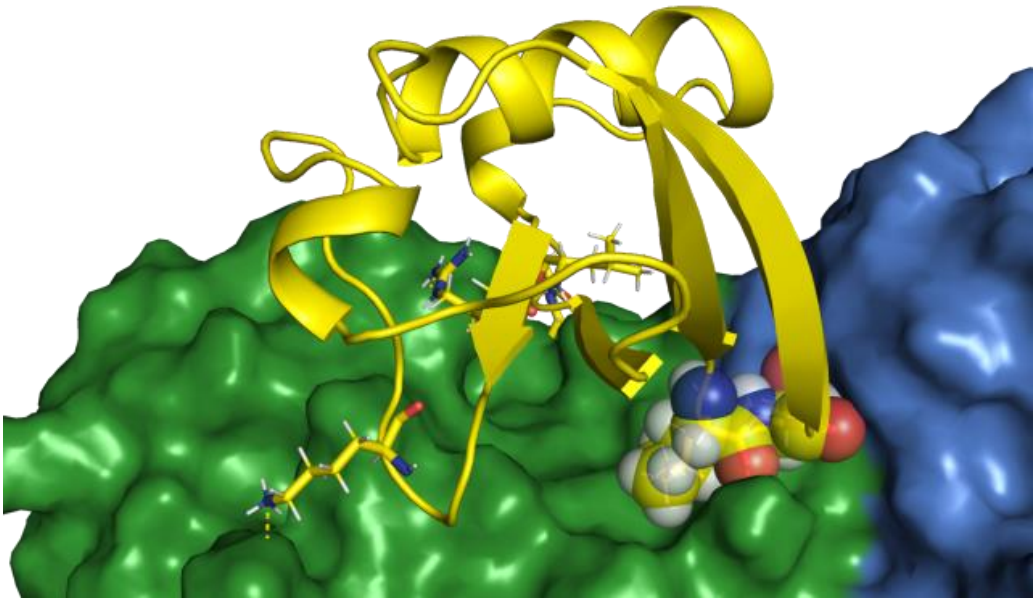

Figure 47. Example analysis of ubiquitin (yellow) complexed with ubiquitin-conjugating enzyme E2 D2 (green) and E3 RING finger protein 165 (blue). Note the burial of the N-terminal turn (TLTG, spheres) at the interface of the E2 and E3 enzymes, and the Arg_{42} side chain polar contact with the E2 enzyme. PDB: 5D0M.

We then identified the most common areas of interaction, avoiding modification of those areas in ubiquitin. For example, we did not modify the first turn of ubiquitin (TLTG) because it frequently appeared to be buried in hydrophobic pockets of the enzymes (**Figure 47**). This highlights the importance of exposed hydrophobic surfaces in protein-protein recognition events,[202] such as those between ubiquitin and the cascade enzymes. We also preserved the side chain of Arg_{42}, which makes a polar contact with all three enzymes in several crystal structures (**Figure 47**). Many other examples of these hydrophobic and polar interactions exist, and we judiciously considered them in our design efforts.

4.2.2 Synthetic Considerations

The sizes of protein targets pursued by our group to date have been limited by our synthetic approach; Fmoc-solid phase synthesis methods can only generate sequences up to ~50 residues long before overall yields begin to suffer. Chemical synthesis of proteins larger than 50 residues generally requires chemoselective ligation techniques, such as native chemical ligation (NCL).[203] Briefly, NCL couples two peptide fragments together using a sulfur nucleophile—typically a cysteine residue—followed by an S→N acyl shift, which forms a native amide bond (**Figure 48**).

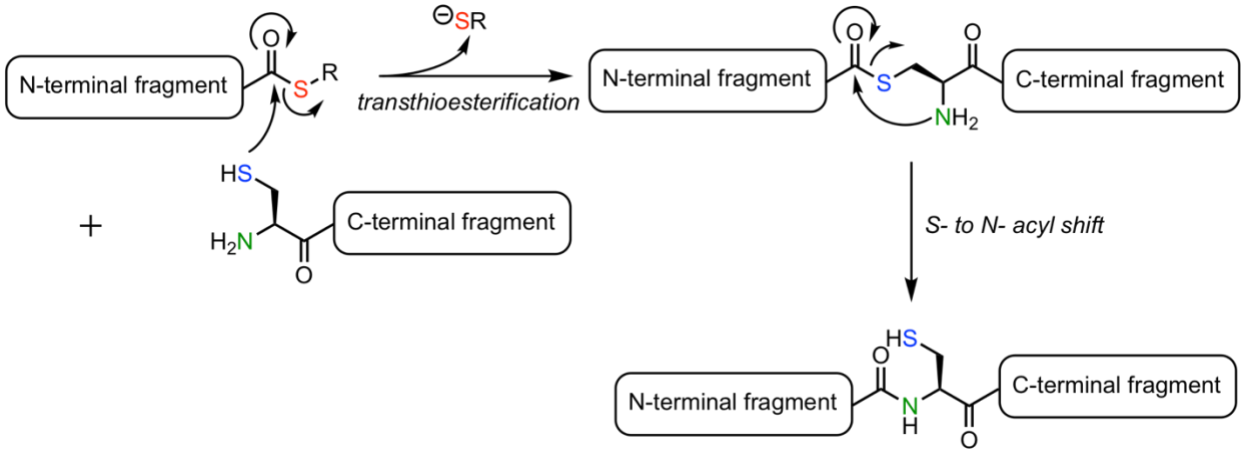

Figure 48. Generalized native chemical ligation mechanism. A transthioesterification couples the N- and C-terminal protein fragments together, then an intramolecular S→N acyl shift generates an amide bond. R = alkyl or aryl group.

For target protein sequences that lack a cysteine, such as ubiquitin, a desulfurization reaction can be used to transform the resulting cysteine to an alanine.[204] There are two potential ligation sites in the sequence of ubiquitin that would allow for simple Cys→Ala desulfurizations: the first at Lys_{27}—Ala_{28}, and the second at Phe_{45}—Ala_{46}. We elected to use the former because we wished to use peptide hydrazides as thioester surrogates;[205] to our knowledge, a peptide hydrazide larger than 40 residues has not been reported. Finally, in both designs we avoided modification near the proposed ligation site (K27-A28). The closest unnatural residues to this ligation site are at least 2-3 amino acids away. This decision was inspired by unpublished work in which we observed reduced reaction rates when unnatural residues were incorporated at—or even 2 residues away—from the ligation site.

We envisioned the following retrosynthetic scheme to generate ubiquitin and variants (**Figure 49**).

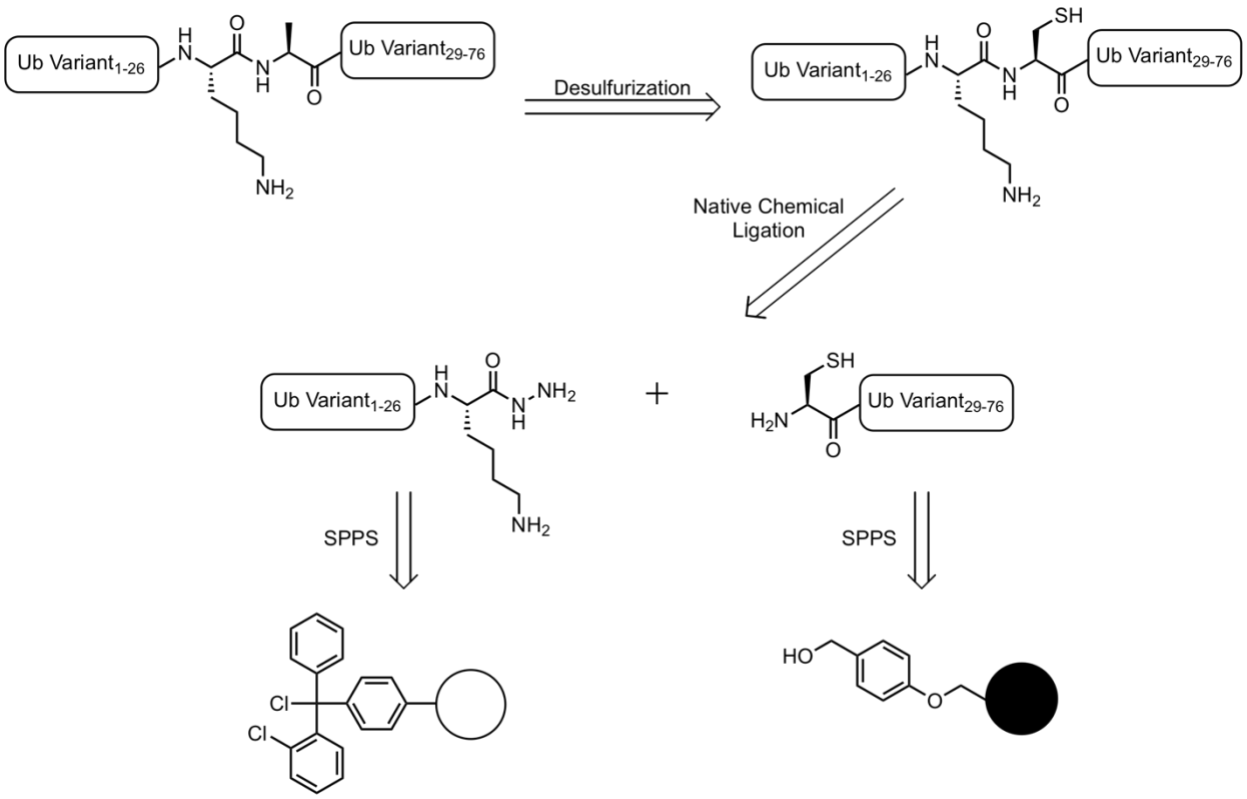

Figure 49. Retrosynthetic scheme showing the proposed synthesis of WT_{chem} and ubiquitin variants. The circles represent the polymeric solid supports of the peptide synthesis resins. SPPS = solid phase peptide synthesis, open circle = polystyrene, filled circle = NovaPEG.

Full-length ubiquitin and variants can be achieved by desulfurization of the corresponding Cys28Ala precursor, which is the product of a native chemical ligation reaction. The two peptide fragment starting materials for this ligation can be generated via Fmoc solid-phase peptide synthesis methods. The left-hand (N-terminal) thioester fragments can be prepared from a hydrazine-functionalized 2-chlorotrityl chloride polystyrene resin; upon cleavage, this generates a peptide hydrazide that can be subsequently converted to the thioester *in situ*.[205] The nucleophilic right-hand (C-terminal) fragments can be synthesized on a NovaPEG Wang Resin.

Finally, while NCL and other ligation techniques have been used to chemically synthesize many proteins with various post-translational modifications,[206] these methods have not yet been used to synthesize a heterogeneous-backbone protein. In addition to closing this gap in the literature, a significant advancement of this work is the modularity of our synthetic approach, which showcases the potential of native chemical ligation to generate backbone-modified protein libraries. While this type approach has accomplished divergent syntheses of natural proteins,[207] to our knowledge it has not yet been used to synthesize highly-modified proteins such as the ones we generate herein.

4.3 RESULTS AND DISCUSSION

Comparing the structure and function of wildtype (WT) ubiquitin with that of the backbone-modified ubiquitin variants enables rigorous examination of our design principles. After synthesizing and characterizing WT and variant ubiquitins by CD spectroscopy, we submitted them to the lab of Jeffrey Brodsky (University of Pittsburgh, Biological Sciences) for biological assays.

4.3.1 Modular Synthesis of Ubiquitin Variant Library

WT_{chem} ubiquitin was synthesized by native chemical ligation, using the peptide hydrazide thioester-masking approach (**Figure 50**).[205]

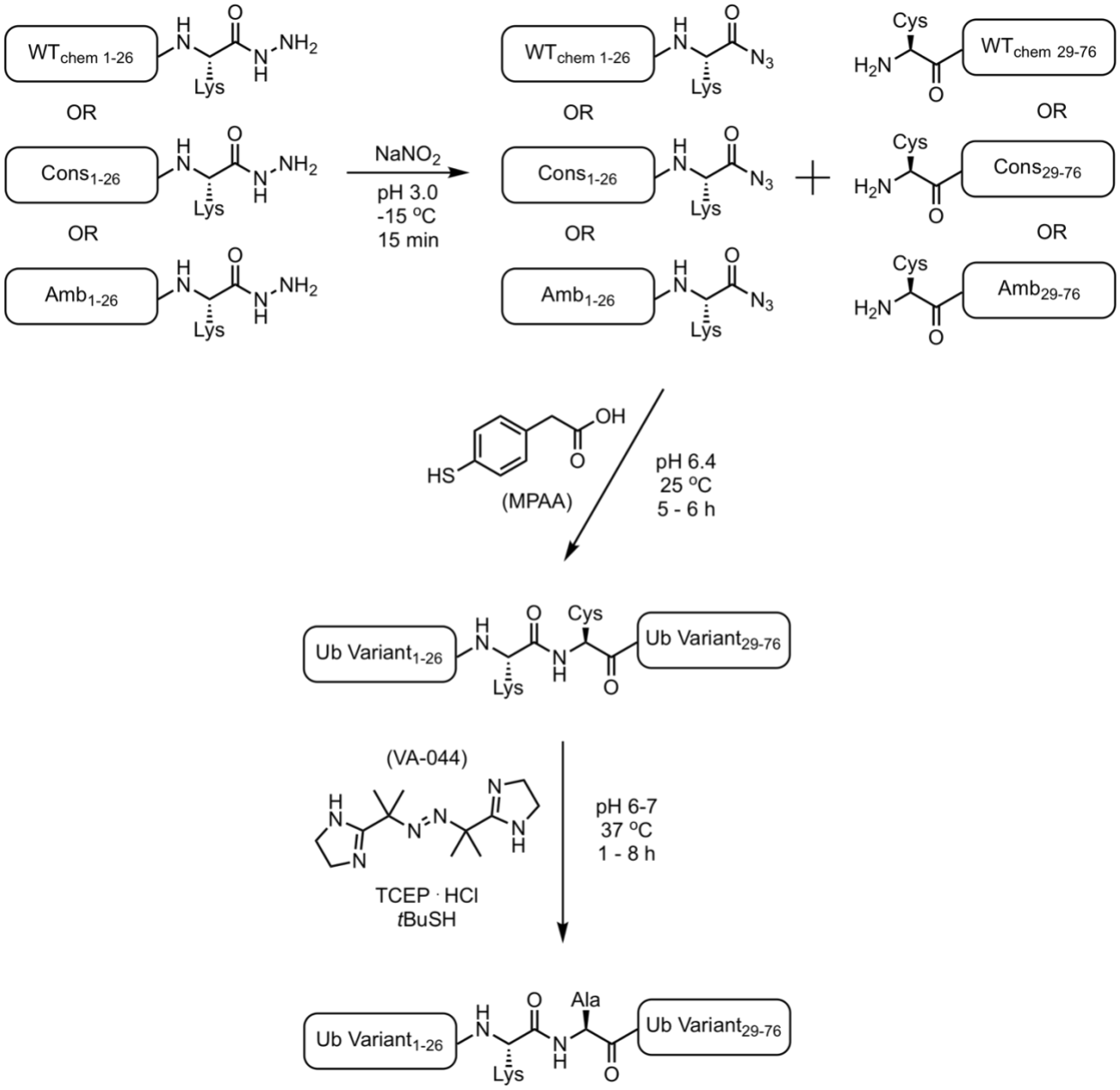

Figure 50. Scheme for the synthesis of ubiquitin variants. One of three N-terminal fragments is first oxidized, then an aryl thiol (MPAA) and one of three C-terminal fragments are added to the reaction simultaneously. The resulting A28C protein is isolated and purified by RP-HPLC, then subjected to a radical-mediated desulfurization, which restores the native alanine sidechain.

The N-terminal and C-terminal fragments—containing an acyl hydrazide and a cysteine, respectively—were synthesized by Fmoc solid phase peptide methods. In one-pot, the acyl hydrazide was oxidized to an acyl azide, converted to an aryl thioester, and the two fragments were ligated together in phosphate buffer at room temperature. Notably, the pH of this ligation is critical to reaction success; a ligation pH of 6.8 or 6.0 resulted in the formation of a byproduct that significantly reduces the yield of desired product. By mass, the byproduct appears to be an intramolecular cyclization of the lysine ε-NH_2 onto the thioester of the N-terminal fragment (**Figure 51**).

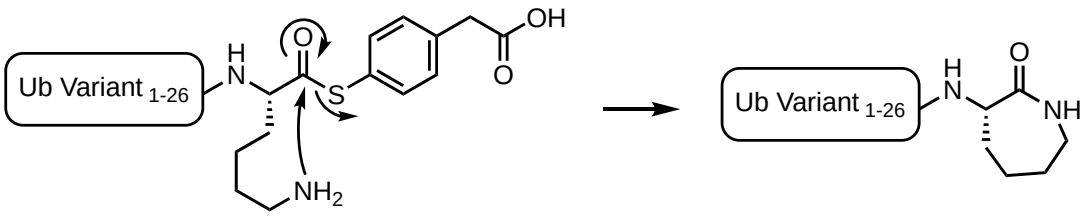

Figure 51. Intramolecular cyclization of the lysine sidechain onto the terminus of the N-terminal peptide fragment resulted in a byproduct.

While the intramolecular cyclization at higher pH (6.8) can be explained by the increased nucleophilicity of the side chain amine, the same byproduct formation at pH 6.0 is somewhat puzzling. We suspect that at a pH < 6.4, the cysteine nucleophilicity is reduced to a sufficient extent that the competing intramolecular cyclization becomes favored over the intermolecular coupling of the two fragments. Allowing the ligation to proceed at pH 6.4 for roughly 5 hours generates the full-length ubiquitin sequence with an Ala28Cys mutation. The native alanine was then restored via radical-mediated desulfurization techniques.[204] Reaction progress and product

purity were assessed by RP-HPLC, and product identity was confirmed by MALDI-TOF-MS (Section 4.5).

With a reliable synthesis for WT_{chem} in hand, we shifted focus to our heterogeneous-backbone ubiquitin designs. Pursuing all possible combinations of the three N- and C-terminal fragments—i.e. WT_{chem}, Cons, and Amb—results in eight ubiquitin variants in addition to WT_{chem} ubiquitin (**Figure 52**).

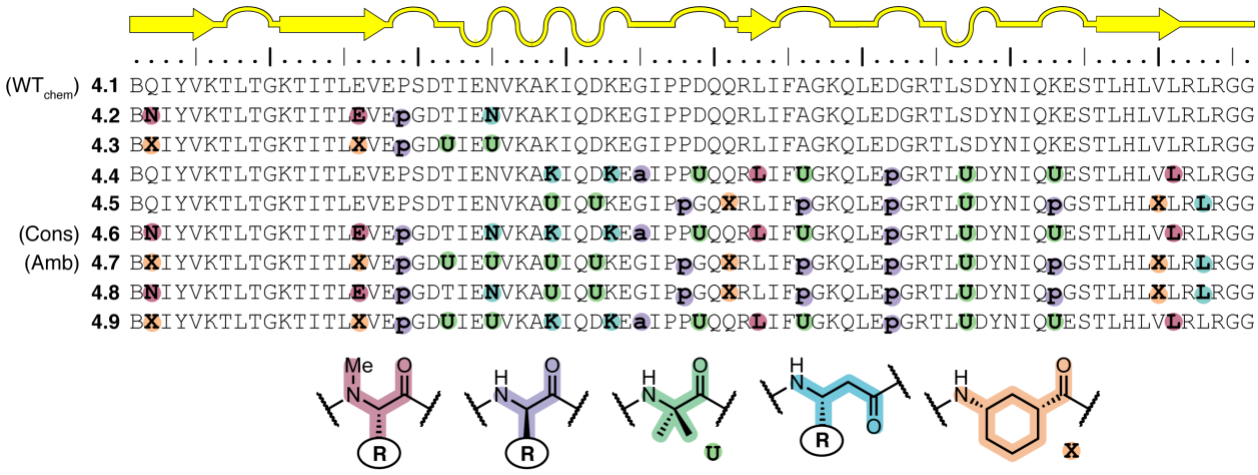

Figure 52. Full library of ubiquitin variants synthesized in this work. Note that proteins **4.1**, **4.6**, and **4.7** are the designed proteins WT_{chem}, Cons, and Amb, respectively (see **Figure 42**). Side-chain R groups, when present, are indicated by the single letter code of the corresponding α-amino acid.

Thus, we proceeded to synthesize the remaining eight proteins by the same route as WT_{chem} (**4.1**) ubiquitin. We first ligated and desulfurized the backbone-modified fragments with the WT_{chem} fragments to generate four "chimera" variants (**4.2**-**4.5**). Combining only the backbone-modified fragments with each other furnish four fully-modified variants: our two original designs (Cons, **4.6** and Amb, **4.7**), and two N-/C-terminal swapped analogs (**4.8** and **4.9**). While there were noticeable differences among the reaction rates of the nine syntheses, no clear trends emerged.

Importantly, the route was able to generate sufficient material of all nine proteins for biophysical and biological characterization.

4.3.2 Examination of Folding by CD Spectroscopy

The structures of WT and variant ubiquitins were characterized through circular dichroism (CD) spectroscopy. While CD signatures can provide qualitative evidence of natural protein structure, comparative analyses become complicated when applied to proteins with modified backbones. Because CD spectroscopy involves a chiral light source, the presence of non-L-α-amino acids in a protein can alter its CD signature. Consequently, the CD signature of a backbone-modified protein can appear distinct from its natural counterpart even if the two proteins have similar folds. For example, the inclusion of β-residues in a helix-bundle quaternary structure resulted in an atypical helical signature with a single minimum at 205 nm.[180] Thus, it is important to consider that an unusual signature could be the result of either an altered fold or the presence of unnatural residues. With this consideration in mind, we were cautious in our comparisons of WT and variant ubiquitin CD signatures.

We first compared the CD signatures of expressed ubiquitin with that of chemically synthesized WT, **4.1** (**Figure 53**).

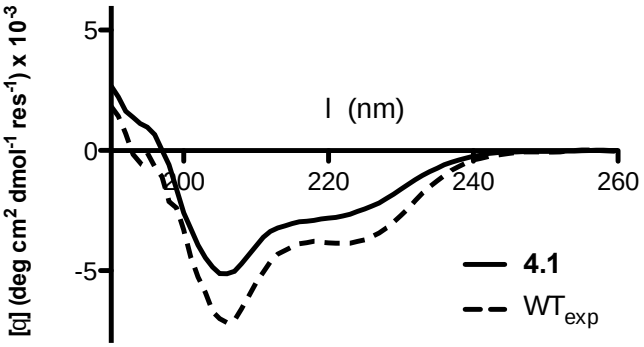

Figure 53. CD scans of chemically synthesized and expressed ubiquitin.

While the 206 and 222 nm minima are less intense in **4.1** compared with WT_{exp}, the qualitative similarities between the two signatures suggest that they have similar tertiary folds. The small differences may arise from the two side chain alterations (Met1Nle, Phe4Tyr).

We next examined the CD signatures of the chimera ubiquitin proteins (**Figure 54**).

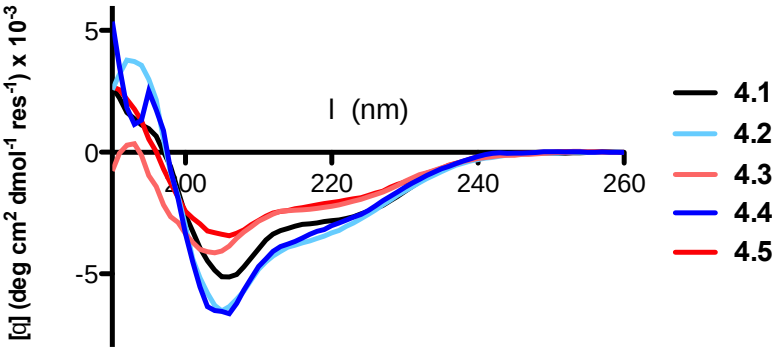

Figure 54. CD scans of chimera ubiquitin variants.

While some differences exist among the chimera variants, we were pleased to see that all signatures show some semblance of structure. Signatures of variants **4.3** and **4.5** show diminished and slightly blue-shifted minima, yet they remain qualitatively similar to that of

WT_{exp} and **4.1**. This suggests that though their tertiary structure may be somewhat perturbed, these variants likely resemble the natural fold of ubiquitin. On the other hand, signatures of variants **4.2** and **4.4** appear to be qualitatively distinct, with enhanced minima at 206 nm (relative to **4.1**) but without a corresponding increase at 222 nm. It is encouraging that the 206 nm minimum is nearly as large in magnitude as WT_{exp}. Though it is tempting to attribute this enhanced minimum solely to β^3-residue incorporation, variants **4.2** and **4.4** only contain one and two β^3-residues, respectively. Thus, we suspect that there may be multiple factors contributing to the dissimilar signatures we observe for the conservative design chimeras.

Finally, we analyzed the CD data for the fully-modified ubiquitin variants (**Figure 55**).

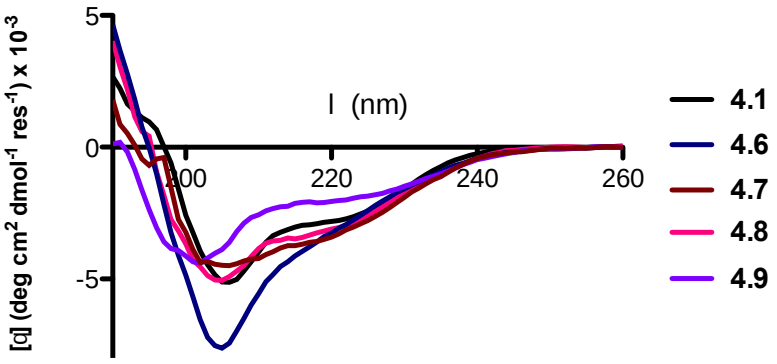

Figure 55. CD scans of fully-modified ubiquitin variants.

Like the chimera variants, the fully-modified ubiquitin variants also appeared to be structured. Variant **4.9** is least like WT_{exp} and **4.1**, with decreased minima intensities and a strongly blue-shifted minimum near 200 nm. While the shape of the signature still indicates some folding, the strong shift toward 200 nm suggests that some population of this variant may exist as a random coil. Variant signatures for **4.7** and **4.8** have intensities similar to **4.1**; however, the signature shape of variant **4.7** appears most disparate from all others. It is notable that this variant has the

most unnatural backbone among all variants. While it is possible that the atypical signature is the result of unnatural amino acid content, an alternative explanation could be the existence of increased β-sheet character. Remarkably, the signature of variant **4.6** shows a 206 nm minimum that is nearly identical to WT_{exp}. Though the shape of the signature is slightly different from that of WT ubiquitin, we were encouraged by the similarities of the spectra.

Initially, we expected that some of the variants would not be folded. Gratifyingly, while perhaps slightly different from the tertiary fold of ubiquitin, it appears that all variants possess some structure. This observation suggests that our design principles are valid and can successfully generate heterogeneous-backbone foldamers that mimic the structure of their natural counterparts.

4.3.3 CHIP E3 Ligase Ubiquitination *in vitro* Assay

After determining that all synthesized variants were structured in solution, we were curious to assess their function. Collaborating with the Brodsky lab, we subjected all variants to an *in vitro* ubiquitination assay. In this ATP-dependent assay, the C-terminus (residues 395-646) of chaperone protein Hsc70 (previously shown to be modified by CHIP) is polyubiquitinated by Ube1 (E1), UbcH5b (E2), and CHIP, a RING-type E3 ubiquitin ligase.[208] The extent of $Hsc70_{395\text{-}646}$ ubiquitination is then detected by Western blotting (for the GST-tag on $Hsc70_{395\text{-}646}$). A reaction using a commercial isolate of WT ubiquitin serves as a positive control, and a reaction without the ATP necessary to drive ubiquitination is a negative control. We tested the ability of our ubiquitin variants to ubiquitinate $Hsc70_{395\text{-}646}$ by adding them to the assay instead of expressed ubiquitin. From these experiments, we determined that variants **4.1**, **4.2**, **4.4**, and **4.6**

ubiquitinated $Hsc70_{395-646}$ to varying degrees, while **4.3**, **4.5**, **4.7**, **4.8**, and **4.9** did not mono- or polyubiquitinate $Hsc70_{395-646}$ to any observable extent (**Figure 56**).

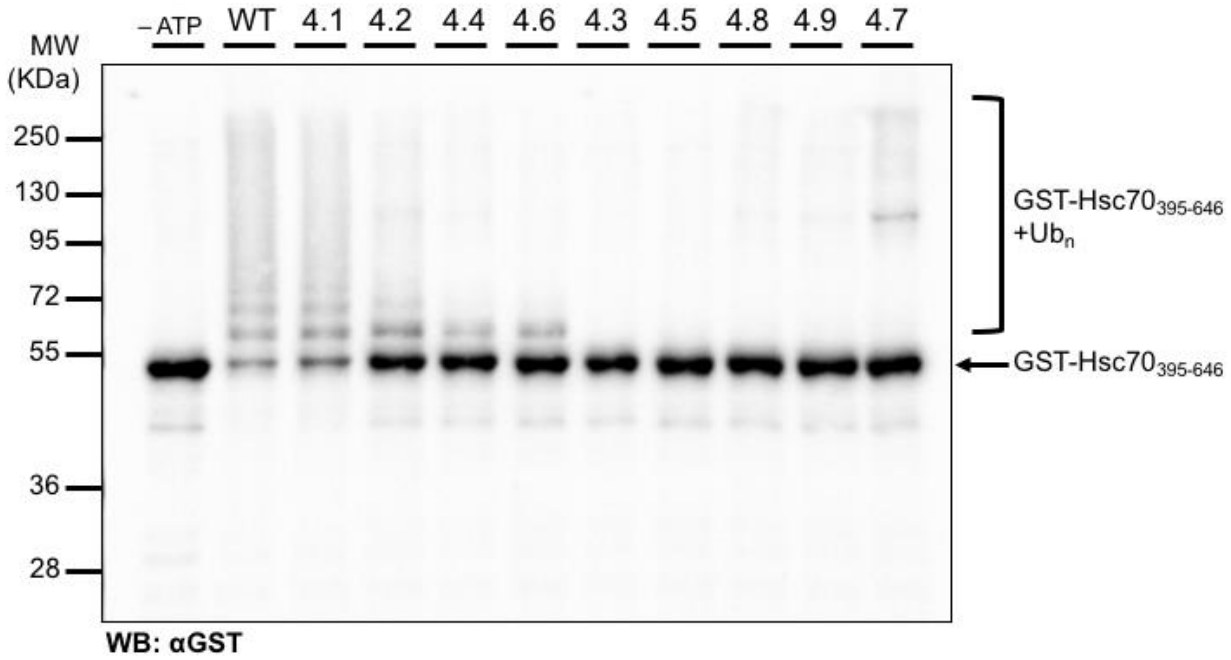

Figure 56. Representative substrate western blot of ubiquitination reactions with expressed and variant ubiquitins.

We were pleased to see that synthetic ubiquitin (**4.1**) and a commercial isolate of WT ubiquitin (WT) exhibited nearly identical substrate polyubiquitination activity. Ubiquitin variant **4.2** also polyubiquitinated the substrate, albeit to a lesser extent than **4.1**. Interestingly, while ubiquitin variants **4.4** and **4.6** successfully monoubiquitinated substrate, they were unable to form significant amounts of polyubiquitinated $Hsc70_{395-646}$. However, these two variants did show minor amounts of diubiquitination in the western blot (**Figure 57**).

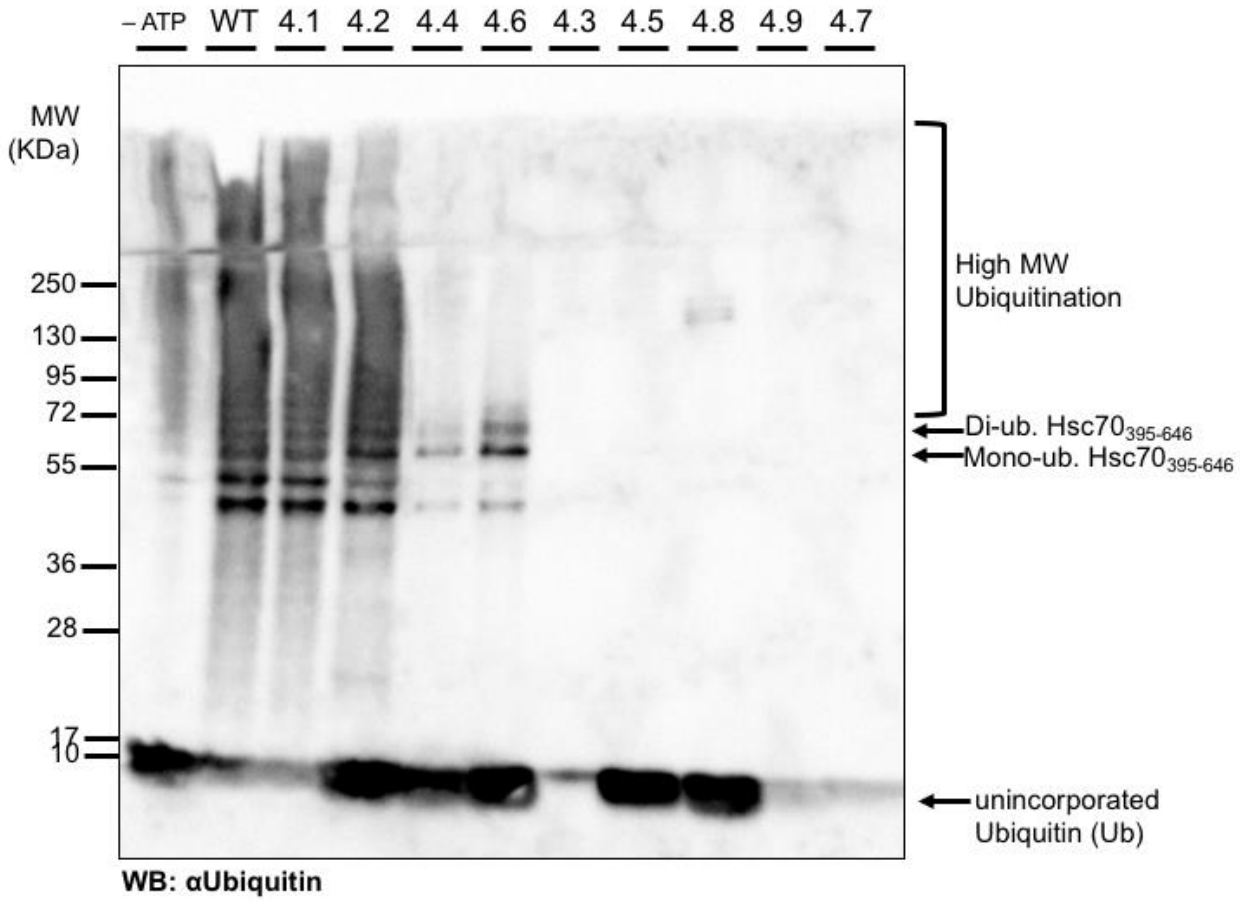

Figure 57. Representative total ubiquitination western blot of reactions with expressed and variant ubiquitins.

Unfortunately, we observed poor solubility in the case of variant **4.7**, which precipitated upon being added to the reaction. As a band for monoubiquitination is not observed for **4.7**, the higher molecular weight species present in the substrate blot are likely the result of aggregation rather than of polyubiquitination (**Figure 56**). It is noteworthy that the α-ubiquitin polyclonal antibody was less efficient in recognizing variants **4.3, 4.7,** and **4.9**. Considering this observation together with the CD data (**Figures 54** and **55**), we suggest that these variants are least structurally comparable to native ubiquitin.

Our qualitative observations prompted us to quantitatively compare the extent of ubiquitination among variants. To accomplish this, we quantified the relative amounts of unubiquitinated, monoubiquitinated, and polyubiquitinated $Hsc70_{395\text{-}646}$ in replicate reactions by densitometric analysis of the scanned gel images (**Figure 58**).

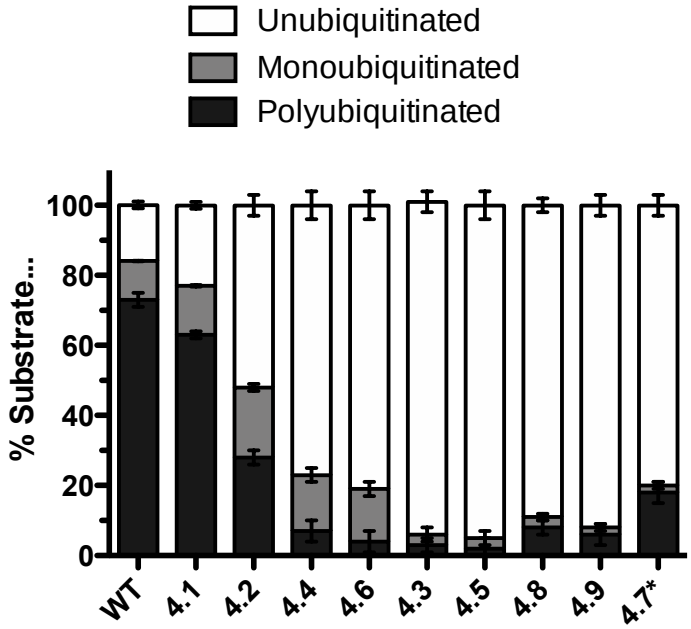

Figure 58. Percentage of Hsc70$_{395-646}$ (substrate) that is unubiquitinated, monoubiquitinated, and polyubiquitinated for each reaction. *Poor solubility of variant **4.7** resulted in an overestimation of polyubiquitinated substrate. Error bars represent the range of the data.

The quantitative data corroborate our qualitative observations: WT ubiquitin and variant **4.1** polyubiquitinate Hsc70$_{395-646}$ to a similar extent, and variant **4.2** to a lesser extent. A minor amount of polyubiquitination is observed with variants **4.4** and **4.6**, but a significant amount of Hsc70$_{395-646}$ is monoubiquitinated. For all successful ubiquitination reactions (WT, **4.1**, **4.2**, **4.4**, and **4.6**), the relative amounts of monoubiquitinated Hsc70$_{395-646}$ are similar.

Our next goal was to investigate the reason for the disparities in polyubiquitination efficiency among variants. We identified the presence or absence of the K_{63} side chain as one possible source of the observed differences. While WT, **4.1**, and **4.2** all contain K_{63}, it is replaced with an Aib residue in variants **4.4** and **4.6**. We hypothesized that the loss of sidechain at this site in variants **4.4** and **4.6** may preclude polyubiquitination by the particular set of ligases employed

in the assay. We were fortunate to be provided a set of Lys→Arg mutant ubiquitins from the lab of Philip Cole (Harvard) to test this hypothesis. For these experiments, we used K48R, K63R, or K48,63R as the ubiquitin source to determine their relative abilities to ubiquitinate $Hsc70_{395-646}$ (**Figure 59**).

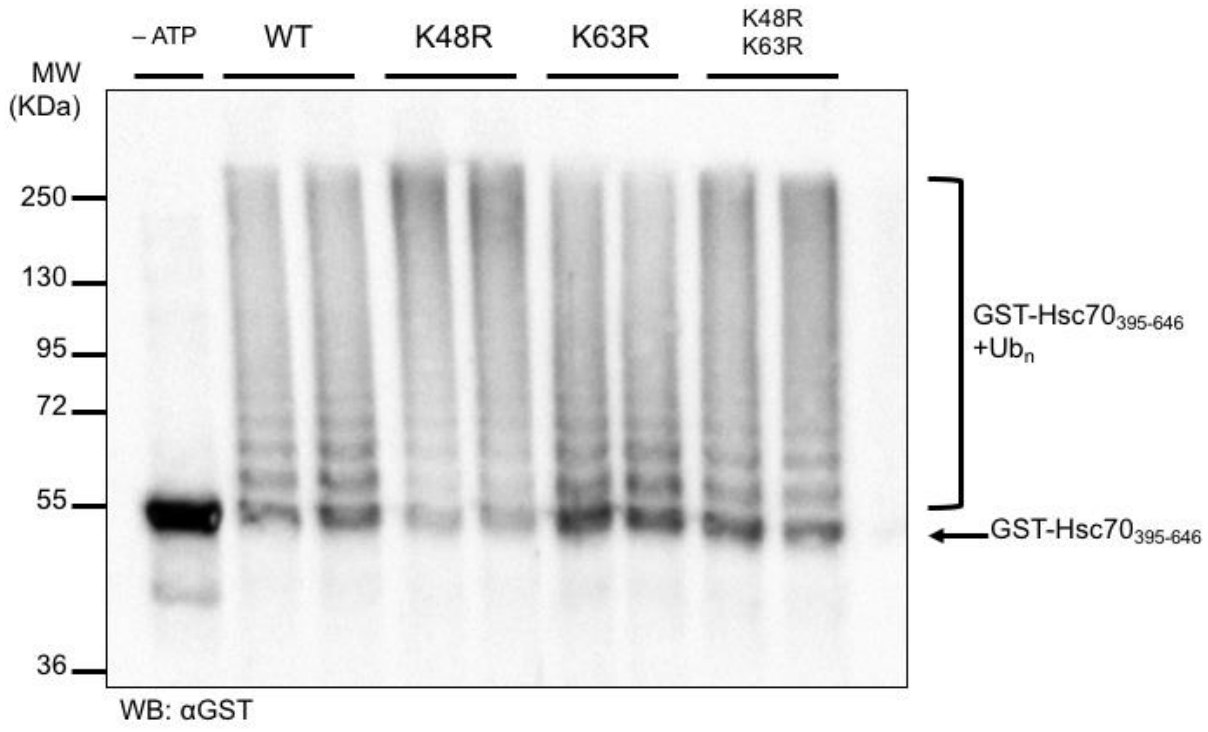

Figure 59. Substrate western blot of ubiquitination reactions with K48R, K63R, or K48,63R mutant ubiquitin proteins.

UbcH5b and CHIP did not show a preference for either K_{63}- or K_{48}-linked polyubiquitin chains. Even the double replacement of both K_{48} and K_{63} resulted in polyubiquitin chains linked through any of the five remaining lysines in the sequence. Thus, our hypothesis was refuted, and the origin of the lack of polyubiquitination by variants **4.4** and **4.6** remains unclear. We suspect that these variants may have structural topology differences that are imperceptible by CD

spectroscopy, but sufficient to disrupt polyubiquitination by UbcH5b and CHIP due to the high selectivity of enzymes in the ubiquitin pathway for substrates and ubiquitin over other highly related ubiquitin-like proteins.

4.3.4 *in vitro* Ubiquitin Conjugation and Retrotranslocation

To further examine functional capabilities of the ubiquitin variants that mono- or polyubiquitinated $Hsc70_{395-646}$ in the CHIP assay, we subjected **4.1, 4.2, 4.4,** and **4.6** to an *in vitro* assay that monitors the ubiquitin-mediated degradation of a misfolded transmembrane protein in the endoplasmic reticulum (ER).[209] After being polyubiquitinated, the substrate is "retrotranslocated" or extracted from the ER membrane and can be delivered for proteasome-dependent degradation. It is important to note the major difference in complexity between these experiments and the CHIP assay. While both are performed *in vitro*, this assay more accurately mimics cellular conditions, containing multiple E3 ubiquitin ligases in addition to other biological machinery such as molecular chaperone complexes that recognize misfolded proteins. In these experiments, radiolabeled (^{125}I) ubiquitin variant was added to a reaction containing cytosol, an ATP regenerating system (or apyrase in negative control), and microsomes displaying the misfolded membrane protein Chimera A*. After incubation, the reactions were separated into solid and liquid components, which contain membrane-bound and cytosolic species, respectively. The extent of membrane protein ubiquitination (**Figure 60A**) and retrotranslocated membrane protein in the cytosol (**Figure 60B**) was visualized by radioactive imaging of each ^{125}I-ubiquitin variant.

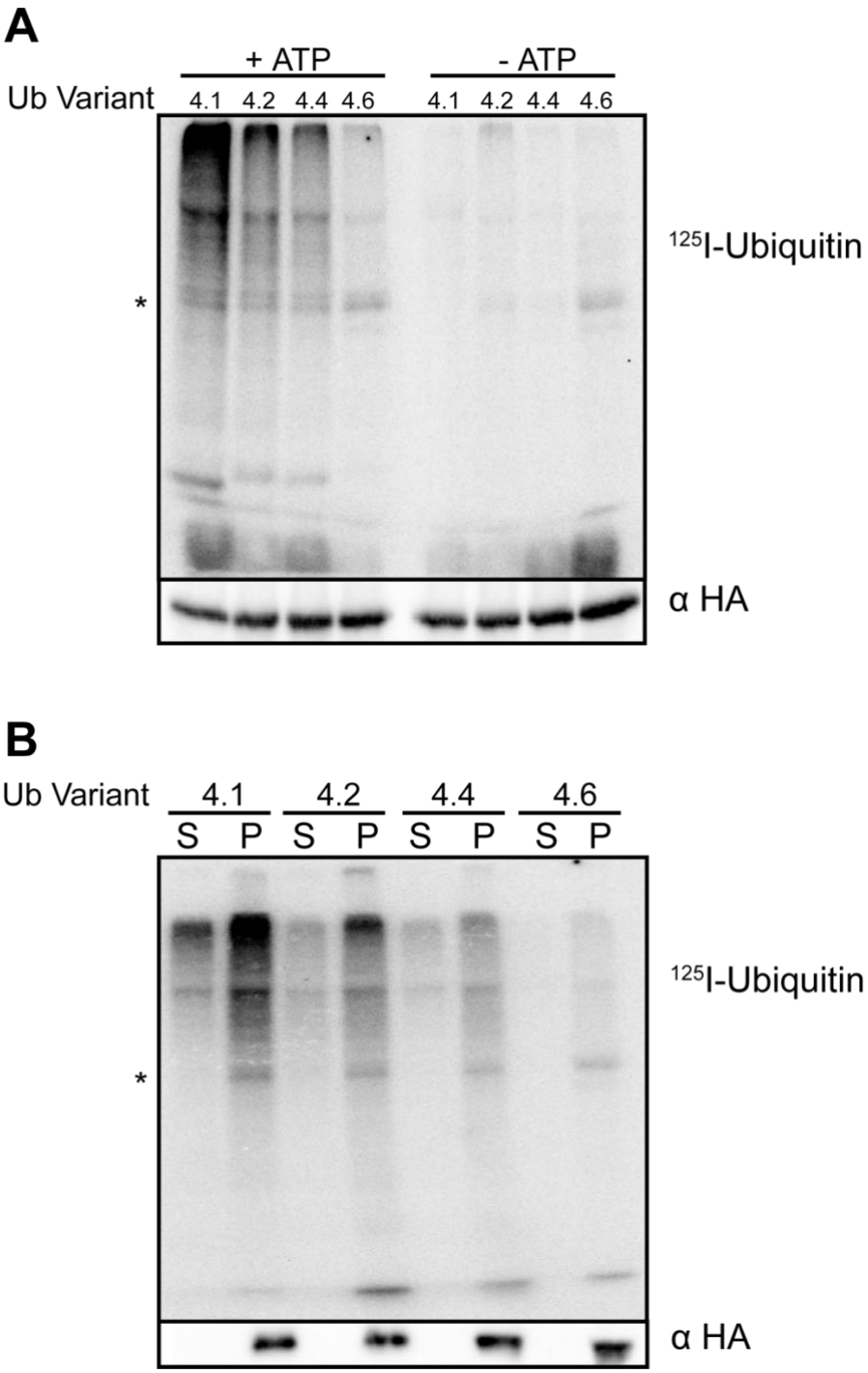

Figure 60. Ubiquitination and retrotranslocation of Chimera A* by ubiquitin variants **4.1**, **4.2**, **4.4**, and **4.6**. * = relative molecular weight of Chimera A*. Bottom portions of gels represent western blots for Chimera A*. A) Total reaction ubiquitination observed for each ubiquitin variant (+ATP) and negative control reactions containing apyrase (-ATP). B) Ubiquitinated Chimera A* retrotranslocated to the cytosolic supernatant (S), and ubiquitinated Chimera A* remaining in the microsomal membrane pellet (P) after centrifugation.

Remarkably, all tested variants successfully ubiquitinated membrane-bound Chimera A*, albeit to varying extents. The amount of ubiquitination appears to be inversely correlated with the percentage of modified backbone in each variant. In **Figure 60B**, we see in reactions with variants **4.1**, **4.2**, and **4.4** that an observable fraction of ubiquitinated Chimera A* is retrotranslocated to the supernatant (S) cytosol. Unfortunately, as the signal for **4.6** is already faint in the total reaction (**Figure 60A**), the corresponding retrotranslocation results are inconclusive. It is unclear whether the signal is absent because the amount retrotranslocated is below the detection threshold, or because retrotranslocation did not occur.

It is imperative to consider the complexity of this assay when assessing the significance of these results. In contrast to the CHIP assay, in which ubiquitin variants were processed by the three added enzymes, the E1, E2, and E3 ubiquitin ligase CHIP, a positive result from this assay indicates that our variants have been recognized by myriad proteins. As in nature, ubiquitination can occur by many possible combinations of E1, E2, and E3 enzymes, many of which are present in these reactions. For retrotranslocation to occur, a polyubiquitin chain of at least four linked ubiquitins must be recognized by a large chaperone complex, which then removes Chimera A* from the membrane. It is noteworthy that our variants, which contain 5-18% unnatural residues, can successfully participate in this many molecular recognition events. Additionally, the observed ubiquitination by **4.4** and **4.6** and retrotranslocation of Chimera A* by **4.4** call into question the negative results observed in the CHIP assay. Perhaps the variants deemed "unsuccessful" in the CHIP assay could successfully mono- and polyubiquitinate a substrate in the presence of other E2 and E3 enzymes that were lacking in the CHIP assay.

4.4 CONCLUSIONS

In summary, we successfully synthesized a library of nine ubiquitin variants through a modular approach of native chemical ligation and desulfurization techniques. While CD scans of these nine variants resulted in varying signatures, all proteins appeared to attain tertiary structures similar to that of ubiquitin. All nine variants were then subjected to a simple ubiquitination assay with purified E1, E2, and an E3 enzyme, where proteins **4.1**, **4.2**, **4.4**, and **4.6** were able to successfully ubiquitinate a known substrate ($Hsc70_{395\text{-}646}$) of this pathway, albeit to different degrees. Expressed WT ubiquitin and **4.1** showed identical ubiquitination profiles, variant **4.2** polyubiquitinated substrate to a lesser extent, and variants **4.4** and **4.6** only monoubiquitinated substrate. We then submitted these four active variants to a more complex *in vitro* assay, measuring their ability to ubiquitinate and facilitate retrotranslocation of a misfolded transmembrane protein (Chimera A*) from a biological membrane. While all four variants successfully ubiquitinated Chimera A*, only variants **4.1**, **4.2**, and **4.4** conclusively facilitated Chimera A* retrotranslocation.

This work represents a significant milestone in the mimicry of natural proteins by heterogeneous-backbone foldamers. We successfully applied our backbone-modification design principles to a larger and functionally complex protein. However, while our principles have proven valid for effective structural mimicry, they appear to need further refinement if we wish to use them for functional mimicry. Notably, all variants derived from only our conservative (or WT_{chem}) design showed some level of function, while variants containing any part of our ambitious design appeared folded but unable to function. This observation sheds light on an important discrepancy; a positive CD scan result indicating folding does not necessarily translate to a functional protein. Our results suggest that more structural information than a CD scan may

be necessary to determine the potential of a backbone-modified protein to mimic the function of its natural counterpart.

4.5 EXPERIMENTAL

4.5.1 Materials

Solvents and reagents were purchased from Sigma Aldrich, Baker, EMD Millipore, Fisher, Acros Organics, Alfa Aesar, or ChemImpex, and used as received. The Fmoc-protected monomer for installation of Acc was synthesized as previously described.[210] MALDI-TOF mass spectrometry was performed on a Bruker ultrafleXtreme instrument. Circular dichroism spectra were recorded on an Olis DSM17 spectrometer equipped with a Peltier temperature controller using quartz cuvettes of 0.1 cm path length. Preparative, semi-preparative, and analytical HPLC were performed on Phenomenex Jupiter C18 columns using gradients between 0.1% TFA in water and 0.1% TFA in acetonitrile.

His-Ube1,[211] His-CHIP,[212] and GST-Hsc70$_{395\text{-}646}$[212] were expressed and purified from BL21(DE3) competent cells (New England Biolabs) for *in vitro* ubiquitination assays with ubiquitin variants. pET21d Ube1 were provided by Dr. Cynthia Wolberger (Addgene plasmid #34965[211]). pET151/D-TOPO CHIP and pGSTǁ2 Hsc70$_{395\text{-}646}$ were obtained from Dr. Saurav Misra.[208] Transformed cells were cultured in Luria broth (LB) + 100 μg/mL ampicillin at 37 °C 225 rpm until reaching an OD600 of 0.3, then induced with 500 μM isopropyl β-D-1-thiogalactopyranoside (IPTG), incubated for 24 hrs. at 15-18 °C, and subsequently harvested at

8000xg. Cell pellets were stored at -80 °C. Ubiquitin variants K48R, K63R, and K48,63R were provided by Dr. Philip Cole.

4.5.2 Fragment Synthesis and Purification

N-terminal ubiquitin fragments were synthesized on 2-chlorotrityl chloride resin as previously described[205] with microwave heating (MARS microwave reactor, CEM). 2-chlorotrityl chloride resin was activated twice with 5% hydrazine monohydrate in DMF (v/v) for 30 minutes each at 30 °C. Unactivated resin sites were then capped with 5% methanol in DMF (v/v) for 10 minutes at room temperature. Amino acid couplings were performed with 5 equivalents of amino acid to resin. Fmoc-protected amino acids were preactivated with HCTU (5 equivalents to resin) and DIEA (7 equivalents to resin) in NMP for 2 minutes. The preactivated amino acid was then added to the resin in a reaction vessel equipped with a stir bar, and a microwave program consisting of a 1.5 minute ramp to 90 °C followed by a 2 minute hold at 90 °C was run. The resin was washed with DMF, DCM, then DMF and treated with 20% 4-methylpiperidine in DMF using a microwave deprotection program consisting of a 1.5 minute ramp to 90 °C followed by a 1 minute hold at 90 °C. The resin was washed with DMF, DCM, then DMF, and the above cycle was repeated until the desired peptide chain was obtained. Peptides were cleaved from resin by treatment with 90% TFA, 8% water, and 2% triisopropylsilane for 3 hours.

C-terminal ubiquitin fragments were synthesized at room temperature on NovaPEG Wang Resin using a Protein Technologies, Inc. Tribute automated peptide synthesizer. The resin was loaded by adding Fmoc-Gly-OH (5 equivalents), N,N'-diisopropylcarbodiimide (5 equivalents), and 4-dimethylaminopyridine (0.1 equivalents) to the NovaPEG Wang resin suspended in anhydrous DMF. The suspension was stirred for 3.5 hours at room temperature.

The resin was acetyl-capped with 4-dimethylaminopyridine (2 equivalents) and acetic anhydride in anhydrous DMF (10% v/v) for 10 minutes at room temperature. The resin was rinsed with DMF, DCM, and methanol, and dried in a desiccator overnight. Resin loading was determined by a spectrophotometric method in which a portion of resin was deprotected with 4-methylpiperidine, and the absorbance of the subsequent dibenzofulvene-4-methylpiperidine adduct (ε_{300} = 6234 M^{-1} cm^{-1}) was measured. The synthesis proceeded in the same couple-wash-deprotect cycle as stated in the above paragraph with the following exceptions. Couplings were performed for 50 minutes at room temperature with 5 equivalents of amino acid relative to resin. Fmoc-protected amino acids were preactivated with HCTU (5 equivalents to resin) and N-methylmorpholine (10 equivalents to resin) in DMF for 2 minutes. When coupling to *N*-methyl-residues, Fmoc-protected amino acids were preactivated with PyAOP (5 equivalents to resin) and N-methylmorpholine (10 equivalents to resin) in DMF for 2 minutes. Deprotections were performed in 2 iterations of 4.5 minutes each. The peptide was cleaved from resin by treatment with 94% TFA, 2.5% water, 2.5% ethanedithiol, and 1% triisopropylsilane for 4 hours.

Following cleavage of peptide fragments from resin, the crude peptide was precipitated in cold diethyl ether and pelleted by centrifugation. The ether was decanted, and the resulting pellet dissolved in water and acetonitrile with 0.1% TFA. Purification was performed by HPLC on a Jupiter C18 preparative column using gradients between 0.1% TFA in water and 0.1% TFA in acetonitrile. Peptide identities and purities were determined by MALDI-TOF mass spectrometry (**Table 5**) and analytical RP-HPLC (**Figure 61**), respectively.

Table 5. MALDI-TOF data for N- and C-terminal Ubiquitin Fragments.

	$[M+H]^+$ (*m/z*)	
Peptide	**Calculated**	**Observed**
N' WT	3048.5	3048.5
N' Cons	3046.5	3046.7
N' Amb	2966.6	2966.0
C' WT	5577.0	5577.6
C' Cons	5571.5	5571.4
C' Amb	5389.3	5389.6

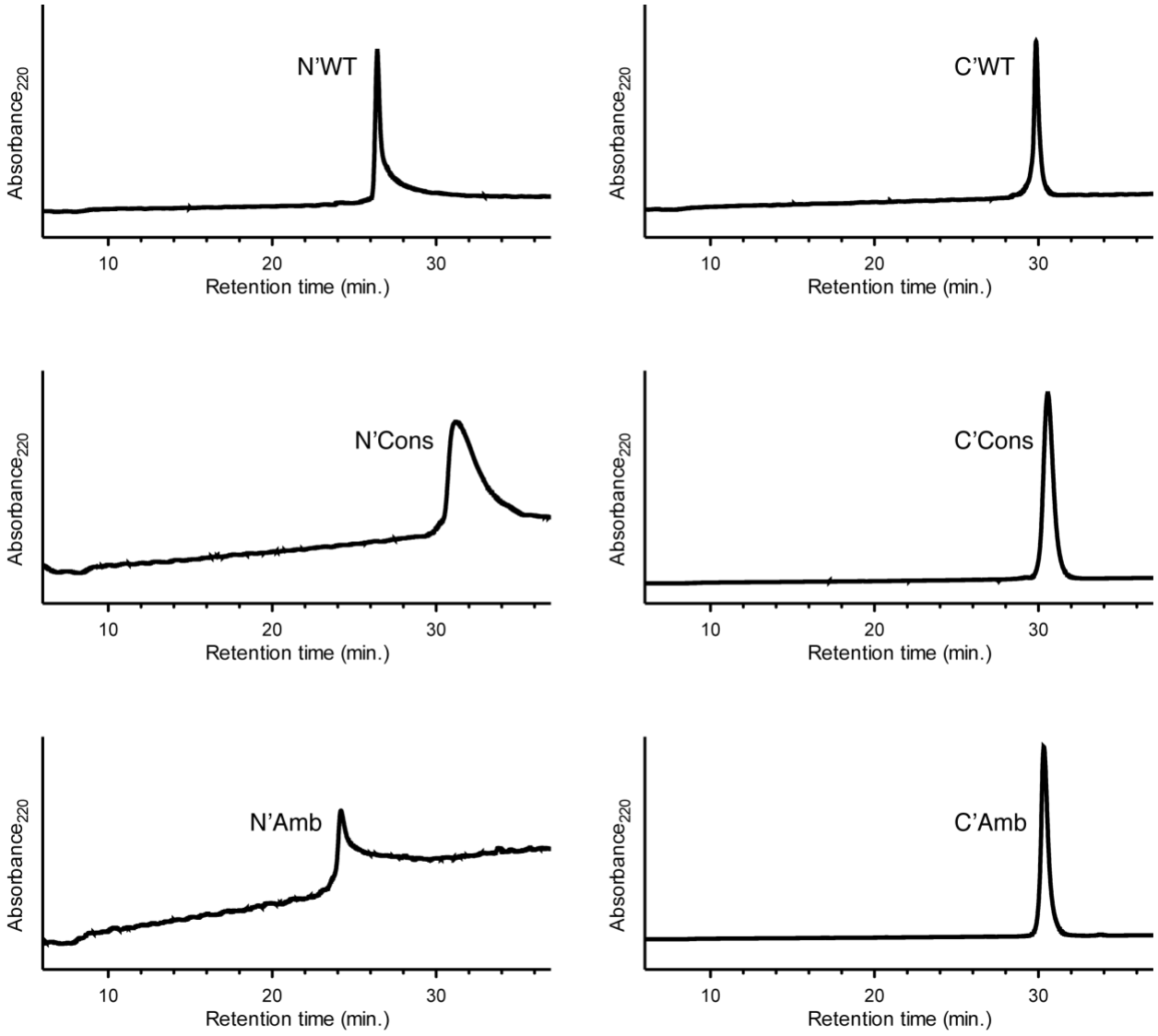

Figure 61. Analytical HPLC chromatograms of purified N- and C-terminal ubiquitin fragments. Notably, the irregular tailing effects observed in the peptide hydrazide chromatograms are precedented.[213]

4.5.3 General Native Chemical Ligation and Desulfurization Procedures

Ubiquitin fragments were coupled by native chemical ligation using the peptide hydrazide thioester-masking approach.[205] An Eppendorf tube containing 600 μL N-terminal ubiquitin fragment (2 mM) in ligation buffer (0.2 M $NaH_2PO_4 \cdot 2H_2O$, 6M Gdn · HCl, pH 3.0) was equipped with a stir bar and cooled to -15 °C in a salt ice bath. 40 μL sodium nitrite in water (0.5 M) was added and the solution was stirred at -15 °C for 15 minutes. To this was added a 600 μL solution containing both the C-terminal ubiquitin fragment (2 mM) and 4-mercaptophenylacetic acid (69 mM) in ligation buffer. The solution was warmed to room temperature and the pH was raised to 6.4. The reaction was monitored by quenching a 1μL aliquot with TCEP (0.1M) and analyzing by RP-HPLC. Upon completion, the reaction was quenched with 250 μL TCEP (0.1M) and purified via semi-preparative HPLC to furnish the Ala28Cys ubiquitin variant. Protein identities and purities were determined by MALDI-TOF mass spectrometry (**Table 6**) and analytical RP-HPLC (**Figure 62**), respectively.

Table 6. MALDI-TOF data for A28C protein ligation products.

	$[M+H]^+$ (*m/z*)	
Protein	**Calculated**	**Observed**
4.1 A28C	8595.8	8596.2
4.2 A28C	8593.8	8594.9
4.3 A28C	8513.8	8513.5
4.4 A28C	8586.9	8587.8
4.5 A28C	8404.8	8407.0
4.6 A28C	8585.0	8585.3
4.7 A28C	8322.8	8322.8
4.8 A28C	8402.8	8405.3
4.9 A28C	8505.0	8505.0

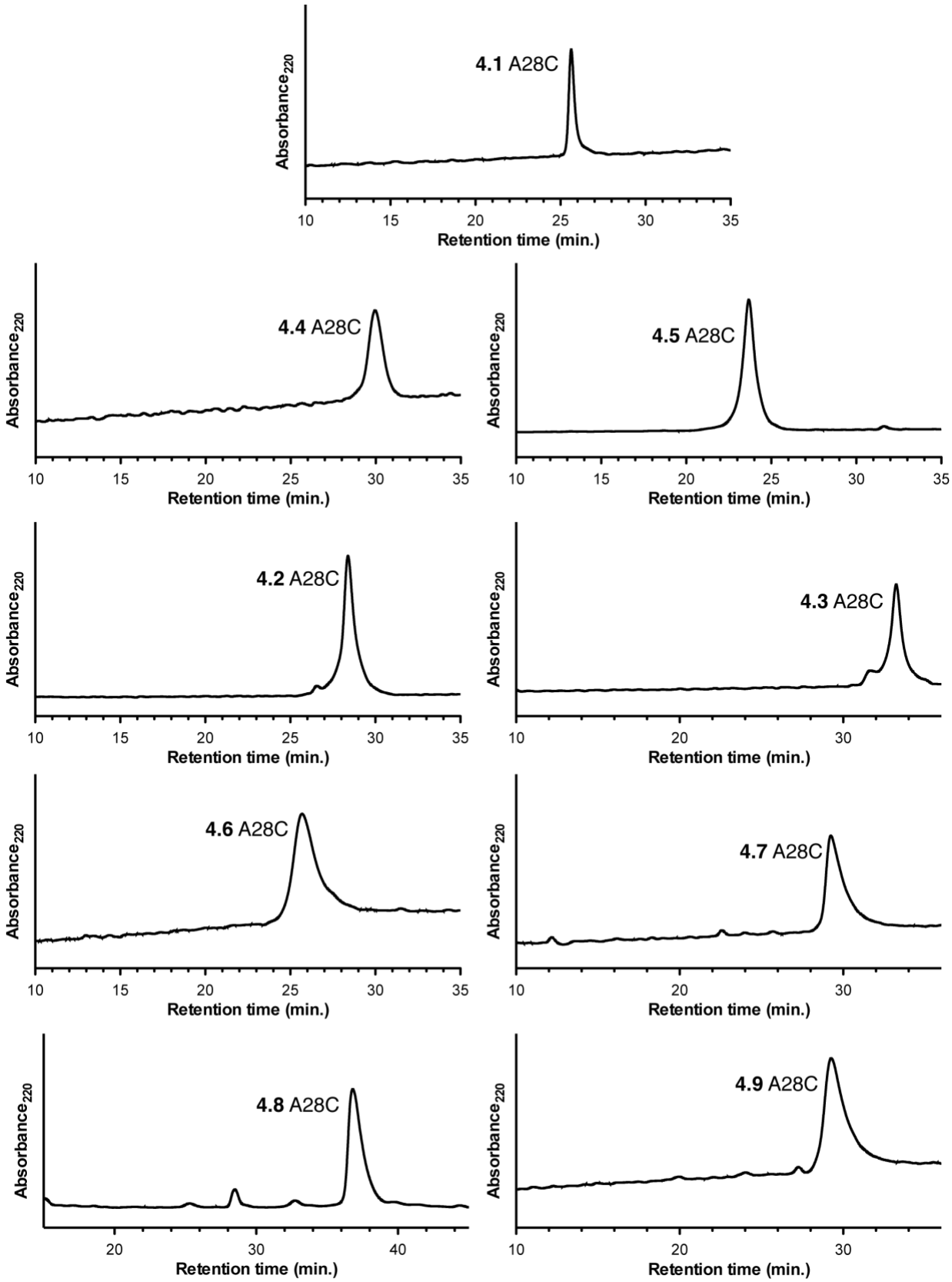

Figure 62. Analytical HPLC chromatograms of ubiquitin A28C intermediates.

Ala28Cys ubiquitin variants were desulfurized using free-radical-mediated desulfurization.[204] Pure, lyophilized protein was dissolved in 500 μL neutral ligation buffer (0.2 M $NaH_2PO_4 \cdot 2H_2O$, 6M Gdn · HCl, pH 6.5). To this solution was added 500 μL TCEP (1 M in water), 100 μL *tert*-butylthiol, and 50 μL VA-044 (0.1 M in water). The reaction was warmed to 37 °C and stirred for 5 hours. Upon completion, the reaction was purified by semi-preparative HPLC. Protein identity and purity were determined by MALDI-TOF mass spectrometry (**Table 7**) and analytical RP-HPLC (**Figure 63**), respectively.

Table 7. MALDI-TOF data for ubiquitin variants.

	$[M+H]^+$ (*m/z*)	
Protein	**Calculated**	**Observed**
4.1	8563.7	8564.8
4.2	8561.7	8562.5
4.3	8481.7	8482.1
4.4	8554.9	8555.5
4.5	8372.7	8375.0
4.6	8552.9	8552.9
4.7	8290.7	8291.4
4.8	8370.7	8372.6
4.9	8472.9	8474.9

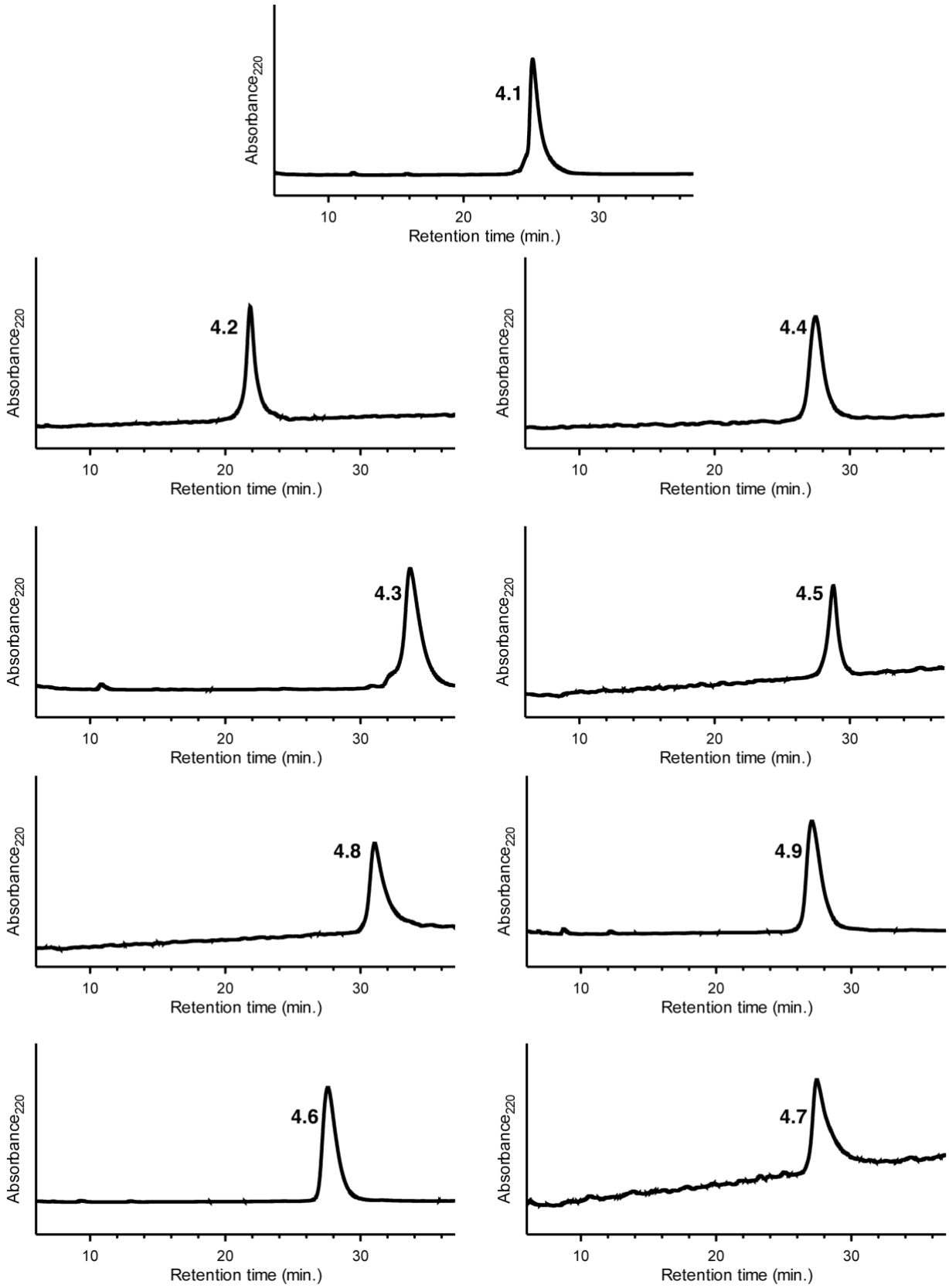

Figure 63. Analytical HPLC chromatograms of ubiquitin variants.

4.5.4 Circular Dichroism Spectroscopy

Stock solutions of ubiquitin variants were prepared in water, and the concentration of peptide was determined by UV-Vis spectroscopy (ε_{280} = 2560 M^{-1} cm^{-1}).[163] Samples for CD analysis were prepared by dilution of the peptide stock with water and buffer stocks to yield solutions consisting of 40 μM peptide in 50 mM phosphate buffer pH 5.6. CD scans were performed from 200-260 nm with 1 nm step size, 2 nm bandwidth, and 5 second integration time at each wavelength. All measurements were baseline corrected against a buffer blank measured in the same cell. Scans were smoothed by the Savitsky-Golay method using GraphPad Prism.

4.5.5 CHIP *In Vitro* Ubiquitination Assay

Note: these experiments were performed by Samuel Estabrooks from the Brodsky Lab in the Department of Biology at the University of Pittsburgh.

Recombinant human CHIP was purified from pelleted cells as described previously.[214] Cell pellets containing Ube1 were lysed in 10 mM imidazole, 50 mM $NaPO_4$ pH 8, 300 mM NaCl, 5 mM 2-mercaptoethanol, 0.25% Triton-100X, 2 mg/mL lysozyme for 30 min. on ice followed by sonication. Recovery of intact Ube1 required addition of protease inhibitors (1% PMSF, 0.2% leupeptin, 0.1% pepstatin A, Roche protease inhibitor cocktail) to lysis buffer and all purification buffers. After centrifugation, cleared Ube1 cell lysates were applied to Ni-NTA agarose resin (Qiagen), washed with 30 mM imidazole, and eluted with 200 mM imidazole. Peak His-Ube1 fractions were pooled, dialyzed into 20 mM HEPES pH 7.4, 20 mM NaCl, and further purified by anion exchange chromatography over DEAE-Sepharose (GE Healthcare). Ube1 was eluted across a 50-300 mM NaCl gradient and peak fractions were pooled, dialyzed into 50 mM HEPES pH 7, 50

mM NaCl, further concentrated by centrifugal filtration (Millipore), flash frozen in liquid nitrogen, and stored at -80 °C. Cell pellets containing GST-Hsc70$_{395-646}$ were lysed in 50 mM Tris pH 7.5, 150 mM NaCl, 5 mM 2-mercaptoethanol, 0.25% Triton-100X, 2 mg/mL lysozyme, sonicated, and cleared lysates applied to glutathione agarose (Sigma). After washing, GST-Hsc70$_{395-646}$ was eluted with 6.8 mg/mL reduced glutathione. Peak fractions were pooled, dialyzed into 50 mM HEPES pH 7, 50 mM NaCl, flash frozen, and stored at -80 °C. Purified proteins were verified by Coomassie Brilliant Blue staining. Protein concentration was determined by Pierce BCA protein concentration assay (Thermo Fisher Scientific).

Protein quantities indicate final reaction molarities in 20 µL reactions. Reactions were initiated by combining 125 nM His-Ube1, 1 µM UbcH5b (Boston Biochem E2-622), and ATP reaction buffer (50 mM HEPES pH 7.0, 50 mM NaCl, 2 mM ATP, 4 mM $MgCl_2$) with 140 µM recombinant human ubiquitin (Boston Biochem U-100H) or a synthetic ubiquitin variant. After incubation at 37 °C, ubiquitin-charged E1/E2 mixtures were dispensed to reaction tubes containing 3 µM His-CHIP, 10 µM GST-Hsc70$_{395-646}$, and excess reaction buffer (50 mM HEPES pH 7.0, 50 mM NaCl) pre-incubated on ice for 20 min. Active reactions proceeded for 1 hr. at 37 °C, before quenching by addition of 2X SDS sample buffer supplemented with 50 mM EDTA. Quenched reactions were resolved by 10% SDS-PAGE, then transferred to nitrocellulose. Transferred reactions were treated with either α-GST HRP-conjugated antibody (Abcam ab3416) to indicate GST-Hsc70$_{395-646}$ substrate ubiquitination, or with α-ubiquitin antibody (P4D1, Santa Cruz Biotechnology sc-8017) followed by α-mouse HRP-conjugated antibody (Cell Signaling Technology 7076S) to indicate total ubiquitination. Reactions were visualized by chemiluminescent detection (Bio-Rad ChemiDoc XRS+) and quantified by densitometry in ImageJ. Western blot chemiluminescence was first converted to grayscale, and the raw integrated densities of unubiquitinated, monoubiquitinated, and polyubiquitinated substrate bands were measured. Relative percentages of each species were then

normalized to the sum of raw integrated density in each lane. Three reaction and western blot replicates were performed for each ubiquitin variant and wildtype ubiquitin.

4.5.6 *in vitro* Ubiquitination Conjugation, and Retrotranslocation Assays

Note: these experiments were performed by G. Michael Preston from the Brodsky Lab in the Department of Biology at the University of Pittsburgh.

A total of 4 reactions were set up, one for each ubiquitin variant. Columns were washed three times with 1 x PBS + 1% BSA and pre-equilibrated in this solution overnight in the cold room. A stock of iodine monochloride (ICl, Apodaca Laboratory, Department of Medicine) was made by diluting 33 mM ICl to a final concentration of 0.66 mM in 2M NaCl. The reaction was initiated by adding 4 µL of $^{125}I_2$ (Perkin Elmer, NEZ033010MC) to 120 µL of an 833 mM Tris, pH 8.0, 0.11 mM ICl solution for exactly 1 min at room temperature. To these reactions, 50 µg of variants **4.1**, **4.4**, and **4.7** and 25 µg of variant **4.2** were added and incubated for 10 minutes at room temperature. The reactions were stopped by the addition of NaI to a final concentration of 0.4 M. Reactions were loaded onto the pre-equilibrated desalting columns and allowed to run into the column. The columns were washed with 300 µL of 1 x PBS + 1% BSA. After the wash, the iodinated ubiquitin variants were collected in 600 µL of 1 x PBS + 1% BSA. The relative counts per µL of each iodinated ubiquitin variant was then determined by scintillation counting, the samples were aliquoted, and stored at -80 °C.

in vitro ubiquitination conjugation reactions were performed using a variation of a previously described method[209] and consisted of 1 mg/ml microsomes purified from wild type yeast expressing Chimera A*,[215] 1 mg/mL cytosol, and an ATP regenerating system (1 mM ATP, 40 mM creatine phosphate, 0.2 mg/mL creatine phosphokinase in 250 mM sorbitol, 150 mM potassium acetate, 5 mM magnesium acetate, 20 mM HEPES pH 6.8) in a final volume of 40 µL. Purified yeast cytosol

was prepared using liquid nitrogen via a modified version of a previously published technique.[216] After cells were grown at 37 °C for 1 h, they were harvested, washed in 250 mM sorbitol, 150 mM potassium acetate, 5 mM magnesium acetate, 20 mM HEPES pH 6.8, and flash frozen in liquid nitrogen. The frozen cells were then lysed using a cold mortar and pestle for 1 min in the presence of liquid nitrogen for a total of 6 rounds of grinding. Addition of apyrase (0.02 units/reaction) instead of the ATP regenerating system served as a negative control. Samples were pre-incubated at room temperature for 10 min, after which ^{125}I-ubiquitin (3.8 x 10^6 cpm/rxn) was added. The samples were then incubated at 35 °C for 55 min. Half of each reaction was removed and kept for a "Total" ubiquitination sample. The remaining reactions were centrifuged 10 minutes at 18,000 x g and 4 °C. The supernatants were removed and placed in a fresh 1.5 mL Eppendorf tube as the retrotranslocated population of ubiquitinated substrate. The pellets were resuspended in an equal volume of fresh buffer (250 mM sorbitol, 150 mM potassium acetate, 5 mM magnesium acetate, 20 mM HEPES pH 6.8). 125 µL of a 1.25% SDS Stop solution (50 mM Tris–Cl, pH 7.4, 150 mM NaCl, 5 mM EDTA, 1.25% sodium dodecyl sulfate (SDS), 1 mM PMSF, 2 mM leupeptin, 0.7 mM pepstatin A, and 10 mM N-ethylmaleimide (NEM)) was added to all samples and incubated at 37 °C for 30 min. A total of 400 µl of a Triton solution (50 mM Tris–Cl, pH 7.4, 150 mM NaCl, 5 mM EDTA, 2% Triton X-100, 1 mM PMSF, 2 mM leupeptin, 0.7 mM pepstatin A, and 10 mM NEM), 35 µl of a 50/50 protein A-sepharose slurry in Protein A bead resuspension solution, and anti-HA antibody were then added to each reaction and samples were immunoprecipitated overnight at 4 °C on a rotator. After centrifugation, the pellets were washed 3 times in an IP wash buffer, and after all fluid was removed from the beads, TCA sample buffer (80 mM Tris, pH 8, 8 mM EDTA, 3.5% SDS, 15% glycerol, 0.08% Tris base, 0.01% bromphenol blue, 5% fresh β-mercaptoethanol) was added, the samples were briefly agitated, and incubated at 37 °C for 30 min. The precipitated chimera was then resolved on duplicate 10% SDS-polyacrylamide gels. One gel was transferred to nitrocellulose

and incubated with anti-HA-HRP antibody to control for IP levels. The second gel was washed in ddH_2O, placed on filter paper, and dried. Dried gels were then exposed to a phosphorfilm for two weeks.

BIBLIOGRAPHY

1. Werner, H. M.; Horne, W. S., Folding and function in α/β-peptides: Targets and therapeutic applications. *Curr. Opin. Chem. Biol.* **2015,** *28*, 75-82.

2. Anfinsen, C. B., The formation and stabilization of protein structure. *Biochem. J.* **1972,** *128* (4), 737-749.

3. Chou, P. Y.; Fasman, G. D., Prediction of protein conformation. *Biochemistry* **1974,** *13* (2), 222-245.

4. Lim, V. I., Structural principles of the globular organization of protein chains. A stereochemical theory of globular protein secondary structure. *J. Mol. Biol.* **1974,** *88* (4), 857-872.

5. Chou, K.-C.; Cai, Y.-D., Predicting protein quaternary structure by pseudo amino acid composition. *Proteins: Struct., Funct., Bioinf.* **2003,** *53* (2), 282-289.

6. Khoury, G. A.; Baliban, R. C.; Floudas, C. A., Proteome-wide post-translational modification statistics: frequency analysis and curation of the swiss-prot database. *Sci. Rep.* **2011,** *1*.

7. Walsh, C. T.; Garneau-Tsodikova, S.; Gatto, G. J., Jr., Protein posttranslational modifications: the chemistry of proteome diversifications. *Angew. Chem. Int. Ed.* **2005,** *44* (45), 7342-72.

8. Lothrop, A. P.; Torres, M. P.; Fuchs, S. M., Deciphering post-translational modification codes. *FEBS Lett.* **2013,** *587* (8), 1247-57.

9. Sevier, C. S.; Kaiser, C. A., Formation and transfer of disulphide bonds in living cells. *Nature Reviews Molecular Cell Biology* **2002,** *3* (11), 836-847.

10. Liu, Y. D.; Goetze, A. M.; Bass, R. B.; Flynn, G. C., N-terminal glutamate to pyroglutamate conversion in vivo for human IgG2 antibodies. *J. Biol. Chem.* **2011,** *286* (13), 11211-7.

11. Laupacis, A.; Keown, P. A.; Ulan, R. A.; McKenzie, N.; Stiller, C. R., Cyclosporin A: a powerful immunosuppressant. *Canadian Medical Association Journal* **1982,** *126* (9), 1041-1046.

12. Lau, Y. H.; de Andrade, P.; Wu, Y.; Spring, D. R., Peptide stapling techniques based on different macrocyclisation chemistries. *Chem. Soc. Rev.* **2015,** *44* (1), 91-102.

13. Walensky, L. D.; Kung, A. L.; Escher, I.; Malia, T. J.; Barbuto, S.; Wright, R. D.; Wagner, G.; Verdine, G. L.; Korsmeyer, S. J., Activation of Apoptosis in Vivo by a Hydrocarbon-Stapled BH3 Helix. *Science* **2004,** *305* (5689), 1466-1470.

14. Felix, A. M.; Heimer, E. P.; Wang, C.-T.; Lambros, T. J.; Fournier, A.; Mowles, T. F.; Maines, S.; Campbell, R. M.; Wegrzynski, B. B.; Toome, V.; Fry, D.; Madison, V. S., Synthesis, biological activity and conformational analysis of cyclic GRF analogs. *Int. J. Pept. Protein Res.* **1988,** *32* (6), 441-454.

15. Wolfe, J. M.; Fadzen, C. M.; Holden, R. L.; Yao, M.; Hanson, G. J.; Pentelute, B. L., Perfluoroaryl Bicyclic Cell-Penetrating Peptides for Delivery of Antisense Oligonucleotides. *Angew. Chem. Int. Ed.* **2018,** *57* (17), 4756-4759.

16. Schafmeister, C. E.; Po, J.; Verdine, G. L., An All-Hydrocarbon Cross-Linking System for Enhancing the Helicity and Metabolic Stability of Peptides. *J. Am. Chem. Soc.* **2000,** *122* (24), 5891-5892.

17. Scrima, M.; Le Chevalier-Isaad, A.; Rovero, P.; Papini, A. M.; Chorev, M.; D'Ursi, A. M., CuI-Catalyzed Azide-Alkyne Intramolecular i-to-(i+4) Side-Chain-to-Side-Chain Cyclization Promotes the Formation of Helix-Like Secondary Structures. *Eur. J. Biochem.* **2010,** *2010* (3), 446-457.

18. Haney, C. M.; Loch, M. T.; Horne, W. S., Promoting peptide alpha-helix formation with dynamic covalent oxime side-chain cross-links. *Chem. Commun.* **2011,** *47* (39), 10915-7.

19. Verdine, G. L.; Hilinski, G. J., Stapled peptides for intracellular drug targets. *Methods Enzymol.* **2012,** *503*, 3-33.

20. Henchey, L. K.; Jochim, A. L.; Arora, P. S., Contemporary strategies for the stabilization of peptides in the alpha-helical conformation. *Curr. Opin. Chem. Biol.* **2008,** *12* (6), 692-7.

21. Reinert, Z. E.; Horne, W. S., Protein backbone engineering as a strategy to advance foldamers toward the frontier of protein-like tertiary structure. *Org. Biomol. Chem.* **2014,** *12* (44), 8796-8802.

22. Rajarathnam, K.; Sykes, B. D.; Kay, C. M.; Dewald, B.; Geiser, T.; Baggiolini, M.; Clark-Lewis, I., Neutrophil activation by monomeric interleukin-8. *Science* **1994,** *264* (5155), 90.

23. Fuller, A. A.; Du, D.; Liu, F.; Davoren, J. E.; Bhabha, G.; Kroon, G.; Case, D. A.; Dyson, H. J.; Powers, E. T.; Wipf, P.; Gruebele, M.; Kelly, J. W., Evaluating beta-turn mimics as beta-sheet folding nucleators. *Proc. Natl. Acad. Sci. USA* **2009,** *106* (27), 11067-72.

24. George, K. L.; Horne, W. S., Heterogeneous-Backbone Foldamer Mimics of Zinc Finger Tertiary Structure. *J. Am. Chem. Soc.* **2017,** *139* (23), 7931-7938.

25. Werner, H. M.; Cabalteja, C. C.; Horne, W. S., Peptide Backbone Composition and Protease Susceptibility: Impact of Modification Type, Position, and Tandem Substitution. *ChemBioChem* **2016,** *17* (8), 712-8.

26. Gellman, S. H., Foldamers: A Manifesto. *Acc. Chem. Res.* **1998,** *31* (4), 173-180.

27. Horne, W. S.; Gellman, S. H., Foldamers with heterogeneous backbones. *Acc. Chem. Res.* **2008,** *41* (10), 1399-1408.

28. Wang, P. S. P.; Nguyen, J. B.; Schepartz, A., Design and High-Resolution Structure of a β3-Peptide Bundle Catalyst. *J. Am. Chem. Soc.* **2014,** *136* (19), 6810-6813.

29. Seebach, D.; Gardiner, J., β-Peptidic Peptidomimetics. *Acc. Chem. Res.* **2008,** *41* (10), 1366-1375.

30. Zhao, L.; Lu, W., Mirror image proteins. *Curr. Opin. Chem. Biol.* **2014,** *22*, 56-61.

31. Ferrand, Y.; Huc, I., Designing Helical Molecular Capsules Based on Folded Aromatic Amide Oligomers. *Acc. Chem. Res.* **2018,** *51* (4), 970-977.

32. and, D. T. C.; Korsmeyer, S. J., BCL-2 FAMILY: Regulators of Cell Death. *Annu. Rev. Immunol.* **1998,** *16* (1), 395-419.

33. Sadowsky, J. D.; Fairlie, W. D.; Hadley, E. B.; Lee, H.-S.; Umezawa, N.; Nikolovska-Coleska, Z.; Wang, S.; Huang, D. C. S.; Tomita, Y.; Gellman, S. H., (α/β+α)-Peptide antagonists of BH3 domain/Bcl-x_L recognition: Toward general strategies for foldamer-based inhibition of protein−protein interactions. *J. Am. Chem. Soc.* **2007,** *129* (1), 139-154.

34. Horne, W. S.; Price, J. L.; Keck, J. L.; Gellman, S. H., Helix bundle quaternary structure from α/β-peptide foldamers. *J. Am. Chem. Soc.* **2007,** *129* (14), 4178-4180.

35. Lee, E. F.; Smith, B. J.; Horne, W. S.; Mayer, K. N.; Evangelista, M.; Colman, P. M.; Gellman, S. H.; Fairlie, W. D., Structural basis of Bcl-x_L recognition by a BH3-mimetic a/b-peptide generated by sequence-based design. *ChemBioChem* **2011,** *12* (13), 2025-2032.

36. Smith, B. J.; Lee, E. F.; Checco, J. W.; Evangelista, M.; Gellman, S. H.; Fairlie, W. D., Structure-guided rational design of α/β-peptide foldamers with high affinity for BCL-2 family prosurvival proteins. *ChemBioChem* **2013,** *14* (13), 1564-1572.

37. Gensure, R. C.; Gardella, T. J.; Jüppner, H., Parathyroid hormone and parathyroid hormone-related peptide, and their receptors. *Biochem. Bioph. Res. Co.* **2005,** *328* (3), 666-678.

38. Vilardaga, J.-P.; Romero, G.; Friedman, P.; Gardella, T., Molecular basis of parathyroid hormone receptor signaling and trafficking: A family B GPCR paradigm. *Cell. Mol. Life Sci.* **2011,** *68* (1), 1-13.

39. Cheloha, R. W.; Maeda, A.; Dean, T.; Gardella, T. J.; Gellman, S. H., Backbone modification of a polypeptide drug alters duration of action in vivo. *Nat. Biotech.* **2014,** *32* (7), 653-655.

40. Reinert, Z. E.; Lengyel, G. A.; Horne, W. S., Protein-like tertiary folding behavior from heterogeneous backbones. *J. Am. Chem. Soc.* **2013,** *135* (34), 12528-12531.

41. Checco, J. W.; Kreitler, D. F.; Thomas, N. C.; Belair, D. G.; Rettko, N. J.; Murphy, W. L.; Forest, K. T.; Gellman, S. H., Targeting diverse protein–protein interaction interfaces with α/β-peptides derived from the Z-domain scaffold. *Proc. Natl. Acad. Sci. USA* **2015,** *112* (15), 4552-4557.

42. Johnson, L. M.; Barrick, S.; Hager, M. V.; McFedries, A.; Homan, E. A.; Rabaglia, M. E.; Keller, M. P.; Attie, A. D.; Saghatelian, A.; Bisello, A.; Gellman, S. H., A potent α/β-peptide analogue of GLP-1 with prolonged action in vivo. *J. Am. Chem. Soc.* **2014,** *136* (37), 12848-12851.

43. Guo, W.; Wisniewski, J. A.; Ji, H., Hot spot-based design of small-molecule inhibitors for protein–protein interactions. *Bioorg. Med. Chem. Lett.* **2014,** *24* (11), 2546-2554.

44. Arkin, Michelle R.; Tang, Y.; Wells, James A., Small-Molecule Inhibitors of Protein-Protein Interactions: Progressing toward the Reality. *Chem. Biol.* **2014,** *21* (9), 1102-1114.

45. Nevola, L.; Giralt, E., Modulating protein-protein interactions: the potential of peptides. *Chem. Commun.* **2015,** *51* (16), 3302-3315.

46. Nestor Jr, J. J., The Medicinal Chemistry of Peptides. *Curr. Med. Chem.* **2009,** *16* (33), 4399-4418.

47. Diao, L.; Meibohm, B., Pharmacokinetics and Pharmacokinetic–Pharmacodynamic Correlations of Therapeutic Peptides. *Clin. Pharmacokinet.* **2013,** *52* (10), 855-868.

48. Rink, R.; Arkema-Meter, A.; Baudoin, I.; Post, E.; Kuipers, A.; Nelemans, S. A.; Akanbi, M. H. J.; Moll, G. N., To protect peptide pharmaceuticals against peptidases. *J. Pharmacol. Toxicol. Method.* **2010,** *61* (2), 210-218.

49. Stevenson, C. L., Advances in Peptide Pharmaceuticals. *Curr. Pharm. Biotechno.* **2009,** *10* (1), 122-137.

50. Werle, M.; Bernkop-Schnürch, A., Strategies to improve plasma half life time of peptide and protein drugs. *Amino Acids* **2006,** *30* (4), 351-367.

51. Weinstock, M. T.; Francis, J. N.; Redman, J. S.; Kay, M. S., Protease-resistant peptide design—empowering nature's fragile warriors against HIV. *Pept. Sci.* **2012,** *98* (5), 431-442.

52. Bellmann-Sickert, K.; Beck-Sickinger, A. G., Peptide drugs to target G protein-coupled receptors. *Trends Pharmacol. Sci.* **2010,** *31* (9), 434-441.

53. Avan, I.; Hall, C. D.; Katritzky, A. R., Peptidomimetics via modifications of amino acids and peptide bonds. *Chem. Soc. Rev.* **2014,** *43* (10), 3575-3594.

54. Dong, J. Z.; Shen, Y.; Zhang, J.; Tsomaia, N.; Mierke, D. F.; Taylor, J. E., Discovery and characterization of taspoglutide, a novel analogue of human glucagon-like peptide-1, engineered for sustained therapeutic activity in type 2 diabetes. *Diabetes Obes. Metab.* **2011,** *13* (1), 19-25.

55. Gaston, F.; Granados, G. C.; Madurga, S.; Rabanal, F.; Lakhdar-Ghazal, F.; Giralt, E.; Bahraoui, E., Development and Characterization of Peptidic Fusion Inhibitors Derived from HIV-1 gp41 with Partial D-Amino Acid Substitutions. *ChemMedChem* **2009,** *4* (4), 570-581.

56. Fiacco, S. V.; Roberts, R. W., N-Methyl Scanning Mutagenesis Generates Protease-Resistant G Protein Ligands with Improved Affinity and Selectivity. *ChemBioChem* **2008,** *9* (14), 2200-2203.

57. Horne, W. S., Peptide and peptoid foldamers in medicinal chemistry. *Expert Opin. Drug Dis.* **2011,** *6* (12), 1247-1262.

58. Guichard, G.; Huc, I., Synthetic foldamers. *Chem. Commun.* **2011,** *47* (21), 5933-5941.

59. Goodman, C. M.; Choi, S.; Shandler, S.; DeGrado, W. F., Foldamers as versatile frameworks for the design and evolution of function. *Nat. Chem. Biol.* **2007,** *3* (5), 252-262.

60. Bautista, A. D.; Craig, C. J.; Harker, E. A.; Schepartz, A., Sophistication of foldamer form and function in vitro and in vivo. *Curr. Opin. Chem. Biol.* **2007,** *11* (6), 685-692.

61. Chatterjee, J.; Gilon, C.; Hoffman, A.; Kessler, H., N-Methylation of Peptides: A New Perspective in Medicinal Chemistry. *Acc. Chem. Res.* **2008,** *41* (10), 1331-1342.

62. Chatterjee, J.; Rechenmacher, F.; Kessler, H., N-Methylation of Peptides and Proteins: An Important Element for Modulating Biological Functions. *Angew. Chem. Int. Ed.* **2013,** *52* (1), 254-269.

63. Sandberg, B. E. B.; Chi-Ming, L.; Hanley, M. R.; Iversen, L. L., Synthesis and Biological Properties of Enzyme-Resistant Analogues of Substance P. *Eur. J. Biochem.* **1981,** *114* (2), 329-337.

64. Haviv, F.; Fitzpatrick, T. D.; Swenson, R. E.; Nichols, C. J.; Mort, N. A.; Bush, E. N.; Diaz, G.; Bammert, G.; Nguyen, A., Effect of N-methyl substitution of the peptide bonds in luteinizing hormone-releasing hormone agonists. *J. Med. Chem.* **1993,** *36* (3), 363-369.

65. Bose, P. P.; Chatterjee, U.; Hubatsch, I.; Artursson, P.; Govender, T.; Kruger, H. G.; Bergh, M.; Johansson, J.; Arvidsson, P. I., In vitro ADMET and physicochemical investigations of poly-N-methylated peptides designed to inhibit Aβ aggregation. *Bioorganic & Medicinal Chemistry* **2010,** *18* (16), 5896-5902.

66. Adessi, C.; Frossard, M.-J.; Boissard, C.; Fraga, S.; Bieler, S.; Ruckle, T.; Vilbois, F.; Robinson, S. M.; Mutter, M.; Banks, W. A.; Soto, C., Pharmacological Profiles of Peptide Drug Candidates for the Treatment of Alzheimer's Disease. *J. Biol. Chem.* **2003,** *278* (16), 13905-13911.

67. Gordon, D. J.; Sciarretta, K. L.; Meredith, S. C., Inhibition of β-Amyloid(40) Fibrillogenesis and Disassembly of β-Amyloid(40) Fibrils by Short β-Amyloid Congeners Containing N-Methyl Amino Acids at Alternate Residues†. *Biochemistry* **2001,** *40* (28), 8237-8245.

68. Biron, E.; Chatterjee, J.; Ovadia, O.; Langenegger, D.; Brueggen, J.; Hoyer, D.; Schmid, H. A.; Jelinek, R.; Gilon, C.; Hoffman, A.; Kessler, H., Improving Oral Bioavailability of Peptides by Multiple N-Methylation: Somatostatin Analogues. *Angew. Chem. Int. Ed.* **2008,** *47* (14), 2595-2599.

69. Cody, W. L.; He, J. X.; Reily, M. D.; Haleen, S. J.; Walker, D. M.; Reyner, E. L.; Stewart, B. H.; Doherty, A. M., Design of a Potent Combined Pseudopeptide Endothelin-A/Endothelin-B Receptor Antagonist, Ac-dBhg16-Leu-Asp-Ile-[NMe]Ile-Trp21 (PD 156252): Examination of Its Pharmacokinetic and Spectral Properties. *J. Med. Chem.* **1997,** *40* (14), 2228-2240.

70. Dechantsreiter, M. A.; Planker, E.; Mathä, B.; Lohof, E.; Hölzemann, G.; Jonczyk, A.; Goodman, S. L.; Kessler, H., N-Methylated Cyclic RGD Peptides as Highly Active and Selective αVβ3 Integrin Antagonists. *J. Med. Chem.* **1999,** *42* (16), 3033-3040.

71. Muppidi, A.; Doi, K.; Edwardraja, S.; Drake, E. J.; Gulick, A. M.; Wang, H.-G.; Lin, Q., Rational Design of Proteolytically Stable, Cell-Permeable Peptide-Based Selective Mcl-1 Inhibitors. *J. Am. Chem. Soc.* **2012,** *134* (36), 14734-14737.

72. Bergmann, M.; Zervas, L.; Fruton, J. S.; Schneider, F.; Schleich, H., ON PROTEOLYTIC ENZYMES: V. ON THE SPECIFICITY OF DIPEPTIDASE. *J. Biol. Chem.* **1935,** *109* (1), 325-346.

73. Banerjee, R.; Basu, G.; Roy, S.; Chène, P., Aib-based peptide backbone as scaffolds for helical peptide mimics. *J. Pept. Res.* **2002,** *60* (2), 88-94.

74. Wada, S.-i.; Tsuda, H.; Okada, T.; Urata, H., Cellular uptake of Aib-containing amphipathic helix peptide. *Bioorg. Med. Chem. Lett.* **2011,** *21* (19), 5688-5691.

75. De Zotti, M.; Biondi, B.; Park, Y.; Hahm, K.-S.; Crisma, M.; Toniolo, C.; Formaggio, F., Antimicrobial lipopeptaibol trichogin GA IV: role of the three Aib residues on conformation and bioactivity. *Amino Acids* **2012,** *43* (4), 1761-1777.

76. Krebs, H. A., Metabolism of amino-acids: Deamination of amino-acids. *Biochem. J.* **1935,** *29* (7), 1620-1644.

77. Koch, Y.; Bram, T.; Hazum, E.; Fridkin, M., Resistance to enzymic degradation of LH-RH analogues possessing increased biological activity. *Biochem. Bioph. Res. Co.* **1977,** *74* (2), 488-491.

78. Marks, N.; Stern, F., Enzymatic mechanisms for the inactivation of luteinizing hormone-releasing hormone (LH-RH). *Biochem. Bioph. Res. Co.* **1974,** *61* (4), 1458-1463.

79. Tugyi, R.; Uray, K.; Iván, D.; Fellinger, E.; Perkins, A.; Hudecz, F., Partial D-amino acid substitution: Improved enzymatic stability and preserved Ab recognition of a MUC2 epitope peptide. *Proc. Natl. Acad. Sci. USA* **2005,** *102* (2), 413-418.

80. Bessalle, R.; Kapitkovsky, A.; Gorea, A.; Shalit, I.; Fridkin, M., All-D-magainin: chirality, antimicrobial activity and proteolytic resistance. *FEBS Lett.* **1990,** *274* (1–2), 151-155.

81. Wiesehan, K.; Willbold, D., Mirror-image Phage Display: Aiming at the Mirror. *ChemBioChem* **2003,** *4* (9), 811-815.

82. Funke, S. A.; Willbold, D., Mirror image phage display-a method to generate d-peptideligands for use in diagnostic or therapeutical applications. *Mol. Biosyst.* **2009,** *5* (8), 783-786.

83. Lew, R. A.; Boulos, E.; Stewart, K. M.; Perlmutter, P.; Harte, M. F.; Bond, S.; Aguilar, M.-I.; Smith, A. I., Bradykinin analogues with β-amino acid substitutions reveal subtle differences in substrate specificity between the endopeptidases EC 3.4.24.15 and EC 3.4.24.16. *J. Pept. Sci.* **2000,** *6* (9), 440-445.

84. Ondetti, M. A.; Engel, S. L., Bradykinin analogs containing .beta.-homoamino acids. *J. Med. Chem.* **1975,** *18* (7), 761-763.

85. Webb, A. I.; Dunstone, M. A.; Williamson, N. A.; Price, J. D.; de Kauwe, A.; Chen, W.; Oakley, A.; Perlmutter, P.; McCluskey, J.; Aguilar, M.-I.; Rossjohn, J.; Purcell, A. W., T Cell

Determinants Incorporating β-Amino Acid Residues Are Protease Resistant and Remain Immunogenic In Vivo. *J. Immunol.* **2005,** *175* (6), 3810-3818.

86. Reinelt, S.; Marti, M.; Dédier, S.; Reitinger, T.; Folkers, G.; de Castro, J. A. L.; Rognan, D., β-Amino acid scan of a class I major histocompatibility complex-restricted alloreactive T-cell epitope. *J. Biol. Chem.* **2001,** *276* (27), 24525-24530.

87. Guichard, G.; Zerbib, A.; Le Gal, F.-A.; Hoebeke, J.; Connan, F.; Choppin, J.; Briand, J.-P.; Guillet, J.-G., Melanoma peptide MART-1(27−35) analogues with enhanced binding capacity to the human class i histocompatibility molecule HLA-A2 by introduction of a β-amino acid residue: Implications for recognition by tumor-infiltrating lymphocytes. *J. Med. Chem.* **2000,** *43* (20), 3803-3808.

88. Sadowsky, J. D.; Murray, J. K.; Tomita, Y.; Gellman, S. H., Exploration of backbone space in foldamers containing α- and β-amino acid residues: Developing protease-resistant oligomers that bind tightly to the BH3-recognition cleft of Bcl-x_L. *ChemBioChem* **2007,** *8* (8), 903-916.

89. Horne, W. S.; Johnson, L. M.; Ketas, T. J.; Klasse, P. J.; Lu, M.; Moore, J. P.; Gellman, S. H., Structural and biological mimicry of protein surface recognition by α/β-peptide foldamers. *Proc. Natl. Acad. Sci. USA* **2009,** *106* (35), 14751-14756.

90. Cabrele, C.; Martinek, T. A.; Reiser, O.; Berlicki, Ł., Peptides containing β-amino acid patterns: Challenges and successes in medicinal chemistry. *J. Med. Chem.* **2014,** *57* (23), 9718-9739.

91. Gráf, L.; Szilágyi, L.; Venekei, I., Chapter 582 - Chymotrypsin. In *Handbook of Proteolytic Enzymes*, Salvesen, N. D. R., Ed. Academic Press: 2013; pp 2626-2633.

92. Hedstrom, L., Serine Protease Mechanism and Specificity. *Chem. Rev.* **2002,** *102* (12), 4501-4524.

93. Southan, C., Assessing the protease and protease inhibitor content of the human genome. *J. Pept. Sci.* **2000,** *6* (9), 453-458.

94. Root, M. J.; Kay, M. S.; Kim, P. S., Protein Design of an HIV-1 Entry Inhibitor. *Science* **2001,** *291* (5505), 884-888.

95. Nord, K.; Gunneriusson, E.; Ringdahl, J.; Stahl, S.; Uhlen, M.; Nygren, P.-A., Binding proteins selected from combinatorial libraries of an [alpha]-helical bacterial receptor domain. *Nat. Biotech.* **1996,** *15* (8), 772-777.

96. O'Shea, E. K.; Lumb, K. J.; Kim, P. S., Peptide 'Velcro': Design of a heterodimeric coiled coil. *Curr. Biol.* **1993,** *3* (10), 658-667.

97. Baeriswyl, V.; Heinis, C., Phage selection of cyclic peptide antagonists with increased stability toward intestinal proteases. *Protein Eng. Des. Sel.* **2013,** *26* (1), 81-89.

98. Berger, A.; Schechter, I., Mapping the Active Site of Papain with the Aid of Peptide Substrates and Inhibitors. *Philos. Trans. R. Soc. London, Ser. B* **1970,** *257* (813), 249-264.

99. Charpentier, B.; Durieux, C.; Pelaprat, D.; Dor, A.; Reibaud, M.; Blanchard, J.-C.; Roques, B. P., Enzyme-resistant CCK analogs with high affinities for central receptors. *Peptides* **1988,** *9* (4), 835-841.

100. Banerjee, R.; Basu, G.; Roy, S.; Chène, P., Aib‐based peptide backbone as scaffolds for helical peptide mimics. *J. Pept. Res.* **2002,** *60* (2), 88-94.

101. Adessi, C.; Frossard, M. J.; Boissard, C.; Fraga, S.; Bieler, S.; Ruckle, T.; Vilbois, F.; Robinson, S. M.; Mutter, M.; Banks, W. A.; Soto, C., Pharmacological profiles of peptide drug candidates for the treatment of Alzheimer's disease. *J. Biol. Chem.* **2003,** *278* (16), 13905-11.

102. Selwyn, M. J., A simple test for inactivation of an enzyme during assay. *Biochim. Biophys. Acta, Enzymol. Biol. Oxid.* **1965,** *105* (1), 193-195.

103. Bizzozero, S. A.; Dutler, H., Stereochemical aspects of peptide hydrolysis catalyzed by serine proteases of the chymotrypsin type. *Bioorg. Chem.* **1981,** *10* (1), 46-62.

104. Wang, D.; Friedmann, M.; Gattin, Z.; Jaun, B.; van Gunsteren, W. F., The Propensity of α-Aminoisobutyric Acid (=2-Methylalanine; Aib) to Induce Helical Secondary Structure in an α-Heptapeptide: A Computational Study. *Helv. Chim. Acta* **2010,** *93* (8), 1513-1531.

105. Clark, E. A.; Walker, N.; Ford, D. C.; Cooper, I. A.; Oyston, P. C.; Acharya, K. R., Molecular recognition of chymotrypsin by the serine protease inhibitor ecotin from Yersinia pestis. *J. Biol. Chem.* **2011,** *286* (27), 24015-22.

106. Kim, H.; Chu, T. T.; Kim, D. Y.; Kim, D. R.; Nguyen, C. M.; Choi, J.; Lee, J. R.; Hahn, M. J.; Kim, K. K., The crystal structure of guamerin in complex with chymotrypsin and the development of an elastase-specific inhibitor. *J. Mol. Biol.* **2008,** *376* (1), 184-92.

107. Roussel, A.; Mathieu, M.; Dobbs, A.; Luu, B.; Cambillau, C.; Kellenberger, C., Complexation of two proteic insect inhibitors to the active site of chymotrypsin suggests decoupled roles for binding and selectivity. *J. Biol. Chem.* **2001,** *276* (42), 38893-8.

108. Frigerio, F.; Coda, A.; Pugliese, L.; Lionetti, C.; Menegatti, E.; Amiconi, G.; Schnebli, H. P.; Ascenzi, P.; Bolognesi, M., Crystal and molecular structure of the bovine α-chymotrypsin-eglin c complex at 2.0 Å resolution. *J. Mol. Biol.* **1992,** *225* (1), 107-123.

109. Hecht, H. J.; Szardenings, M.; Collins, J.; Schomburg, D., Three-dimensional structure of the complexes between bovine chymotrypsinogen A and two recombinant variants of human pancreatic secretory trypsin inhibitor (Kazal-type). *J. Mol. Biol.* **1991,** *220* (3), 711-722.

110. Fujinaga, M.; Sielecki, A. R.; Read, R. J.; Ardelt, W.; Laskowski, M.; James, M. N. G., Crystal and molecular structures of the complex of α-chymotrypsin with its inhibitor Turkey ovomucoid third domain at 1.8 Å resolution. *J. Mol. Biol.* **1987,** *195* (2), 397-418.

111. Schweitzer-Stenner, R.; Gonzales, W.; Bourne, G. T.; Feng, J. A.; Marshall, G. R., Conformational Manifold of α-Aminoisobutyric Acid (Aib) Containing Alanine-Based Tripeptides in Aqueous Solution Explored by Vibrational Spectroscopy, Electronic Circular Dichroism Spectroscopy, and Molecular Dynamics Simulations. *J. Am. Chem. Soc.* **2007,** *129* (43), 13095-13109.

112. Venkatraman, J.; Shankaramma, S. C.; Balaram, P., Design of Folded Peptides†. *Chem. Rev.* **2001,** *101* (10), 3131-3152.

113. Segal, D. M., Kinetic investigation of the crystallographically deduced binding subsites of bovine chymotrypsin Aγ. *Biochemistry* **1972,** *11* (3), 349-356.

114. Wilcox, P. E.; Segal, D. M.; Powers, J. C.; Cohen, G. H.; Davies, D. R., Substrate binding site in bovine chymotrypsin Aγ. Crystallographic study using peptide chloromethyl ketones as site-specific inhibitors. *Biochemistry* **1971,** *10* (20), 3728-3738.

115. Schellenberger, V.; Braune, K.; Hofmann, H.-J.; Jakubke, H.-D., The specificity of chymotrypsin. *Eur. J. Biochem.* **1991,** *199* (3), 623-636.

116. Lengyel, G. A.; Horne, W. S., Design Strategies for the Sequence-Based Mimicry of Side-Chain Display in Protein β-Sheets by α/β-Peptides. *J. Am. Chem. Soc.* **2012,** *134* (38), 15906-15913.

117. Tavenor, N. A.; Reinert, Z. E.; Lengyel, G. A.; Griffith, B. D.; Horne, W. S., Comparison of design strategies for alpha-helix backbone modification in a protein tertiary fold. *Chem. Commun.* **2016,** *52* (19), 3789-92.

118. Pelay-Gimeno, M.; Glas, A.; Koch, O.; Grossmann, T. N., Structure-Based Design of Inhibitors of Protein-Protein Interactions: Mimicking Peptide Binding Epitopes. *Angew. Chem. Int. Ed.* **2015,** *54* (31), 8896-927.

119. Reinert, Z. E.; Horne, W. S., Folding thermodynamics of protein-like oligomers with heterogeneous backbones. *Chem. Sci.* **2014,** *5* (8), 3325-3330.

120. Savitzky, A.; Golay, M. J. E., Smoothing and Differentiation of Data by Simplified Least Squares Procedures. *Anal. Chem.* **1964,** *36* (8), 1627-1639.

121. Haney, C. M.; Werner, H. M.; McKay, J. J.; Horne, W. S., Thermodynamic origin of alpha-helix stabilization by side-chain cross-links in a small protein. *Org. Biomol. Chem.* **2016,** *14* (24), 5768-73.

122. Gao, M.; Cheng, K.; Yin, H., Targeting protein−protein interfaces using macrocyclic peptides. *Pept. Sci.* **2015,** *104* (4), 310-316.

123. Laraia, L.; McKenzie, G.; Spring, David R.; Venkitaraman, Ashok R.; Huggins, David J., Overcoming Chemical, Biological, and Computational Challenges in the Development of Inhibitors Targeting Protein-Protein Interactions. *Chem. Biol.* **2015,** *22* (6), 689-703.

124. Leader, B.; Baca, Q. J.; Golan, D. E., Protein therapeutics: a summary and pharmacological classification. *Nat. Rev. Drug Discov.* **2008,** *7*, 21.

125. Jochim, A. L.; Arora, P. S., Systematic Analysis of Helical Protein Interfaces Reveals Targets for Synthetic Inhibitors. *ACS Chem. Biol.* **2010,** *5* (10), 919-923.

126. Jayatunga, M. K.; Thompson, S.; Hamilton, A. D., alpha-Helix mimetics: outwards and upwards. *Bioorg. Med. Chem. Lett.* **2014,** *24* (3), 717-24.

127. Hill, T. A.; Shepherd, N. E.; Diness, F.; Fairlie, D. P., Constraining cyclic peptides to mimic protein structure motifs. *Angew. Chem. Int. Ed.* **2014,** *53* (48), 13020-41.

128. White, C. J.; Yudin, A. K., Contemporary strategies for peptide macrocyclization. *Nat. Chem.* **2011,** *3* (7), 509-24.

129. Shepherd, N. E.; Hoang, H. N.; Abbenante, G.; Fairlie, D. P., Single Turn Peptide Alpha Helices with Exceptional Stability in Water. *J. Am. Chem. Soc.* **2005,** *127* (9), 2974-2983.

130. Spokoyny, A. M.; Zou, Y.; Ling, J. J.; Yu, H.; Lin, Y.-S.; Pentelute, B. L., A Perfluoroaryl-Cysteine SNAr Chemistry Approach to Unprotected Peptide Stapling. *J. Am. Chem. Soc.* **2013,** *135* (16), 5946-5949.

131. Haney, C. M.; Horne, W. S., Dynamic covalent side-chain cross-links via intermolecular oxime or hydrazone formation from bifunctional peptides and simple organic linkers. *J. Pept. Sci.* **2014,** *20* (2), 108-14.

132. Lau, Y. H.; Wu, Y.; de Andrade, P.; Galloway, W. R.; Spring, D. R., A two-component 'double-click' approach to peptide stapling. *Nat. Protoc.* **2015,** *10* (4), 585-94.

133. Kawamoto, S. A.; Coleska, A.; Ran, X.; Yi, H.; Yang, C.-Y.; Wang, S., Design of Triazole-Stapled BCL9 α-Helical Peptides to Target the β-Catenin/B-Cell CLL/lymphoma 9 (BCL9) Protein–Protein Interaction. *J. Med. Chem.* **2012,** *55* (3), 1137-1146.

134. Wang, C. K.; Swedberg, J. E.; Northfield, S. E.; Craik, D. J., Effects of Cyclization on Peptide Backbone Dynamics. *J. Phys. Chem. B.* **2015,** *119* (52), 15821-15830.

135. Miller, S. E.; Watkins, A. M.; Kallenbach, N. R.; Arora, P. S., Effects of side chains in helix nucleation differ from helix propagation. *Proc. Natl. Acad. Sci. USA* **2014,** *111* (18), 6636-41.

136. Frankiewicz, L.; Betti, C.; Guillemyn, K.; Tourwé, D.; Jacquot, Y.; Ballet, S., Stabilisation of a shortα-helical VIP fragment by side chain to side chain cyclisation: a comparison of common cyclisation motifs by circular dichroism. *J. Pept. Sci.* **2013,** *19* (7), 423-432.

137. Houston, M. E.; Gannon, C. L.; Kay, C. M.; Hodges, R. S., Lactam bridge stabilization of α-helical peptides: Ring size, orientation and positional effects. *J. Pept. Sci.* **1995,** *1* (4), 274-282.

138. Haney, C. M.; Horne, W. S., Oxime side-chain cross-links in an alpha-helical coiled-coil protein: structure, thermodynamics, and folding-templated synthesis of bicyclic species. *Chemistry* **2013,** *19* (34), 11342-51.

139. Kim, Y.-W.; Kutchukian, P. S.; Verdine, G. L., Introduction of All-Hydrocarbon i,i+3 Staples into α-Helices via Ring-Closing Olefin Metathesis. *Org. Lett.* **2010,** *12* (13), 3046-3049.

140. Harrison, R. S.; Shepherd, N. E.; Hoang, H. N.; Ruiz-Gomez, G.; Hill, T. A.; Driver, R. W.; Desai, V. S.; Young, P. R.; Abbenante, G.; Fairlie, D. P., Downsizing human, bacterial, and viral proteins to short water-stable alpha helices that maintain biological potency. *Proc. Natl. Acad. Sci. USA* **2010,** *107* (26), 11686-91.

141. Glas, A.; Bier, D.; Hahne, G.; Rademacher, C.; Ottmann, C.; Grossmann, T. N., Constrained peptides with target-adapted cross-links as inhibitors of a pathogenic protein-protein interaction. *Angew. Chem. Int. Ed.* **2014,** *53* (9), 2489-93.

142. Udugamasooriya, D. G.; Spaller, M. R., Conformational constraint in protein ligand design and the inconsistency of binding entropy. *Biopolymers* **2008,** *89* (8), 653-67.

143. Sia, S. K.; Carr, P. A.; Cochran, A. G.; Malashkevich, V. N.; Kim, P. S., Short constrained peptides that inhibit HIV-1 entry. *Proc. Natl. Acad. Sci. USA* **2002,** *99* (23), 14664-9.

144. Luo, P.; Braddock, D. T.; Subramanian, R. M.; Meredith, S. C.; Lynn, D. G., Structural and Thermodynamic Characterization of a Bioactive Peptide Model of Apolipoprotein E: Side-Chain Lactam Bridges To Constrain the Conformation. *Biochemistry* **1994,** *33* (41), 12367-12377.

145. Chiu, T. K.; Kubelka, J.; Herbst-Irmer, R.; Eaton, W. A.; Hofrichter, J.; Davies, D. R., High-resolution x-ray crystal structures of the villin headpiece subdomain, an ultrafast folding protein. *Proc. Natl. Acad. Sci. USA* **2005,** *102* (21), 7517-22.

146. McKnight, C. J.; Matsudaira, P. T.; Kim, P. S., NMR structure of the 35-residue villin headpiece subdomain. *Nat. Struct. Biol.* **1997,** *4*, 180.

147. Xiao, S.; Patsalo, V.; Shan, B.; Bi, Y.; Green, D. F.; Raleigh, D. P., Rational modification of protein stability by targeting surface sites leads to complicated results. *Proc. Natl. Acad. Sci. USA* **2013,** *110* (28), 11337-42.

148. Brown, J. W.; Farelli, J. D.; McKnight, C. J., On the unyielding hydrophobic core of villin headpiece. *Protein Sci.* **2012,** *21* (5), 647-654.

149. Cellmer, T.; Buscaglia, M.; Henry, E. R.; Hofrichter, J.; Eaton, W. A., Making connections between ultrafast protein folding kinetics and molecular dynamics simulations. *Proc. Natl. Acad. Sci. USA* **2011,** *108* (15), 6103-8.

150. Godoy-Ruiz, R.; Henry, E. R.; Kubelka, J.; Hofrichter, J.; Muñoz, V.; Sanchez-Ruiz, J. M.; Eaton, W. A., Estimating Free-Energy Barrier Heights for an Ultrafast Folding Protein from Calorimetric and Kinetic Data. *J. Phys. Chem. B.* **2008,** *112* (19), 5938-5949.

151. Glasscock, J. M.; Zhu, Y.; Chowdhury, P.; Tang, J.; Gai, F., Using an Amino Acid Fluorescence Resonance Energy Transfer Pair To Probe Protein Unfolding: Application to the Villin Headpiece Subdomain and the LysM Domain. *Biochemistry* **2008,** *47* (42), 11070-11076.

152. Brewer, S. H.; Vu, D. M.; Tang, Y.; Li, Y.; Franzen, S.; Raleigh, D. P.; Dyer, R. B., Effect of modulating unfolded state structure on the folding kinetics of the villin headpiece subdomain. *Proc. Natl. Acad. Sci. USA* **2005,** *102* (46), 16662-7.

153. Kubelka, J.; Eaton, W. A.; Hofrichter, J., Experimental Tests of Villin Subdomain Folding Simulations. *J. Mol. Biol.* **2003,** *329* (4), 625-630.

154. Tang, Y.; Grey, M. J.; McKnight, J.; Palmer Iii, A. G.; Raleigh, D. P., Multistate Folding of the Villin Headpiece Domain. *J. Mol. Biol.* **2006,** *355* (5), 1066-1077.

155. Frank, B. S.; Vardar, D.; Buckley, D. A.; McKnight, C. J., The role of aromatic residues in the hydrophobic core of the villin headpiece subdomain. *Protein Sci.* **2002,** *11* (3), 680-7.

156. Taylor, J. W., The synthesis and study of side-chain lactam-bridged peptides. *Biopolymers* **2002,** *66* (1), 49-75.

157. Cantel, S.; Le Chevalier Isaad, A.; Scrima, M.; Levy, J. J.; DiMarchi, R. D.; Rovero, P.; Halperin, J. A.; D'Ursi, A. M.; Papini, A. M.; Chorev, M., Synthesis and Conformational Analysis of a Cyclic Peptide Obtained via i to i+4 Intramolecular Side-Chain to Side-Chain Azide−Alkyne 1,3-Dipolar Cycloaddition. *J. Org. Chem.* **2008,** *73* (15), 5663-5674.

158. Buer, B. C.; Levin, B. J.; Marsh, E. N. G., Influence of Fluorination on the Thermodynamics of Protein Folding. *J. Am. Chem. Soc.* **2012,** *134* (31), 13027-13034.

159. Kuhlman, B.; Raleigh, D. P., Global analysis of the thermal and chemical denaturation of the N‐terminal domain of the ribosomal protein L9 in H2O and D2O. Determination of the thermodynamic parameters, ΔH°, ΔS°, and ΔC°p, and evaluation of solvent isotope effects. *Protein Sci.* **1998,** *7* (11), 2405-2412.

160. Bi, Y.; Cho, J.-H.; Kim, E.-Y.; Shan, B.; Schindelin, H.; Raleigh, D. P., Rational Design, Structural and Thermodynamic Characterization of a Hyperstable Variant of the Villin Headpiece Helical Subdomain. *Biochemistry* **2007,** *46* (25), 7497-7505.

161. Myers, J. K.; Pace, C. N.; Scholtz, J. M., Denaturant m values and heat capacity changes: Relation to changes in accessible surface areas of protein unfolding. *Protein Sci.* **1995,** *4* (10), 2138-2148.

162. Katayama, H.; Hojo, H.; Ohira, T.; Nakahara, Y., An efficient peptide ligation using azido-protected peptides via the thioester method. *Tet. Lett.* **2008,** *49* (38), 5492-5494.

163. Gill, S. C.; von Hippel, P. H., Calculation of protein extinction coefficients from amino acid sequence data. *Anal. Biochem.* **1989,** *182* (2), 319-326.

164. Rauscher, E.; Csekő, G.; Horváth, A. K., On the Complexity of Kinetics and the Mechanism of the Thiosulfate–Periodate Reaction. *Inorg. Chem.* **2011,** *50* (12), 5793-5802.

165. Mortenson, D. E.; Satyshur, K. A.; Guzei, I. A.; Forest, K. T.; Gellman, S. H., Quasiracemic Crystallization as a Tool To Assess the Accommodation of Noncanonical Residues in Nativelike Protein Conformations. *J. Am. Chem. Soc.* **2012,** *134* (5), 2473-2476.

166. Shortle, D.; Meeker, A. K.; Freire, E., Stability mutants of staphylococcal nuclease: large compensating enthalpy-entropy changes for the reversible denaturation reaction. *Biochemistry* **1988,** *27* (13), 4761-4768.

167. Kato, T.; Yamashita, H.; Misawa, T.; Nishida, K.; Kurihara, M.; Tanaka, M.; Demizu, Y.; Oba, M., Plasmid DNA delivery by arginine-rich cell-penetrating peptides containing unnatural amino acids. *Bioorg Med Chem* **2016,** *24* (12), 2681-7.

168. Dietrich, L.; Rathmer, B.; Ewan, K.; Bange, T.; Heinrichs, S.; Dale, T. C.; Schade, D.; Grossmann, T. N., Cell Permeable Stapled Peptide Inhibitor of Wnt Signaling that Targets beta-Catenin Protein-Protein Interactions. *Cell Chem. Biol.* **2017,** *24* (8), 958-968 e5.

169. Oba, M.; Kunitake, M.; Kato, T.; Ueda, A.; Tanaka, M., Enhanced and Prolonged Cell-Penetrating Abilities of Arginine-Rich Peptides by Introducing Cyclic α,α-Disubstituted α-Amino Acids with Stapling. *Bioconjug. Chem.* **2017,** *28* (7), 1801-1806.

170. Comegna, D.; Zannetti, A.; Del Gatto, A.; de Paola, I.; Russo, L.; Di Gaetano, S.; Liguoro, A.; Capasso, D.; Saviano, M.; Zaccaro, L., Chemical Modification for Proteolytic Stabilization of the Selective αvβ3 Integrin RGDechi Peptide: in Vitro and in Vivo Activities on Malignant Melanoma Cells. *J. Med. Chem.* **2017,** *60* (23), 9874-9884.

171. de Lucio, H.; Gamo, A. M.; Ruiz-Santaquiteria, M.; de Castro, S.; Sanchez-Murcia, P. A.; Toro, M. A.; Gutierrez, K. J.; Gago, F.; Jimenez-Ruiz, A.; Camarasa, M. J.; Velazquez, S., Improved proteolytic stability and potent activity against Leishmania infantum trypanothione reductase of alpha/beta-peptide foldamers conjugated to cell-penetrating peptides. *Eur. J. Med. Chem.* **2017,** *140*, 615-623.

172. Zhao, H.; Jiang, Y.; Tian, Y.; Yang, D.; Qin, X.; Li, Z., Improving cell penetration of helical peptides stabilized by N-terminal crosslinked aspartic acids. *Org. Biomol. Chem.* **2017,** *15* (2), 459-464.

173. Hentzen, N. B.; Smeenk, L. E. J.; Witek, J.; Riniker, S.; Wennemers, H., Cross-Linked Collagen Triple Helices by Oxime Ligation. *J. Am. Chem. Soc.* **2017,** *139* (36), 12815-12820.

174. Jiang, Y.; Deng, Q.; Zhao, H.; Xie, M.; Chen, L.; Yin, F.; Qin, X.; Zheng, W.; Zhao, Y.; Li, Z., Development of Stabilized Peptide-Based PROTACs against Estrogen Receptor α. *ACS Chem. Biol.* **2018,** *13* (3), 628-635.

175. Virgilio, A.; Amato, T.; Petraccone, L.; Esposito, F.; Grandi, N.; Tramontano, E.; Romero, R.; Haider, S.; Gomez-Monterrey, I.; Novellino, E.; Mayol, L.; Esposito, V.; Galeone, A., Improvement of the activity of the anti-HIV-1 integrase aptamer T30175 by introducing a modified thymidine into the loops. *Scientific Reports* **2018,** *8* (1).

176. Zhang, P.; Ma, J.; Yan, Y.; Chen, B.; Liu, B.; Jian, C.; Zhu, B.; Liang, S.; Zeng, Y.; Liu, Z., Arginine modification of lycosin-I to improve inhibitory activity against cancer cells. *Org. Biomol. Chem.* **2017,** *15* (44), 9379-9388.

177. Bang, D.; Makhatadze, G. I.; Tereshko, V.; Kossiakoff, A. A.; Kent, S. B., Total chemical synthesis and X-ray crystal structure of a protein diastereomer: [D-Gln 35]ubiquitin. *Angew. Chem. Int. Ed.* **2005,** *44* (25), 3852-6.

178. Uppalapati, M.; Lee, D. J.; Mandal, K.; Li, H.; Miranda, L. P.; Lowitz, J.; Kenney, J.; Adams, J. J.; Ault-Riché, D.; Kent, S. B. H.; Sidhu, S. S., A Potent d-Protein Antagonist of VEGF-A is Nonimmunogenic, Metabolically Stable, and Longer-Circulating in Vivo. *ACS Chem. Biol.* **2016,** *11* (4), 1058-1065.

179. Ulas, G.; Lemmin, T.; Wu, Y.; Gassner, G. T.; DeGrado, W. F., Designed metalloprotein stabilizes a semiquinone radical. *Nat. Chem.* **2016,** *8* (4), 354-9.

180. Boersma, M. D.; Haase, H. S.; Peterson-Kaufman, K. J.; Lee, E. F.; Clarke, O. B.; Colman, P. M.; Smith, B. J.; Horne, W. S.; Fairlie, W. D.; Gellman, S. H., Evaluation of Diverse α/β-Backbone Patterns for Functional α-Helix Mimicry: Analogues of the Bim BH3 Domain. *J. Am. Chem. Soc.* **2012,** *134* (1), 315-323.

181. Giuliano, M. W.; Horne, W. S.; Gellman, S. H., An α/β-Peptide helix bundle with a pure β^3-amino acid core and a distinctive quaternary structure. *J. Am. Chem. Soc.* **2009,** *131* (29), 9860-9861.

182. Horne, W. S.; Price, J. L.; Gellman, S. H., Interplay among side chain sequence, backbone composition, and residue rigidification in polypeptide folding and assembly. *Proc. Natl. Acad. Sci. USA* **2008,** *105* (27), 9151-9156.

183. Horne, W. S.; Boersma, M. D.; Windsor, M. A.; Gellman, S. H., Sequence-based design of α/β-peptide foldamers that mimic BH3 domains. *Angew. Chem. Int. Ed.* **2008,** *47* (15), 2853-2856.

184. Lengyel, G. A.; Eddinger, G. A.; Horne, W. S., Introduction of Cyclically Constrained γ-Residues Stabilizes an α-Peptide Hairpin in Aqueous Solution. *Org. Lett.* **2013,** *15* (4), 944-947.

185. Lengyel, G. A.; Frank, R. C.; Horne, W. S., Hairpin folding behavior of mixed a/b-peptides in aqueous solution. *J. Am. Chem. Soc.* **2011,** *133* (12), 4246-4249.

186. Lengyel, G. A.; Reinert, Z. E.; Griffith, B. D.; Horne, W. S., Comparison of backbone modification in protein beta-sheets by alpha-->gamma residue replacement and alpha-residue methylation. *Org. Biomol. Chem.* **2014,** *12* (29), 5375-81.

187. Reinert, Z. E.; Musselman, E. D.; Elcock, A. H.; Horne, W. S., A PEG-based oligomer as a backbone replacement for surface-exposed loops in a protein tertiary structure. *ChemBioChem* **2012,** *13* (8), 1107-11.

188. Cheloha, R. W.; Chen, B.; Kumar, N. N.; Watanabe, T.; Thorne, R. G.; Li, L.; Gardella, T. J.; Gellman, S. H., Development of Potent, Protease-Resistant Agonists of the Parathyroid Hormone Receptor with Broad β Residue Distribution. *J. Med. Chem.* **2017,** *60* (21), 8816-8833.

189. Cheloha, R. W.; Watanabe, T.; Dean, T.; Gellman, S. H.; Gardella, T. J., Backbone Modification of a Parathyroid Hormone Receptor-1 Antagonist/Inverse Agonist. *ACS Chem. Biol.* **2016,** *11* (10), 2752-2762.

190. W., C. J.; H., G. S., Iterative Nonproteinogenic Residue Incorporation Yields α/β-Peptides with a Helix-Loop-Helix Tertiary Structure and High Affinity for VEGF. *ChemBioChem* **2017,** *18* (3), 291-299.

191. Kumar, K. S.; Bavikar, S. N.; Spasser, L.; Moyal, T.; Ohayon, S.; Brik, A., Total chemical synthesis of a 304 amino acid K48-linked tetraubiquitin protein. *Angew. Chem. Int. Ed.* **2011,** *50* (27), 6137-41.

192. Ramage, R.; Green, J.; Muir, T. W.; Ogunjobi, O. M.; Love, S.; Shaw, K., Synthetic, structural and biological studies of the ubiquitin system: the total chemical synthesis of ubiquitin. *Biochem. J.* **1994,** *299* (Pt 1), 151-158.

193. Love, S. G.; Muir, T. W.; Ramage, R.; Shaw, K. T.; Alexeev, D.; Sawyer, L.; Kelly, S. M.; Price, N. C.; Arnold, J. E.; Mee, M. P.; Mayer, R. J., Synthetic, structural and biological studies of the ubiquitin system: synthesis and crystal structure of an analogue containing unnatural amino acids. *Biochem. J.* **1997,** *323* (Pt 3), 727-734.

194. Marshall, G. R.; Hodgkin, E. E.; Langs, D. A.; Smith, G. D.; Zabrocki, J.; Leplawy, M. T., Factors governing helical preference of peptides containing multiple alpha,alpha-dialkyl amino acids. *Proc. Natl. Acad. Sci. USA* **1990,** *87* (1), 487-491.

195. Yokum, T. S.; Gauthier, T. J.; Hammer, R. P.; McLaughlin, M. L., Solvent Effects on the 310-/α-Helix Equilibrium in Short Amphipathic Peptides Rich in α,α-Disubstituted Amino Acids. *J. Am. Chem. Soc.* **1997,** *119* (5), 1167-1168.

196. Vijayakumar, E. K. S.; Sudha, T. S.; Balaram, P., Circular dichroism studies of α-aminoisobutyric acid-containing peptides: Chain length and solvent effects in alternating Aib-L-Ala and Aib-L-Val sequences. *Biopolymers* **1984,** *23* (5), 877-886.

197. Masterson, L. R.; Etienne, M. A.; Porcelli, F.; Barany, G.; Hammer, R. P.; Veglia, G., Nonstereogenic α-aminoisobutyryl-glycyl dipeptidyl unit nucleates type I′ β-turn in linear peptides in aqueous solution. *Pept. Sci.* **2007,** *88* (5), 746-753.

198. Haque, T. S.; Little, J. C.; Gellman, S. H., Stereochemical Requirements for β-Hairpin Formation: Model Studies with Four-Residue Peptides and Depsipeptides. *J. Am. Chem. Soc.* **1996,** *118* (29), 6975-6985.

199. Mali, S. M.; Singh, S. K.; Eid, E.; Brik, A., Ubiquitin Signaling: Chemistry Comes to the Rescue. *J. Am. Chem. Soc.* **2017,** *139* (14), 4971-4986.

200. Kerscher, O.; Felberbaum, R.; Hochstrasser, M., Modification of proteins by ubiquitin and ubiquitin-like proteins. *Annu Rev Cell Dev Biol* **2006,** *22*, 159-80.

201. Komander, D., The emerging complexity of protein ubiquitination. *Biochem. Soc. Trans.* **2009,** *37* (Pt 5), 937-53.

202. Chothia, C.; Janin, J., Principles of protein–protein recognition. *Nature* **1975,** *256*, 705.

203. Dawson, P.; Muir, T.; Clark-Lewis, I.; Kent, S., Synthesis of proteins by native chemical ligation. *Science* **1994,** *266* (5186), 776-779.

204. Wan, Q.; Danishefsky, S. J., Free-radical-based, specific desulfurization of cysteine: a powerful advance in the synthesis of polypeptides and glycopolypeptides. *Angew. Chem. Int. Ed.* **2007,** *46* (48), 9248-52.

205. Zheng, J. S.; Tang, S.; Qi, Y. K.; Wang, Z. P.; Liu, L., Chemical synthesis of proteins using peptide hydrazides as thioester surrogates. *Nat. Protoc.* **2013,** *8* (12), 2483-95.

206. Bondalapati, S.; Jbara, M.; Brik, A., Expanding the chemical toolbox for the synthesis of large and uniquely modified proteins. *Nat. Chem.* **2016,** *8* (5), 407-18.

207. Tornøe, C.; Johansson, E.; Wahlund, P.-O., Divergent Protein Synthesis of Bowman–Birk Protease Inhibitors, their Hydrodynamic Behavior and Co-crystallization with α-Chymotrypsin. *Synlett* **2017,** *28* (15), 1901-1906.

208. Zhang, H.; Amick, J.; Chakravarti, R.; Santarriaga, S.; Schlanger, S.; McGlone, C.; Dare, M.; Nix, J. C.; Scaglione, K. M.; Stuehr, D. J.; Misra, S.; Page, R. C., A bipartite interaction

between Hsp70 and CHIP regulates ubiquitination of chaperoned client proteins. *Structure* **2015,** *23* (3), 472-82.

209. Nakatsukasa, K.; Huyer, G.; Michaelis, S.; Brodsky, J. L., Dissecting the ER-associated degradation of a misfolded polytopic membrane protein. *Cell* **2008,** *132* (1), 101-12.

210. Badland, M.; Bains, C. A.; Howard, R.; Laity, D.; Newman, S. D., An improved synthesis of (1R,3S)-3-[(tert-butoxycarbonyl)amino]cyclohexanecarboxylic acid. *Tetrahedron-Asymmetr.* **2010,** *21* (7), 864-866.

211. Berndsen, C. E.; Wolberger, C., A spectrophotometric assay for conjugation of ubiquitin and ubiquitin-like proteins. *Anal. Biochem.* **2011,** *418* (1), 102-10.

212. Sheffield, P.; Garrard, S.; Derewenda, Z., Overcoming Expression and Purification Problems of RhoGDI Using a Family of "Parallel" Expression Vectors. *Protein Expression and Purification* **1999,** *15* (1), 34-39.

213. Loibl, S. F.; Harpaz, Z.; Zitterbart, R.; Seitz, O., Total chemical synthesis of proteins without HPLC purification. *Chem Sci* **2016,** *7* (11), 6753-6759.

214. Ye, Z.; Needham, P. G.; Estabrooks, S. K.; Whitaker, S. K.; Garcia, B. L.; Misra, S.; Brodsky, J. L.; Camacho, C. J., Symmetry breaking during homodimeric assembly activates an E3 ubiquitin ligase. *Sci. Rep.* **2017,** *7* (1), 1789.

215. Guerriero, C. J.; Reutter, K.-R.; Augustine, A. A.; Preston, G. M.; Weiberth, K. F.; Mackie, T. D.; Cleveland-Rubeor, H. C.; Bethel, N. P.; Callenberg, K. M.; Nakatsukasa, K.; Grabe, M.; Brodsky, J. L.; Spang, A., Transmembrane helix hydrophobicity is an energetic barrier during the retrotranslocation of integral membrane ERAD substrates. *Molecular Biology of the Cell* **2017,** *28* (15), 2076-2090.

216. Nakatsukasa, K.; Brodsky, J. L., in vitro reconstitution of the selection, ubiquitination, and membrane extraction of a polytopic ERAD substrate. *Methods Mol. Biol.* **2010,** *619*, 365-76.